

THE LAMINAR BOUNDARY LAYER OF A STEADY,
COMPRESSIBLE FLOW IN THE ENTRANCE REGION OF A TUBE

by

TAU-YI TONG

B.S.M.E., National Chiao-Tung University, China
(1940)

S.M., Massachusetts Institute of Technology
(1948)

SUBMITTED IN PARTIAL FULFILLMENT OF THE
REQUIREMENTS FOR THE DEGREE OF
DOCTOR OF SCIENCE

at the

MASSACHUSETTS INSTITUTE OF TECHNOLOGY
(1952)

Signature of Author

Department of Mechanical Engineering
January 5, 1952

Certified by
Thesis Supervisor

.
Chairman, Departmental Committee on Graduate Students

THE LAMINAR BOUNDARY LAYER OF A STEADY,
COMPRESSIBLE FLOW IN THE ENTRANCE REGION OF A TUBE

by

TAU-YI TOONG

Submitted to the Department of Mechanical Engineering
on January 5, 1952 in Partial Fulfillment of the Requirements
for the Degree of Doctor of Science

ABSTRACT

The partial differential equations of continuity, momentum, and energy were developed for the laminar boundary layer of a steady, compressible flow in the entrance region of a tube. These were transformed into ordinary differential equations, and then solved with the aid of the M.I.T. Differential Analyzer for particular boundary conditions and a constant Prandtl number of the fluid equal to 0.74.

The solution was developed in terms of a power series of the "length parameter". The first two or three terms of this power series were obtained for seven cases of different entrance Mach numbers and different thermal conditions at the tube wall. Rapid convergence was obtained for the cases where the entrance Mach number equalled 2.8.

The effects of compressibility, pressure gradient, and heating or cooling at the tube wall were studied. The theoretical results were compared with those for laminar flow over a flat plate with zero pressure gradient, and also with experimental measurements made in the entrance region of a tube. In the region where a laminar boundary

layer appears to exist and does not fill the entire cross-section of the tube, close agreement was observed between the predicted and measured values of static pressure, adiabatic-wall temperature, and heat-transfer rate.

Comparisons between theory and experiments indicate also that, when the entrance diameter Reynolds number is large, the transition from laminar to turbulent flow seems to have occurred before the entire cross-section of the tube is filled with the laminar boundary layer. When the entrance diameter Reynolds number is sufficiently low, the entire cross-section may be filled with laminar boundary layer before transition occurs. However, the analysis presented here is not valid when the laminar boundary layer fills the entire cross-section of the tube or the boundary layer become turbulent.

Thesis Supervisor: Joseph Kaye
Title: Associate Professor of Mechanical
 Engineering

MASSACHUSETTS INSTITUTE OF TECHNOLOGY

77 Massachusetts Avenue
Cambridge, Massachusetts

January 5, 1952

Professor J. P. Den Hartog
Chairman, Departmental Committee on Graduate Students
Department of Mechanical Engineering
Massachusetts Institute of Technology
Cambridge, Massachusetts

Dear Professor Den Hartog:

In partial fulfillment of the requirements for the degree of Doctor of Science in Mechanical Engineering at the Massachusetts Institute of Technology, I herewith submit my thesis entitled "The Laminar Boundary Layer of a Steady, Compressible Flow in the Entrance Region of a Tube".

Respectfully submitted,

Tau-Yi Toong

ACKNOWLEDGMENTS

The author wishes to extend his sincere thanks to the many people who helped in the course of this work.

The author is especially grateful to Professor Joseph Kaye, who, as supervisor of the thesis and one of the directors of the project for which this present work was done, not only suggested the problem but also gave freely of his time and advice.

The author also wishes to express his deep appreciation to Professor Joseph H. Keenan, co-director of this project, for his various suggestions.

Thanks are also due to Professors A. H. Shapiro and C. C. Lin for their valuable opinions, to Mr. R. H. Shoulberg for his help in the checking of the derivation of the boundary-layer equations, to Mr. G. A. Brown for his assistance in the computation of results, and to Dr. E. J. Frey, Messrs. F. M. Verzuh, R. B. Fredrickson, W. F. O'Connell, Jr., E. Weiss, Mrs. E. C. Hogan, and Miss M. Sullivan for their efforts in solving the differential equations with the differential analyzer.

To his wife, Miranda, the author wishes to express his sincere gratitude for her help in the computation of results and the preparation of the final manuscript.

This work is sponsored as Contract Number N5-ori-07805 by the Office of Naval Research of the United States Navy.

TABLE OF CONTENTS

	Page
Title Page	i
Abstract	ii
Letter of Transmittal	iv
Acknowledgments	v
Table of Contents	vi
List of Figures	vii
Nomenclature	x
Introduction	1
Results	4
Conclusions	25
Appendix A: Derivation of Equations for the Laminar Boundary Layer of a Steady, Compressible Flow in the Entrance Region of a Tube	30
Appendix B: Method of Solving the Differential Equations with the Aid of the M.I.T. Differential Analyzer	53
Appendix C: Tabulation of Results	59
Appendix D: Recommendations for Future Work	64
Appendix E: Bibliography	66
Appendix F: Biographical Note	68
Figures	70

LIST OF FIGURES

<u>Figure No.</u>	<u>Title</u>
1	Variation of f_1 , \dot{f}_1 , and \ddot{f}_1 in Boundary Layer, for Adiabatic Cases of Different Entrance Mach Numbers
2	Variation of \dot{f}_1 in Boundary Layer, for Different Entrance Mach Numbers and Thermal Conditions at Tube Wall
3	Variation of θ_1 in Boundary Layer, for Different Entrance Mach Numbers and Thermal Conditions at Tube Wall
4	Variation of $\dot{\theta}_1$ in Boundary Layer, for Different Entrance Mach Numbers and Thermal Conditions at Tube Wall
5	First Approximation to Velocity Profile in Boundary Layer, for Different Entrance Mach Numbers and Thermal Conditions at Tube Wall
6	Boundary-Layer Thickness-Ratio Versus Length Parameter, for Entrance Mach Number of 2.8 and Different Thermal Conditions at Tube Wall
7	Boundary-Layer Thickness-Ratio Versus Length Reynolds Number, for Entrance Mach Number of 2.8 and Different Thermal Conditions at Tube Wall
8	Boundary-Layer Thickness-Ratio Versus Length-Radius Ratio, for Entrance Mach Number of 2.8 and Different Thermal Conditions at Tube Wall
9	Region of Validity of Present Analysis (Criteria: Maximum Length Parameter and Maximum Length Reynolds Number)
10	Velocity Profile in Boundary Layer, for Entrance Mach Number of 2.8 and Different Thermal Conditions at Tube Wall
11	Temperature Profile in Boundary Layer, for Entrance Mach Number of 2.8 and Different Thermal Conditions at Tube Wall
12	Pressure Ratio Versus Length Parameter, for Adiabatic Case of Entrance Mach Number of 2.8
13	Measured Value of Pressure Ratio Versus Modified Length Parameter, Test Combination B, Adiabatic Apparatus (3, 4)

<u>Figure No.</u>	<u>Title</u>
14	Measured Value of Pressure Ratio Versus Length Reynolds Number, Test Combination B, Adiabatic Apparatus (3, 4)
15	Pressure Ratio Versus Length Parameter for Entrance Mach Number of 2.8 with Heating at Tube Wall ($\theta_w = 3$)
16	Measured Value of Pressure Ratio Versus Modified Length Parameter, Heat-Transfer Apparatus (13)
17	Measured Value of Pressure Ratio Versus Modified Length Parameter, Heat-Transfer Apparatus (13)
18	First Approximation to Pressure Ratio Versus Length Parameter, for Different Entrance Mach Numbers and Thermal Conditions at Tube Wall
19	Adiabatic-Wall Temperature-Ratio Versus Length Parameter, for Entrance Mach Number of 2.8
20	Measured Value of Adiabatic-Wall Temperature-Ratio Versus Modified Length Parameter, Test Combination B, Adiabatic Apparatus (3, 4)
21	Adiabatic-Wall Temperature-Ratio Versus Length Parameter, for Entrance Mach Numbers of 2 and 2.8
22	Local Recovery Factor Versus Length Parameter, for Entrance Mach Numbers of 2 and 2.8
23	Local True Friction Coefficient Versus Length Reynolds Number, for Adiabatic Case of Entrance Mach Number of 2.8
24	Local True Friction Coefficient Versus Length Reynolds Number, for Adiabatic Cases of Different Entrance Mach Numbers
25	Local True Friction Coefficient Versus Length Reynolds Number, for Adiabatic Cases of Different Entrance Mach Numbers
26	Local True Friction Coefficient Versus Length Reynolds Number, for Entrance Mach Number of 2.8 and Different Thermal Conditions at Tube Wall
27	$f_3 (w_j / v_o)^{1/2}$ Versus Length Parameter, for Different Entrance Mach Numbers and Thermal Conditions at Tube Wall

<u>Figure No.</u>	<u>Title</u>
28	First Approximation to $f_z (u_e \beta / \lambda_e)^{1/2}$ Versus Length Parameter, for Different Entrance Mach Numbers and Thermal Conditions at Tube Wall
29	$4\bar{f}_a (\beta/D)$ Versus Length Parameter, for Different Entrance Mach Numbers and Thermal Conditions at Tube Wall
30	Local Nusselt Number Versus Length Parameter, for Entrance Mach Number of 2.8 with Heating at Tube Wall ($\theta_w = 3$)
31	Local Stanton Number Versus Length Reynolds Number, for Entrance Mach Number of 2.8 with Heating at Tube Wall ($\theta_w = 3$)
32	Local Stanton Number Versus Length Reynolds Number, for Entrance Mach Number of 2.8 with Heating at Tube Wall ($\theta_w = 3$)
33	First Approximation to Local Nusselt Number Versus Length Parameter, for Different Entrance Mach Numbers and Thermal Conditions at Tube Wall
34	Measured Value of $ga/(\lambda T)_{c1}$ Versus Modified Length Parameter, Heat-Transfer Apparatus (13)
35	Local Core Mach Number Versus Length Parameter, for Different Entrance Mach Numbers and Thermal Conditions at Tube Wall
36	Local Core Mach-Number-Ratio Versus Length Parameter, for Different Entrance Mach Numbers and Thermal Conditions at Tube Wall
37	Local Core Density-Ratio Versus Length Parameter, for Different Entrance Mach Numbers and Thermal Conditions at Tube Wall
38	Local Core Temperature-Ratio Versus Length Parameter, for Different Entrance Mach Numbers and Thermal Conditions at Tube Wall

NOMENCLATURE

a	inside radius of tube
C_m	constant of integration, see equation (A-69)
c_p	specific heat at constant pressure
c_v	specific heat at constant volume
D	inside diameter of tube
E	internal energy per unit mass
\vec{F}	vector body force per unit mass
F_n	function of η , see equation (B-2)
\bar{f}_a	mean apparent friction coefficient, defined in equation (A-80)
f_m	function of η , see equation (A-15)
f_z	local true friction coefficient, defined in equation (A-77)
G	mass rate of flow per unit area, defined in equation (A-89)
$\left. \begin{array}{l} g \\ h \\ i \\ j \\ l \\ m \\ n \end{array} \right\}$	any positive integer for either exponent or subscript repeated indices indicate summation from 1, 2, 3, ... ∞
h_z	local heat-transfer coefficient
K_m	function of η , see equations (A-42) and (A-53)
k	ratio of specific heats, c_p/c_v
k_m	coefficient of ξ^m in velocity polynomial, see equation (A-19)
L	distance from end of curved contour of nozzle
M	Mach number, $w/(kRT)^{1/2}$

p	static pressure
q	rate of radial heat transfer per unit circumferential area
R	perfect-gas constant
r \varnothing z }	cylindrical coordinates
\bar{r}	recovery factor, defined in equation (A-85)
Re_D	diameter Reynolds number, wD/ν
Re_L	length Reynolds number, based on distance from end of curved contour of nozzle, wL/ν
Re_z	length Reynolds number, based on distance from entrance section of tube, wz/ν
T	absolute temperature
t	time
t_m	coefficient of S^m in temperature polynomial, see equation (A-21)
u	velocity component in radial direction
v	velocity component in circumferential direction
\vec{v}	velocity vector
w	velocity component in axial direction
α_m	coefficient of S^m in density polynomial, see equation (A-22)
β_m	coefficient of S^m in pressure polynomial, see equation (A-20)
δ	thickness of either velocity- or temperature-boundary layer
S	length parameter, defined in equation (A-13)
η	independent variable in transformed boundary-layer equations, defined in equation (A-14)
θ_m	function of η , see equation (A-16)

λ	thermal conductivity
μ	absolute viscosity
ν	kinematic viscosity
ρ	mass density
σ	Prandtl number, $c_p \mu / \lambda$
τ	shear stress
Ψ	stream function, defined in equation (A-12)
ψ	stress dyndic

Subscripts:

aw	refers to adiabatic-wall conditions
c	refers to isentropic core conditions
cl	refers to measured core conditions at the first station
o	refers to entrance conditions
oi	refers to measured upstream stagnation conditions
s	refers to isentropic stagnation conditions
T	refers to temperature-boundary layer
v	refers to velocity-boundary layer
w	refers to conditions at tube wall

Dot above a symbol denotes differentiation with respect to η

INTRODUCTION

The growing importance of problems involving compressible-fluid flow in ducts, with or without heat transfer, has been emphasized in many fields during the past decade. However, most of the analytical and experimental work carried out previous to this decade was devoted to incompressible flow. Although this work may be successfully applied to the low-subsonic regime, extrapolation to the high-subsonic or supersonic regime is inadequate.

Within the past several years, in a research program sponsored by the Office of Naval Research and conducted at M.I.T., an extensive amount of experimental data was obtained on recovery factors, apparent friction coefficients, and heat-transfer coefficients for supersonic flow of air in a tube. These results, which have been systematically reported in a series of papers (1, 2, 3)*, were calculated on the basis of a simple one-dimensional flow model, which assumes uniform properties of the stream at any cross-section of the tube. This simple flow model, although adequate for fully-developed flow, was found inadequate to interpret some of the results (3). It was realized that in the supersonic regime the flow could never attain the fully-developed stage and that the entrance-region effects were important. It was found necessary to

* Numbers in parentheses refer to items in Bibliography.

consider the growth of the boundary layer in the direction of flow. A simplified two-dimensional approach based on the Karman-Pohlhausen integral method was attempted, and the results were encouraging (4).

Theoretical investigations of the flow of an incompressible fluid in the entrance region of a circular tube have been carried out by Hagenbach (5), Neumann (6), Couette (7), Boussinesq (8), Schiller (9), Atkinson and Goldstein (10), Langhaar (11). In this thesis, the effects of compressibility and heat transfer have been studied. The basic partial differential equations of continuity, momentum, and energy, simplified within the usual assumptions of the boundary-layer theory, were transformed into a series of simultaneous ordinary differential equations. These transformed differential equations were then solved with the aid of the M.I.T. Differential Analyzer, for combinations of two different Mach numbers at the entrance of the tube and three different thermal conditions at the tube wall, namely, adiabatic, cooling, and heating. The transformed boundary-layer equations for incompressible flow derived in Atkinson and Goldstein (10) were also solved for comparison. It should be noted, however, that the present analysis is valid only when the boundary layer remains laminar, with the coexistence of an isentropic core in the center of the tube. For other assumptions and the derivation of these equations, see Appendix A.

Variations of the static pressure, adiabatic-wall temperature, and rate of heat transfer, predicted from the theoretical analysis, were compared with the experimental measurements made in the entrance region

of a tube. Comparisons were also made between the predicted values of local true friction coefficients, local recovery factors, and local heat-transfer coefficients for laminar flow in the entrance region of a tube and those for laminar flow over a flat plate with zero pressure gradient. Effects of compressibility, pressure gradient, and heating or cooling at the tube wall were also studied.

RESULTS

The transformed boundary-layer equations derived in Appendix A (A-37, A-42, A-48, and A-53) were solved with the aid of the M.I.T. Differential Analyzer for the six cases shown below in Table 1. The solution of each of these six cases was carried up to terms containing S^{n-1} , as indicated in the table. The Prandtl number of the fluid was assumed constant at 0.74. The differential equations for the incompressible laminar boundary layer given by Atkinson and Goldstein (10) were also solved for comparison. For the method of solving the differential equations, see Appendix B.

TABLE 1

<u>Case</u>	<u>Entrance Mach Number</u>	<u>Thermal Condition at Wall</u>	<u>n</u>
A	2.8	Adiabatic	3
B	2.8	Cooling, $\theta_w = 2$	2
C	2.8	Heating, $\theta_w = 3$	3
D	2.0	Adiabatic	2
E	2.0	Cooling, $\theta_w = 1.445$	2
F	2.0	Heating, $\theta_w = 2.167$	2
G	Incompressible	Adiabatic	2

1. The Functions f_n , θ_n , and Their Derivatives

Fig. 1 shows the variation of the functions f_1 , \dot{f}_1 , and \ddot{f}_1

versus the parameter η for the three adiabatic cases with different entrance Mach numbers. It is shown in Appendix A that η is the independent variable used in the transformed boundary-layer equations, and is defined through equation (A-14). The functions f_n are functions of η and are the coefficients of the different powers of the length parameter ξ (defined through equation A-13) in the stream function ψ (equation A-15). Fig. 2 shows the variation of \dot{f}_1 versus the same parameter η for the seven cases given in Table 1. The variations of θ_1 and $\dot{\theta}_1$ versus η are shown respectively in Figs. 3 and 4 for the six compressible cases. The functions θ_n are functions of η only and are the coefficients of the different powers of the length parameter ξ in the temperature ratio T/T_0 (equation A-16). They are related also to the temperature profiles inside the boundary layer through equation (A-75).

It should be noted that a simple relationship between \dot{f}_n and the velocity profile inside the boundary layer exists only in the incompressible case (10). If the effects of compressibility are included, the velocity profile inside the boundary layer is represented by equation (A-74), in which θ_n also appears. Fig. 5 shows the first approximations to the velocity profile for the seven cases given in Table 1. These approximations were obtained by taking the terms containing only the zero power of the length parameter ξ — from equation (A-74) for the compressible cases, and equations (25) and (27) in Atkinson and Goldstein (10) for the incompressible case. Equation (A-75) indicates that Fig. 3 also shows the first approximations to the temperature

profile inside the boundary layer.

2. Boundary-Layer Thickness

The boundary-layer thickness δ is related through equation (A-14) to the value of η at which the velocity or temperature inside the boundary layer reaches a certain arbitrary fraction of the core velocity or core temperature. In view of the trial-and-error procedure involved in the solution of the first set of the differential equations (Appendix B), it seems that this arbitrary value of η may be chosen as one at which either F_1 (the transformed variable introduced in Appendix B for the machine solution of the differential equations) or θ_1 becomes constant within the accuracy of the differential analyzer. The values of η corresponding to the boundary-layer thickness are tabulated for the different cases in Table C-1, Appendix C.

It is shown in equations (A-74) and (A-75) that F_1 and θ_1 are related respectively to the first approximations of the velocity and temperature profiles inside the boundary layer. Figs. 3 and 5 indicate that the thickness of the velocity-boundary layer is smaller than that of the temperature-boundary layer, for given entrance Mach numbers and thermal conditions at the wall. The ratio between the velocity-boundary-layer thickness and temperature-boundary-layer thickness, which may also be predicted from a study of the basic equations, is of the order of the square root of the Prandtl number of the fluid flowing inside the tube. For given thermal conditions at the wall, the velocity-and temperature-boundary-layer thicknesses increase with increasing entrance Mach number.

For given entrance Mach numbers, the effect of heating at the wall is to increase the boundary-layer thicknesses, while the effect of cooling is to decrease the boundary-layer thicknesses.

The variation of the ratio of the boundary-layer thickness to the tube radius, δ/a , versus the length parameter, ξ , the length Reynolds number based on the local core conditions, $u_{\infty} z/\nu$, and the length-to-radius ratio, z/a , is shown in Figs. 6, 7, and 8 respectively for cases A and C. The boundary-layer thickness-ratio estimated from Howarth's result (12) for compressible laminar flow over a flat plate with zero pressure gradient was also plotted in Fig. 6, using the values of the local core Mach number and the local length Reynolds number calculated for case A. It is to be noted from Fig. 8 that the boundary-layer thickness has a tendency to increase rapidly with increasing length, when the length parameter approaches its limiting value (to be discussed below).

3. Region of Validity of the Present Analysis

Since the present analysis is valid only when the boundary layer does not fill the entire cross-section of the tube (Assumption c, Appendix A), the theoretical results, for the entrance Mach numbers of 2.0 and 2.8, should not be extended too far beyond a value of the length parameter of about 0.05 (Fig. 6 and Table C-1, Appendix C). Since the present analysis is valid only for the laminar boundary layer (Assumption b, Appendix A), the theoretical results should not be extended also beyond the approximate value of a transitional length Reynolds number of

1 to 3×10^6 (3, 4).

In view of the above limiting conditions, the value of the ratio of the length to the radius over which this present analysis is applicable was plotted in Fig. 9 versus the entrance diameter Reynolds number, for the entrance Mach numbers of 2.0 and 2.8. Since the transitional length Reynolds number quoted above is only approximate, the length Reynolds number based on the entrance conditions is used instead of that based on the local core conditions. These two length Reynolds numbers are related to each other through equation (A-84). The values of the ratio of the length to the radius below the straight lines of constant length parameter and the rectangular hyperbolas of constant length Reynolds number are those over which this present analysis is valid. It is observed from Figs. 7 and 9 that the limiting condition at low entrance diameter Reynolds numbers is the value of the length parameter, while that at high entrance diameter Reynolds numbers is the value of the transitional length Reynolds number.

4. Velocity and Temperature Profiles

Both cases A and C were solved in series form to the terms containing ξ^2 (equations A-42 and A-53). The velocity and temperature profiles across the boundary layer were computed through equations (A-74) and (A-75), and plotted versus the radial positions in Figs. 10 and 11 respectively, for different values of the length parameter. The curves represent the sum of terms up to ξ^2 . (Necessary data for computations are given in Tables C-2 and C-3, Appendix C). A slight bump may be observed for both the velocity and temperature profiles at high

values of the length parameter. Whether this bump is significant or is mainly due to computation error inherent in the differential analyzer needs further study.

5. Static Pressure Distribution

The ratio of the static pressure at any section along the tube to that at the entrance section was plotted for case A in Fig. 12 versus the length parameter (equation A-20). Three curves are shown, representing the sum of terms up to ξ^n , with values of n equal to 1, 2, and 3 respectively. (For values of β_n , see Table C-3, Appendix C). It was explained above that the solution should not be extended too far beyond a value of the length parameter of approximately 0.05, although the boundary layer may still remain laminar. At a value of ξ of 0.05, the value of $\beta_3 \xi^3$, which represents the correction of curve 3 over curve 2, constitutes only about 2% of the value represented by curve 3 at this same value of ξ . The next correction term, $\beta_4 \xi^4$, has been estimated by extrapolation to be only about 1% of the value represented by curve 3 at the value of ξ of 0.05. Since this 1% is within the computation accuracy of the differential analyzer for the sum of terms up to ξ^3 , it is not worthwhile to calculate this fourth-power term.

The static pressure distribution along the tube, obtained experimentally with the adiabatic apparatus described in Kaye, et al. (3, 4) as test combination B, was plotted in Fig. 13 versus the "modified length parameter" $2\left(\frac{L}{D}\right)\left(\frac{1}{(Re_L)_{cl}}\right)^{1/2}$. Since the entrance condition of the test section was not measured experimentally, the pressure ratio is

formed by dividing the static pressure by the upstream stagnation pressure. The modified length parameter is formed in a manner analogous to the length parameter (equation A-13), except that the former is based on the measured values corresponding to the first station instead of the actual entrance conditions.

It has been pointed out in the earlier papers (3, 4) that it is very confusing to plot experimental values corresponding to the different entrance diameter Reynolds numbers on a single chart. However, if the pressure ratio is plotted versus this modified length parameter as shown in Fig. 13, a definite trend may be observed. The experimental points fall on a curve close to the theoretical curve calculated for case A, for a length of tube depending on the entrance diameter Reynolds numbers. At higher entrance diameter Reynolds numbers, the experimental points deviate from this curve at an earlier station. The points of deviation appear to correspond to the approximate transitional length Reynolds number cited above.

Several facts should be borne in mind, however, in making any interpretation of Fig. 13. Firstly, the theoretical curve was calculated for the adiabatic case of an entrance Mach number of 2.8, which is very close to the exit Mach number of the supersonic nozzle used in test combination B, based on the isentropic area ratio. However, due to frictional effects, it is difficult to estimate the actual Mach number at the entrance of the tube. Secondly, the modified length parameter was calculated on the basis of the measured conditions at the first station, while in the theoretical analysis, the length parameter was

calculated on the basis of the entrance conditions. Thirdly, all static pressures were measured at the tube wall. It seems hardly justified to ignore the effects of interactions between shock and transition on these wall-tap measurements. Fourthly, in the theoretical analysis, the variation of absolute viscosity with temperature was neglected. The effect of this variation on the predicted pressure distribution needs further investigation.

The ratio of the local static pressure to the stagnation pressure, measured with test combination B (3, 4), was also plotted in Fig. 14 versus the length Reynolds number, based on the local length and the core conditions at the first station. For comparison, the predicted values of the pressure ratio, calculated for case A for three different entrance diameter Reynolds numbers up to the sum of terms containing ζ^3 , were also plotted versus the length Reynolds number, based on the local length and the entrance conditions. Agreement between the predicted and measured values is fairly good for that portion of the experimental curve where a laminar boundary layer appears to be present.

Fig. 15 shows for case C the variation of the ratio of the static pressure at any section along the tube to that at the entrance section versus the length parameter (equation A-20). Again, three curves are shown, representing the sum of terms up to ζ^n , with values of n equal to 1, 2, and 3 respectively. (For values of β_n , see Table C-3, Appendix C).

In Fig. 16, the static pressure distribution along the tube,

obtained in the experimental heat exchanger described in Shoulberg, et al. (13) was plotted versus the modified length parameter. The entrance diameter Reynolds number based on the measured conditions at the first station and the ratio of the tube-wall temperature to the core temperature at the first station are also indicated for each experimental curve. The theoretical curve calculated for case C up to the sum of terms containing \int^3 is also shown for comparison. It should be noted that the actual entrance conditions were not measured in the test set-up, that the Mach number, according to the isentropic area ratio, is about 3.0 at the exit plane of the supersonic nozzle, and that the total length-to-diameter ratio of the heat exchanger is about 31, in comparison with a value of about 42 for the test combination B.

In order to get a clearer picture, Fig. 16 was blown up to a larger scale in Fig. 17. Comparison between Fig. 17 and Fig. 16 of Shoulberg, et al. (13) indicates again the advantage of plotting the pressure ratio versus the modified length parameter.

The theoretical prediction of the pressure distribution along the tube is shown in Fig. 18 in terms of the static pressure ratio versus the length parameter for the six compressible cases given in Table 1. Only the first approximations representing the sum of terms up to the first power of the length parameter were plotted. (Values of β_n for the various cases are given in Table C-3, Appendix C). For given supersonic entrance Mach numbers, the effect of heating is to increase the rate of rise of the static pressure ratio with increasing length parameter, while that of cooling is to decrease the

rate of rise of the pressure ratio with increasing length parameter. For given thermal conditions at the wall, the case of higher supersonic entrance Mach number shows a more rapid rise of the static pressure ratio with increasing length parameter.

6. Adiabatic-Wall Temperature and Recovery Factor

Fig. 19 shows the variation of the ratio of the adiabatic-wall temperature to the stagnation temperature, predicted for case A, versus the length parameter. Three curves are shown, representing the sum of terms up to ξ^n , with values of n equal to 0, 1, and 2 respectively (equations A-16, A-26, and A-27). The rapid convergence of the series solution is apparent.

Fig. 20 shows the variation of the ratio of the adiabatic-wall temperature to the upstream stagnation temperature, obtained with the adiabatic apparatus described in Kaye, et al. (3, 4) as test combination B, versus the modified length parameter. Curve 3 of Fig. 19, representing the sum of terms up to ξ^2 , was carried over for comparison. In making any interpretation of this plot, the facts pointed out above for interpreting pressure distributions should also be kept in mind. In addition, with the present test set-up, longitudinal heat transfer to the first and last stations of the test section has not been entirely eliminated. This heat transfer probably accounts for the abnormal rise of the measured "adiabatic-wall" temperatures at the two ends of the test section.

The variation of the ratio of the adiabatic-wall temperature

to the stagnation temperature versus the length parameter is shown in Fig. 21 for cases A and D. Both curves represent the sum of terms up to the first power of the length parameter. The chart indicates that this ratio increases as the entrance Mach number decreases. This same trend has been predicted for laminar flow over a flat plate with zero pressure gradient by Emmons and Brainerd (14).

The recovery factor, defined by equation (A-85) and calculated through equation (A-87) up to the sum of terms containing ξ^n , (with values of n equal to 0, 1, and 2 for case A, and equal to 0 and 1 for case D), was plotted for the same two cases in Fig. 22. The case of the lower entrance Mach number (case D) gives a higher recovery factor at the same value of the length parameter. The theoretical analysis of Emmons and Brainerd for compressible laminar flow over a flat plate (14) indicates that, as a good first approximation, the recovery factor may be calculated as the square root of the Prandtl number. Fig. 4 of Emmons and Brainerd (14) also indicates that for the range of Prandtl number between 0 and 1 the recovery factor increases as the free-stream Mach number decreases. The line representing the square root of the Prandtl number (0.74) used in this theoretical analysis is also shown in Fig. 22 for comparison.

The values of $\theta_m(0)$ for the various cases cited above are given in Table C-4, Appendix C. The values of t_n for the different cases are also given in Table C-3, Appendix C.

7. Local True Friction Coefficient

With the information given in Tables C-3 and C-4, Appendix C, the local true friction coefficient f_z , defined by equations (A-76) and (A-77), may be calculated through equation (A-78). It is recognized from equation (A-78) that this friction coefficient is a function of the length parameter and the length Reynolds number. Using equations (A-13) and (A-84), f_z may be plotted for the different entrance diameter Reynolds numbers versus the length Reynolds number based on the local core conditions. Fig. 23 shows such a plot for case A, for two different entrance diameter Reynolds numbers. Three curves are shown for each entrance diameter Reynolds number, representing the sum of terms up to S^n , with values of n equal to 0, 1, and 2 respectively. Convergence of the series solution seems fairly rapid.

In Fig. 24, the comparison of the local true friction coefficient for the adiabatic cases of different entrance Mach numbers is shown at two different entrance diameter Reynolds numbers. For case A, the curves represent the sum of terms up to S^2 ; while for cases D and G, the curves represent the sum of terms up to S . In the same figure, curves for laminar flow over a flat plate with zero pressure gradient are also shown. The incompressible curve was obtained by Blasius (15), and the compressible curve for a free-stream Mach number of 2 was obtained by Emmons and Brainerd (14) for constant absolute viscosity.

In order to make a clearer comparison, the lower part of Fig. 24 was expanded into a larger plot as shown in Fig. 25. The curve

for laminar flow over a flat plate for a free-stream Mach number of 2.8 was also added for comparison. The following facts are observed from these figures:

(i) Unlike the plate-flow, the local true friction coefficient for the tube-flow, when plotted versus the length Reynolds number, depends also on the entrance diameter Reynolds numbers.

(ii) For constant entrance diameter Reynolds number, the friction coefficient decreases with increasing length Reynolds number.

(iii) For the same supersonic entrance Mach number and at the same length Reynolds number, the friction coefficient at higher entrance diameter Reynolds number is larger than that at lower entrance diameter Reynolds number. For incompressible tube-flow and at the same length Reynolds number, on the other hand, the friction coefficient at higher entrance diameter Reynolds number is smaller than that at lower entrance diameter Reynolds number.

(iv) The curve representing the friction coefficient for the tube-flow at higher entrance diameter Reynolds number lies closer to the curve representing the friction coefficient for the plate-flow, with a free-stream Mach number equal to the entrance Mach number pertaining to the tube-flow.

(v) For supersonic flow, the friction coefficient for the tube-flow is lower than that for the plate-flow of corresponding free-stream Mach number. For incompressible flow, the friction coefficient for the tube-flow is higher than that for the plate-flow. This

reversal may be accounted for by the fact that the pressure gradient along the tube in these two cases is just opposite. It seems reasonable to predict that for subsonic flow, the friction coefficient for the tube-flow will be higher than that for the plate-flow of corresponding free-stream Mach number.

(vi) As in the case of the plate-flow, the effect of compressibility is to decrease the friction coefficient for the same entrance diameter Reynolds number and length Reynolds number.

Fig. 26 shows the comparison of the local true friction coefficient for cases A and C at different entrance diameter Reynolds numbers. All curves represent the sum of terms up to S^2 (equation A-78). For the same entrance diameter Reynolds number and at the same length Reynolds number, the effect of heating is to decrease the local true friction coefficient.

Equation (A-79) indicates that $f_3 \left(\frac{w_0 z}{\nu_0} \right)^{1/2}$ is a function of the length parameter only. Fig. 27 shows a plot of $f_3 \left(\frac{w_0 z}{\nu_0} \right)^{1/2}$ versus the length parameter for cases A, C, D, and G. For cases A and C, the ordinate was calculated up to the sum of terms containing S^2 , while for cases D and G, this was calculated up to the sum of terms containing S . (For convergence of the series solution, see Fig. 23). Corresponding values for laminar flow over a flat plate are also shown for comparison. The effects of compressibility, pressure gradient, and heating at the tube wall are shown clearly.

First approximations to $f_3 \left(\frac{w_0 z}{\nu_0} \right)^{1/2}$ were plotted in Fig. 28

versus the length parameter for the seven cases given in Table 1. The effects of compressibility, heating and cooling at the tube wall are clearly shown.

8. Mean Apparent Friction Coefficient

The mean apparent friction coefficient, defined according to equation (A-80), was calculated through equation (A-81) for incompressible flow and through equation (A-82) for compressible flow. Fig. 29 shows a plot of the product of the mean apparent friction coefficient and the length-to-diameter ratio versus the length parameter, for different entrance Mach numbers and thermal conditions at the tube wall. For cases A and C, the curves represent the sum of terms up to ξ^3 , while for cases D and G, they represent the sum of terms up to ξ^2 .

Comparison of Fig. 29 with Fig. 27 indicates that the effect of compressibility is the same on both the mean apparent friction coefficient and the local true friction coefficient; viz., to give higher values of the friction coefficient at lower entrance Mach numbers. However, the effect of heating at the tube wall on the mean apparent friction coefficient is just opposite to that on the local true friction coefficient; viz., heating gives higher values of the mean apparent friction coefficient, and yet lower values of the local true friction coefficient. This apparent discrepancy is due to the way the two friction coefficients are defined. The mean apparent friction coefficient is related to the static pressure change along the length of the tube. Using the knowledge developed in one-dimensional compressible-flow inside

a constant-area duct that the effects on pressure change due to heating and friction are in the same direction, it seems justified that the value of the mean apparent friction coefficient will be increased, when there is heating at the wall. On the other hand, the local true friction coefficient is related to the radial velocity gradient at the wall. When there is heating at the wall, the boundary-layer thickness is increased, the radial velocity gradient at the wall is decreased, and therefore the local true friction coefficient is decreased.

9. Local Heat-Transfer Coefficient

The local heat-transfer coefficient h_z , defined through equation (A-88), may be calculated from equation (A-93) in terms of the Nusselt number, from equation (A-90) in terms of the Stanton number based on the entrance mass velocity, or from equation (A-91) in terms of the Stanton number based on the local mass velocity. Necessary data for computation are given in Tables C-3 and C-4, Appendix C.

It is to be noted from equation (A-93) that the local Nusselt number is a function of the length parameter only. Fig. 30 shows for case C a plot of the Nusselt number versus the length parameter. The curves represent the sum of terms up to ζ^n , with values of n equal to 0, 1, and 2 (equation A-93). The convergence of the solution is apparent.

For comparison, curves for laminar flow over a flat plate with zero pressure gradient were also plotted in Fig. 30 for both the incompressible case (16) and the compressible case of free-stream Mach number equal to 2.8 (17, 14). It is to be noted that the curve for compressible

plate-flow was deduced from equation (63) of Chapman and Rubesin (17), using the skin friction drag coefficient obtained in Emmons and Brainerd (14) for an insulated plate. The usual assumption of neglecting the effect of heating or cooling on the shape of the velocity profile within the boundary layer was made in the computation of this curve for compressible plate-flow.

It is shown in equations (A-90) and (A-91) that the local Stanton number, like the local true friction coefficient from equation (A-78), is a function of both the length parameter and the length Reynolds number. In Fig. 31, the local Stanton number based on the entrance mass velocity was plotted for case C at different entrance diameter Reynolds numbers versus the length Reynolds number based on the local core conditions. However, just contrary to what has been observed for the local true friction coefficient (Fig. 26), the local Stanton number based on the entrance mass velocity is higher at lower entrance diameter Reynolds number for the same length Reynolds number. This apparent discrepancy is eliminated when the Stanton number based on the local mass velocity was plotted in Fig. 32 versus the length Reynolds number at different entrance diameter Reynolds numbers.

For comparison, Figs. 31 and 32 also show the local Stanton number for laminar flow over a flat plate with zero pressure gradient for both the incompressible case (16) and the compressible case of free-stream Mach number equal to 2.8 (17, 14).

First approximations to the local Nusselt number were plotted versus the length parameter in Fig. 33 for cases B, C, E, and F. They

were calculated through equation (A-93), using only the terms of zero power of the length parameter. Curves for laminar flow over a flat plate with zero pressure gradient were also plotted for comparison for both the incompressible case (16) and the compressible cases of free-stream Mach numbers equal to 2.0 and 2.8 (17, 14). It is shown that the effect of compressibility is to decrease the local Nusselt number for the same length parameter and that, for a given entrance Mach number, the local Nusselt number for heating is smaller than that for cooling.

10. Local Rate of Heat Transfer

Equation (A-88) indicates that the local heat-transfer coefficient is defined on the basis of the difference between the actual wall temperature and the adiabatic-wall temperature, the latter being obtained as a function of the length parameter for the adiabatic case of identical entrance Mach number.

It seems, however, that some sort of justification should be made for using this temperature difference as the effective thermal potential which causes the radial heat transfer. On the contrary, there is reason to believe that this temperature difference should not be the effective thermal potential for the radial heat transfer. For example, due to the effect of heating or cooling upstream of a certain location on the shape of the velocity and temperature profiles within the boundary layer, it seems doubtful that the "equilibrium" temperature of the wall, if it should be insulated at that location, would be the same as

the "adiabatic-wall" temperature for the case of a wall insulated all along the length.

Difficulties with this usual definition of the local heat transfer coefficient were encountered for the case of variable surface temperature for the plate-flow (17). Difficulties may likely be present also with the tube problem, even for the case of constant surface temperature, if this surface temperature should be fairly close to the adiabatic-wall temperature. For example, in equation (A-93), the denominator may become zero at a certain value of the length parameter, while the numerator may still remain finite, thus giving a heat-transfer coefficient of infinity!

A different parameter is found necessary to correlate the rate of heat transfer. A typical one, $\frac{f a}{\lambda T_0}$, related to the radial temperature gradient at the tube wall, is suggested through equation (A-94). It was plotted for case C in Fig. 34 versus the length parameter. In this same figure, the measured values of the heat-transfer rate, obtained in the experimental heat exchanger described in Shoulberg, et al. (13), were also plotted versus the modified length parameter. It is to be noted that the measured rate of heat transfer is expressed in a form analogous to the suggested parameter, except that in the experimental case, the measured conditions at the first station were used instead of the actual entrance conditions. Where the flow appears to be laminar, fair agreement is observed between the measured and predicted values of the rate of heat transfer.

11. Mach-Number, Fluid-Density, and Static-Temperature Distribution Inside the Isentropic Core

Fig. 35 shows the variation of the Mach number inside the isentropic core for cases A, C, and D. The core Mach number was calculated from the isentropic pressure ratio, using Table 30 of "Gas Tables" (18). For case A, two curves are shown, representing respectively the values calculated from the pressure ratios up to the sum of terms containing S^2 and S^3 (equation A-20). Convergence of the series solution is fairly rapid. For case C, the curve was calculated from the pressure ratios up to the sum of terms containing S^3 , while for case D, the curve was calculated from the pressure ratios up to the sum of terms containing S^2 .

The ratio of the local core Mach number to the entrance Mach number was plotted in Fig. 36 versus the length parameter for the same three cases. Here, all the curves were calculated from the pressure ratios up to the sum of terms containing S^2 . It is observed that, as compared with case A, the drop in the value of this ratio of the local core Mach number to the entrance Mach number with increasing length parameter is more rapid for cases C and D.

The ratios of the local core fluid density and the local core static temperature to their respective entrance values were plotted for cases A, C, and D in Figs. 37 and 38 versus the length parameter. They were calculated through equations (A-22) and (A-21), using the values of α_n and t_n given in Table C-3, Appendix C. For case A, the ratios were computed up to the sum of terms containing S^2 and S^3 . Rapid

convergence is again observed. For case C, the ratio was computed up to the sum of terms containing S^3 , while for case D, the ratio was computed up to the sum of terms containing S^2 .

For given supersonic entrance Mach numbers, the effect of heating is to increase the rate of rise of both the density and temperature ratios with increasing length parameter. For given thermal conditions at the wall, the case of higher supersonic Mach number shows a more rapid rise of both the density and temperature ratios with increasing length parameter.

CONCLUSIONS

The differential equations for a steady, laminar, boundary-layer flow in the entrance region of a tube were solved for the incompressible case and six compressible cases of constant Prandtl number (0.74) for different entrance Mach numbers and different thermal conditions at the tube wall (Table 1). The effects of compressibility, pressure gradient, and radial heat transfer at the wall were studied. The theoretical results were compared with those for laminar flow over a flat plate with zero pressure gradient and also with experimental measurements made in the entrance region of a tube.

The theoretical results obtained in this thesis are valid only where the laminar boundary layer exists and does not fill the entire cross-section of the tube. The limiting ratio of the tube length to tube radius, over which this present analysis is applicable, is shown in Fig. 9, corresponding to entrance Mach numbers of 2.0 and 2.8 and different entrance diameter Reynolds numbers. It indicates that the limiting condition at low entrance diameter Reynolds numbers is the value of the length parameter of about 0.05, while at high entrance diameter Reynolds numbers it is the value of the transitional length Reynolds number of about 10^6 .

It is observed from Figs. 12, 15, 19, 22, 23, 30, 35, 37, and 38 that, since the value of the length parameter is small, the series solution employed in this analysis converges very rapidly.

For given thermal conditions at the tube wall, both the

velocity-and temperature-boundary-layer thicknesses increase with increasing entrance Mach numbers. For given entrance Mach numbers, the effect of heating at the wall is to increase the boundary-layer thicknesses, while that of cooling is to decrease the boundary-layer thicknesses.

The measured values of static pressure, adiabatic-wall temperature, and rate of heat transfer, obtained in the entrance region of a tube, were compared with the respective predicted values. It is observed from Figs. 13, 14, 16, 17, 20, and 34 that the agreement is good where the boundary-layer flow appears to be laminar and does not fill the entire cross-section of the tube.

With increasing length parameter, the fluid density, static pressure, and static temperature inside the isentropic core increase for all cases of supersonic flow. For given thermal conditions at the tube wall, the ratios of the local core fluid density, local static pressure, and local core static temperature to their respective values at the entrance section increase more rapidly with increasing length parameter at higher supersonic entrance Mach numbers. For given supersonic entrance Mach numbers, these ratios increase more rapidly with increasing length parameter, when there is heating at the wall.

With increasing length parameter, the core Mach number decreases for all cases of supersonic flow. For given supersonic entrance Mach numbers, the effect of heating is to decrease the core Mach number at the same length parameter. The ratio of the local core Mach number to the entrance Mach number drops faster with increasing

length parameter, if the supersonic entrance Mach number is closer to unity.

The ratio of the adiabatic-wall temperature to the stagnation temperature at a given length parameter decreases with increasing entrance Mach number. Likewise, the recovery factor at a given length parameter decreases with increasing entrance Mach number. Both the recovery factor and the ratio of the adiabatic-wall temperature to the stagnation temperature increase with increasing length parameter. The recovery factor for the entrance laminar flow inside a round tube agrees fairly well with that predicted for laminar flow over a flat plate.

The following facts are observed for the local true friction coefficient:

- (i) Unlike the case of the plate-flow, the local true friction coefficient for the tube-flow, when plotted versus the length Reynolds number, depends also on the entrance diameter Reynolds numbers.
- (ii) For constant entrance diameter Reynolds number, the local true friction coefficient decreases with increasing length Reynolds number.
- (iii) For the same supersonic entrance Mach number and at the same length Reynolds number, the value of the friction coefficient increases with increasing entrance diameter Reynolds number. However, for incompressible flow, its value decreases with increasing entrance diameter Reynolds number.
- (iv) The value of the friction coefficient at higher

entrance diameter Reynolds number also lies closer to that for the corresponding plate-flow, with a free-stream Mach number equal to the entrance Mach number pertaining to the tube-flow.

(v) For supersonic flow, the friction coefficient for the tube-flow is lower than that for the plate-flow of corresponding free-stream Mach number. For incompressible flow, on the other hand, the friction coefficient for the tube-flow is higher than that for the plate-flow. This reversal may be accounted for by the fact that the pressure gradient along the tube in these two cases is just opposite.

(vi) As in the case of the plate-flow, the effect of compressibility is to decrease the friction coefficient, for the same entrance diameter Reynolds number and at the same local length Reynolds number.

(vii) The effect of heating is to decrease the friction coefficient, while that of cooling is to increase the friction coefficient.

A mean apparent friction coefficient, defined through the change in static pressure along the tube according to equation (A-80), is found convenient for design purposes. It is shown that the value of this coefficient is decreased due to the effect of compressibility and is increased due to the effect of heating at the tube wall.

The local Nusselt number is found to decrease with increasing length parameter. Its value is decreased due to the effect of compressibility. For the same entrance Mach number and at the same length parameter, higher Nusselt numbers are obtained with cooling than with heating.

The local Stanton number is a function of both the length parameter and the length Reynolds number. Hence, unlike the case of the plate-flow, it depends also on the entrance diameter Reynolds number, when plotted versus the length Reynolds number. However, just contrary to what has been observed for the local true friction coefficient, the local Stanton number for supersonic flow, defined on the basis of the entrance mass velocity, decreases with increasing entrance diameter Reynolds number. This is probably due to the manner this local Stanton number was defined. When the Stanton number is formed on the basis of the local mass velocity, it is found that its value increases with increasing entrance diameter Reynolds number.

The local heat-transfer coefficient, defined on the basis of the difference between the actual wall temperature and the adiabatic-wall temperature, is found somewhat unsatisfactory for correlating radial heat transfers at the tube wall. This is due to the fact that the difference between the actual wall temperature and the adiabatic-wall temperature is not necessarily the true thermal potential causing the radial heat transfer. A new parameter $\frac{q_w}{\lambda T_w}$ is defined through the radial temperature gradient at the wall. Its value depends only on the length parameter, and is found to decrease with increasing length parameter.

APPENDIX A

DERIVATION OF EQUATIONS FOR THE LAMINAR BOUNDARY LAYER
OF A STEADY, COMPRESSIBLE FLOW IN THE ENTRANCE REGION OF A TUBE

1. Assumptions

- (a) Steady flow
- (b) Laminar boundary layer
- (c) One-dimensional, isentropic flow inside the core
- (d) Perfect gas, with constant c_p , μ , and λ
- (e) Negligible external body force
- (f) Inside the boundary layer,

$$u \ll w, \quad v = \frac{\partial}{\partial \varphi} = 0$$
- (g) $\delta_v/z \ll 1$, and since $c_p \mu/\lambda = O(1)$ for most gases,

$$\delta_T/z \ll 1$$

2. Basic Equations

The basic equations of continuity, momentum, and energy in terms of the Gibbs vector notation are:

$$\frac{\partial \rho}{\partial t} + \nabla \cdot (\rho \vec{v}) = 0 \quad (\text{A-1})$$

$$\begin{aligned} \rho \frac{\partial \vec{v}}{\partial t} + \rho \vec{v} \cdot \nabla \vec{v} &= \rho \vec{F} - \nabla \cdot \psi \\ &= \rho \vec{F} - \nabla p - \frac{2}{3} \nabla (\mu \nabla \cdot \vec{v}) + \nabla \cdot (\mu \Phi) \end{aligned} \quad (\text{A-2})$$

where
$$\Phi = \nabla \vec{v} + (\nabla \vec{v})_{\text{conjugate}}$$

$$\frac{\partial}{\partial t}(\rho E) + \nabla \cdot (E \rho \vec{v}) = (\psi \cdot \nabla) \cdot \vec{v} + \nabla \cdot (\lambda \nabla T) \quad (\text{A-3})$$

In terms of the cylindrical coordinates, with $\frac{\partial}{\partial t} = \frac{\partial}{\partial \varphi} = v = \vec{F} = 0$, constant c_p , μ , and λ , and using perfect-gas relationships,

$$p = \rho R T, \quad E = c_v T, \quad \text{and} \quad c_p - c_v = R \quad (\text{A-4})$$

the basic equations become,

$$\frac{\partial}{\partial r} (r \rho u) + \frac{\partial}{\partial z} (r \rho w) = 0 \quad (\text{A-5})$$

$$\begin{aligned} \rho \left(u \frac{\partial u}{\partial r} + w \frac{\partial u}{\partial z} \right) &= - \frac{\partial p}{\partial r} + \frac{1}{3} \mu \frac{\partial}{\partial r} \left(\frac{\partial u}{\partial r} + \frac{u}{r} + \frac{\partial w}{\partial z} \right) \\ &\quad + \mu \left(\frac{\partial^2 u}{\partial r^2} + \frac{1}{r} \frac{\partial u}{\partial r} - \frac{u}{r^2} + \frac{\partial^2 u}{\partial z^2} \right) \end{aligned} \quad (\text{A-6})$$

$$\begin{aligned} \rho \left(u \frac{\partial w}{\partial r} + w \frac{\partial w}{\partial z} \right) &= - \frac{\partial p}{\partial z} + \frac{1}{3} \mu \frac{\partial}{\partial z} \left(\frac{\partial u}{\partial r} + \frac{u}{r} + \frac{\partial w}{\partial z} \right) \\ &\quad + \mu \left(\frac{\partial^2 w}{\partial r^2} + \frac{1}{r} \frac{\partial w}{\partial r} + \frac{\partial^2 w}{\partial z^2} \right) \end{aligned} \quad (\text{A-7})$$

$$\begin{aligned} &\rho c_p \left(u \frac{\partial T}{\partial r} + w \frac{\partial T}{\partial z} \right) - \left(u \frac{\partial p}{\partial r} + w \frac{\partial p}{\partial z} \right) \\ &= \lambda \left(\frac{\partial^2 T}{\partial r^2} + \frac{1}{r} \frac{\partial T}{\partial r} + \frac{\partial^2 T}{\partial z^2} \right) + 2\mu \left[\left(\frac{\partial u}{\partial r} \right)^2 + \left(\frac{u}{r} \right)^2 + \left(\frac{\partial w}{\partial z} \right)^2 \right] \\ &\quad - \frac{2}{3} \mu \left(\frac{\partial u}{\partial r} + \frac{u}{r} + \frac{\partial w}{\partial z} \right)^2 + \mu \left(\frac{\partial u}{\partial z} + \frac{\partial w}{\partial r} \right)^2 \end{aligned} \quad (\text{A-8})$$

3. Boundary-Layer Equations

Assuming $\delta/z \ll 1$, and neglecting the small quantities of

second order, the basic equations are reduced to

$$\frac{\partial}{\partial r}(r\rho u) + \frac{\partial}{\partial z}(r\rho w) = 0 \quad (\text{A-5})$$

$$\frac{\partial p}{\partial r} = 0 \quad (\text{A-9})$$

$$\rho(u \frac{\partial w}{\partial r} + w \frac{\partial w}{\partial z}) = -\frac{\partial p}{\partial z} + \mu(\frac{\partial^2 w}{\partial r^2} + \frac{1}{r} \frac{\partial w}{\partial r}) \quad (\text{A-10})$$

$$\begin{aligned} \rho C_p(u \frac{\partial T}{\partial r} + w \frac{\partial T}{\partial z}) &= w \frac{\partial p}{\partial z} + \lambda(\frac{\partial^2 T}{\partial r^2} + \frac{1}{r} \frac{\partial T}{\partial r}) \\ &+ \mu(\frac{\partial w}{\partial r})^2 \end{aligned} \quad (\text{A-11})$$

4. Transformations

The continuity equation (A-5) is automatically satisfied by defining a stream function Ψ , such that

$$\left. \begin{aligned} r u r &\equiv -\frac{\partial \Psi}{\partial z} \\ r w r &\equiv \frac{\partial \Psi}{\partial r} \end{aligned} \right\} \quad (\text{A-12})$$

Set

$$\xi \equiv \left(\frac{2z}{a Re_{D_0}}\right)^{1/2} = \frac{z}{a} \left(\frac{1}{Re_{D_0}}\right)^{1/2} = \frac{2(Re_{D_0})^{1/2}}{Re_{D_0}} \quad (\text{A-13})$$

$$\eta \equiv \frac{(1 - \frac{r^2}{a^2})}{4\xi} = \frac{1}{4} \left(1 - \frac{r^2}{a^2}\right) \left(\frac{a}{z}\right) (Re_{D_0})^{1/2} \quad (\text{A-14})$$

where

$$Re_{D_0} \equiv \frac{2w_0 a}{\nu_0}$$

$$Re_{z_0} \equiv \frac{w_0 z}{\nu_0}$$

Assume that the stream function and the temperature within the boundary layer can each be expressed in terms of a convergent series as follows:

$$\begin{aligned} \Psi &= -a^2 \rho_0 w_0 [\zeta f_1(\eta) + \zeta^2 f_2(\eta) + \zeta^3 f_3(\eta) + \dots] \\ &= -a^2 \rho_0 w_0 [\zeta^m f_m(\eta)] \end{aligned} \quad (A-15)$$

$$\begin{aligned} T &= T_0 [\theta_1(\eta) + \zeta \theta_2(\eta) + \zeta^2 \theta_3(\eta) + \dots] \\ &= T_0 [\zeta^{m-1} \theta_m(\eta)] \end{aligned} \quad (A-16)$$

Denoting $f_m(\eta)$ by f_m , $\frac{df_m}{d\eta}$ by \dot{f}_m , etc. and using equations (A-12) and (A-15), one obtains

$$\begin{aligned} w &= \frac{w_0}{2} \frac{\rho_0}{\rho} (f_1 + \zeta \dot{f}_2 + \zeta^2 \dot{f}_3 + \dots) \\ &= \frac{w_0}{2} \frac{\rho_0}{\rho} (\zeta^{m-1} \dot{f}_m) \\ u &= \frac{w_0}{2} \frac{\rho_0}{\rho} \frac{a^2}{\nu_0} [\zeta(f_1 - \eta \dot{f}_1) + \zeta^2(2f_2 - \eta \dot{f}_2) \\ &\quad + \zeta^3(3f_3 - \eta \dot{f}_3) + \dots] \end{aligned} \quad (A-17)$$

$$u = \frac{w_0}{2} \frac{\rho_0}{\rho} \frac{a^2}{r_j} \left[\zeta^m (m f_m - \eta \dot{f}_m) \right] \quad (\text{A-18})$$

5. Velocity, Pressure, Temperature, and Density Relationships

Inside the Isentropic Core

Assume

$$\begin{aligned} w_c &= w_0 (1 + k_1 \zeta + k_2 \zeta^2 + k_3 \zeta^3 + \dots) \\ &= w_0 (1 + \zeta^m k_m) \end{aligned} \quad (\text{A-19})$$

$$\begin{aligned} p &= p_0 (1 + \beta_1 \zeta + \beta_2 \zeta^2 + \beta_3 \zeta^3 + \dots) \\ &= p_0 (1 + \zeta^m \beta_m) \end{aligned} \quad (\text{A-20})$$

$$\begin{aligned} T_c &= T_0 (1 + t_1 \zeta + t_2 \zeta^2 + t_3 \zeta^3 + \dots) \\ &= T_0 (1 + \zeta^m t_m) \end{aligned} \quad (\text{A-21})$$

$$\begin{aligned} \rho_c &= \rho_0 (1 + \alpha_1 \zeta + \alpha_2 \zeta^2 + \alpha_3 \zeta^3 + \dots) \\ &= \rho_0 (1 + \zeta^m \alpha_m) \end{aligned} \quad (\text{A-22})$$

The relationships between k_m , β_m , t_m , and α_m may be derived by using the perfect-gas equation and the isentropic conditions inside the core.

With the perfect-gas equation,

$$p = \rho R T, \quad (\text{A-4})$$

$$p_0 (1 + \zeta^m \beta_m) = \rho_0 R T_0 (1 + \zeta^l \alpha_l) (1 + \zeta^n t_n)$$

Using the binomial expansion for $(1+x)^k$ and the expansion of $\ln(1+x)$ in powers of x , the coefficients of T_c in the expansion of $\ln T_c$ in powers of x are, one obtains,

$$\left. \begin{aligned} \beta_1 &= \alpha_1 + k, \\ \beta_2 &= \alpha_2 + \alpha_1 k_1 + k_2, \\ \beta_3 &= \alpha_3 + \alpha_2 k_1 + \alpha_1 k_2 + k_3 \end{aligned} \right\} \quad (A-24)$$

Using the isentropic condition inside the core,

$$\frac{p}{p_0} = \left(\frac{p_c}{p_0} \right)^{\frac{k}{k-1}} \quad (A-25)$$

$$(1 + \sum^m \beta_m) = (1 + \sum^l \alpha_l)^{\frac{k}{k-1}}$$

Equating the coefficients of the terms in same powers of the length parameter, one gets,

$$\left. \begin{aligned} \beta_1 &= k\alpha_1, \\ \beta_2 &= k\alpha_2 + \frac{k(k-1)}{2} \alpha_1^2, \\ \beta_3 &= k\alpha_3 + k(k-1)\alpha_2\alpha_1 + \frac{k(k-1)(k-2)}{3!} \alpha_1^3 \end{aligned} \right\} \quad (A-25)$$

With the adiabatic condition inside the core,

$$T_c + \frac{w_c^2}{2C_p} = T_s = T_0 + \frac{w_0^2}{2C_p}, \quad (A-26)$$

$$T_0(1 + \sum^m t_m) + \frac{w_0^2}{2C_p} (1 + \sum^n k_n)^2 = T_0 + \frac{w_0^2}{2C_p}$$

Equating the coefficients of the terms in same powers of the length parameter and with the entrance Mach number M_0 defined by

$$M_0^2 \equiv \frac{w_0^2}{kRT_0} \quad (\text{A-27})$$

one obtains,

$$\left. \begin{aligned} t_1 &= -(k-1)M_0^2 k_1 \\ t_2 &= -\left(\frac{k-1}{2}\right)M_0^2 (k_1^2 + 2k_2) \\ t_3 &= -(k-1)M_0^2 (k_1 k_2 + k_3) \end{aligned} \right\} \quad (\text{A-28})$$

By eliminating the β 's from equations (A-23) and (A-25) and using equation (A-28), there results,

$$\left. \begin{aligned} \alpha_1 &= -M_0^2 k_1 \\ \alpha_2 &= M_0^2 \left\{ [(2-k)M_0^2 - 1] \frac{k_1^2}{2} - k_2 \right\} \\ \alpha_3 &= \left(1 - \frac{k}{2}\right) M_0^4 \left[1 - \left(\frac{3-2k}{3}\right) M_0^2 \right] k_1^3 \\ &\quad + M_0^2 [(2-k)M_0^2 - 1] k_1 k_2 - M_0^2 k_3 \end{aligned} \right\} \quad (\text{A-29})$$

and

$$\left. \begin{aligned}
 \beta_1 &= -k M_0^2 k_1 \\
 \beta_2 &= \frac{k M_0^2}{2} (M_0^2 - 1) k_1^2 - k M_0^2 k_2 \\
 \beta_3 &= \frac{k M_0^4}{2} \left[1 - \left(\frac{2-k}{3} \right) M_0^2 \right] k_1^3 \\
 &\quad + k M_0^2 (M_0^2 - 1) k_1 k_2 - k M_0^2 k_3
 \end{aligned} \right\} \quad (A-30)$$

6. Transformed Boundary-Layer Equations

The continuity equation (A-5) is automatically satisfied by the introduction of the stream function defined in equation (A-12).

With the following substitutions, the momentum equation (A-10) combined with equation (A-9) may be transformed into equation (A-36):

$$w = \frac{w_0}{2} \frac{\rho_0}{\rho} (\zeta^{m-1} \dot{f}_m) \quad (A-17)$$

$$u = \frac{w_0}{2} \frac{\rho_0}{\rho} \frac{a^2}{r \zeta} \left[\zeta^m (m \dot{f}_m - \eta \ddot{f}_m) \right] \quad (A-18)$$

$$\frac{\partial w}{\partial r} = - \left(\frac{w_0}{4} \right) \left(\frac{w_0}{r \zeta} \right)^{1/2} \left(\frac{\rho_0}{\rho} \right) \left(\frac{r}{a} \right) \left(\zeta^{m+n-2} \ddot{\theta}_m \dot{f}_n + \zeta^{i+j-2} \ddot{\theta}_i \dot{f}_j \right) \quad (A-31)$$

$$\frac{\partial w}{\partial \zeta} = \left(\frac{w_0}{4 \zeta} \right) \left(\frac{\rho_0}{\rho} \right) \left\{ \begin{aligned}
 &\zeta^{m+n-2} \ddot{\theta}_m [(n-1) \dot{f}_n - \eta \ddot{f}_n] \\
 &+ \zeta^{i+j-2} \dot{f}_i [(j-1) \ddot{\theta}_j - \eta \dot{\theta}_j] \\
 &- \frac{\zeta^{m+i+j-2} m \beta_m \ddot{\theta}_i \dot{f}_j}{1 + \zeta^n \beta_n}
 \end{aligned} \right\} \quad (A-32)$$

$$\frac{\partial p}{\partial z} = \frac{dp}{dz} = \frac{p_0}{z_0} (\sum^m m \beta_m) \quad (\text{A-33})$$

$$\begin{aligned} \frac{\partial^2 w}{\partial z^2} = & -\left(\frac{w_0}{4a}\right)\left(\frac{w_0}{z_0}\right)^{1/2} \left(\frac{p_0}{p}\right) \left(\sum^{m+n-2} \theta_m f_n'' + \sum^{i+j-2} \theta_i f_j''\right) \\ & + \left(\frac{w_0}{8}\right)\left(\frac{w_0}{z_0}\right)\left(\frac{p_0}{p}\right)(1-4\eta)\left\{ \begin{array}{l} \sum^{m+n-2} \theta_m f_n'' \\ + 2\sum^{i+j-2} \theta_i f_j'' \\ + \sum^{k+l-2} \theta_k f_l'' \end{array} \right\} \quad (\text{A-34}) \end{aligned}$$

$$S \equiv \frac{\delta}{a} \left(\frac{z_0}{w_0}\right)^{1/2} \quad (\text{A-13})$$

$$z_0 \equiv \frac{\mu}{\rho_0} \quad (\text{A-35})$$

$$p = p_0 (1 + \sum^m \beta_m) \quad (\text{A-20})$$

$$M_0^2 \equiv \frac{w_0^2}{kRT_0} \quad (\text{A-27})$$

$$\frac{z^2}{a^2} = 1 - 4\eta S \quad (\text{A-14})$$

$$\begin{aligned}
& -(1 + \xi^n \beta_n) [\xi^{m-1} (m f_m - \eta f_m)] (\xi^{i+j-2} \ddot{\theta}_i f_j + \xi^{k+l-2} \dot{\theta}_k f_l) \\
& + (1 + \xi^n \beta_n) (\xi^{m-1} f_m) \left\{ \begin{array}{l} \xi^{i+j-2} \ddot{\theta}_i [(j-1) f_j - \eta f_j] \\ + \xi^{k+l-2} \dot{\theta}_k [(\ell-1) \theta_\ell - \eta \dot{\theta}_\ell] \end{array} \right\} \\
& - \xi^{m+n+i+j-3} m \beta_m \theta_n f_i f_j \\
& = - \frac{4}{k M_0^2} (\xi^m m \beta_m) (1 + \xi^n \beta_n)^2 \\
& - 4 \xi (1 + \xi^n \beta_n) (\xi^{i+j-2} \ddot{\theta}_i f_j + \xi^{k+l-2} \dot{\theta}_k f_l) \\
& + (1 - 4 \eta \xi) (1 + \xi^n \beta_n) (\xi^{i+j-2} \ddot{\theta}_i f_j + 2 \xi^{k+l-2} \dot{\theta}_k f_l + \xi^{m+g-2} \ddot{\theta}_m f_g) \quad (\text{A-36})
\end{aligned}$$

This equation (A-36) should be valid at any length x or length parameter ξ . Hence, the coefficients of the terms in same powers of the length parameter, after being grouped together on one side of the equation, should be identically equal to zero.

For the terms containing ξ^0 :

$$\ddot{\theta}_i f_i + (2 \dot{\theta}_i + \theta_i f_i) \dot{f}_i + (\ddot{\theta}_i + \dot{\theta}_i f_i) f_i = 0 \quad (\text{A-37})$$

For the terms containing ξ , after simplification and combination with equation (A-37):

$$\begin{aligned}
& \theta_1 \ddot{f}_2 + (2\dot{\theta}_1 + \theta_1 \dot{f}_1) \dot{f}_2 + (\ddot{\theta}_1 + \dot{\theta}_1 \dot{f}_1 - \theta_1 \ddot{f}_1) f_2 \\
& + 2(\theta_1 \ddot{f}_1 + \dot{\theta}_1 \dot{f}_1) f_2 + \dot{f}_1 \ddot{\theta}_2 + (2\dot{f}_1 + f_1 \dot{f}_1) \dot{\theta}_2 \\
& + (\ddot{f}_1 + f_1 \ddot{f}_1 - \dot{f}_1^2) \theta_2 = K_1(\eta)
\end{aligned} \tag{A-38}$$

where

$$K_1(\eta) \equiv 4(1-\eta) f_1 (\theta_1 \ddot{f}_1 + \dot{\theta}_1 \dot{f}_1) - \beta_1 \theta_1 \dot{f}_1^2 - 4k_1 \tag{A-39}$$

For the terms containing ξ^2 , after simplification and combination with equations (A-37) and (A-38):

$$\begin{aligned}
& \theta_1 \ddot{f}_3 + (2\dot{\theta}_1 + \theta_1 \dot{f}_1) \dot{f}_3 + (\ddot{\theta}_1 + \dot{\theta}_1 \dot{f}_1 - 2\theta_1 \ddot{f}_1) f_3 \\
& + 3(\theta_1 \ddot{f}_1 + \dot{\theta}_1 \dot{f}_1) f_3 + \dot{f}_1 \ddot{\theta}_3 + (2\dot{f}_1 + f_1 \dot{f}_1) \dot{\theta}_3 \\
& + (\ddot{f}_1 + f_1 \ddot{f}_1 - 2\dot{f}_1^2) \theta_3 = K_3(\eta)
\end{aligned} \tag{A-40}$$

where

$$\begin{aligned}
K_3(\eta) \equiv & (4\eta \theta_1 - \theta_2) \ddot{f}_2 + (-2\theta_1 \dot{f}_2 - 2\dot{\theta}_2 - \dot{f}_1 \theta_2 + 8\eta \dot{\theta}_1 + 4\theta_1) \dot{f}_2 \\
& + (\theta_1 \ddot{f}_2 - 2\dot{\theta}_1 \dot{f}_2 - \ddot{\theta}_2 - \dot{f}_1 \dot{\theta}_2 + 3\dot{f}_1 \theta_2 - 2\beta_1 \theta_1 \dot{f}_1 + 4\eta \ddot{\theta}_1 + 4\dot{\theta}_1) \dot{f}_2 \\
& + 4\eta \dot{f}_1 \ddot{\theta}_2 + (-2\dot{f}_1 \dot{f}_2 + 8\eta \ddot{f}_1 + 4\dot{f}_1) \dot{\theta}_2 \\
& + (-2\dot{f}_1 \dot{f}_2 + 4\eta \ddot{f}_1 + 4\dot{f}_1 - \beta_1 \dot{f}_1^2) \theta_2 \\
& + (\beta_1^2 - 2\beta_2) \theta_1 \dot{f}_1^2 + \frac{8}{kM_0^2} (\beta_1^2 + \beta_2) + 4k_1/\beta_1
\end{aligned} \tag{A-41}$$

In a similar manner, it can be shown that for the terms containing S^{n-1} ($n \geq 2$) the equation will be of the form,

$$\begin{aligned} \theta_1 \ddot{f}_n + (2\dot{\theta}_1 + \theta_1 \dot{f}_1) \dot{f}_n + [\ddot{\theta}_1 + \dot{\theta}_1 \dot{f}_1 - (n-1)\theta_1 \ddot{f}_1] f_n \\ + n(\theta_1 \ddot{f}_1 + \dot{\theta}_1 \dot{f}_1) f_n + \dot{f}_1 \ddot{\theta}_n + (2\dot{f}_1 + f_1 \dot{f}_1) \dot{\theta}_n \\ + [\ddot{f}_1 + f_1 \dot{f}_1 - (n-1)\dot{f}_1^2] \theta_n = K_{2n-3}(\eta) \end{aligned} \quad (\text{A-42})$$

where $K_{2n-3}(\eta)$ will be a function of η , containing f_1, f_2, \dots, f_{n-1} ; $\theta_1, \theta_2, \dots, \theta_{n-1}$; and their derivatives. Note that when the value of n is set to be equal to 1, equation (A-42) is not reducible to equation (A-37).

With the following substitutions, in addition to equations (A-13), (A-14), (A-17), (A-18), (A-20), (A-27), (A-31), (A-33), and (A-35), the energy equation (A-11) may be transformed into equation (A-47).

$$T = T_0 (S^{m-1} \theta_m) \quad (\text{A-16})$$

$$\frac{\partial T}{\partial \dot{\eta}} = -\left(\frac{w_0}{v_0 \dot{\eta}}\right)^{1/2} \left(\frac{\eta}{2a}\right) T_0 (S^{m-1} \dot{\theta}_m) \quad (\text{A-43})$$

$$\frac{\partial T}{\partial \dot{\eta}} = \frac{T_0}{2\dot{\eta}} \left\{ S^{m-1} [(m-1)\theta_m - \eta \dot{\theta}_m] \right\} \quad (\text{A-44})$$

$$\frac{\partial^2 T}{\partial \dot{\eta}^2} = -\left(\frac{w_0}{v_0 \dot{\eta}}\right)^{1/2} \left(\frac{T_0}{2a}\right) (S^{m-1} \dot{\theta}_m) + \left(\frac{w_0}{v_0 \dot{\eta}}\right) \left(\frac{T_0}{4}\right) (1-4\eta S) (S^{m-1} \ddot{\theta}_m) \quad (\text{A-45})$$

$$\sigma \equiv \frac{c_p \mu}{\lambda} \quad (\text{A-46})$$

$$\begin{aligned}
& -(1 + \zeta^m \beta_m)^2 [\zeta^{i+j-2} \dot{\theta}_i (j f_j - \eta f_j)] \\
& + (1 + \zeta^m \beta_m)^2 \left\{ \zeta^{i+j-2} f_i [(j-1) \theta_j - \eta \dot{\theta}_j] \right\} \\
& - \left(\frac{k-1}{k} \right) (1 + \zeta^m \beta_m) (\zeta^{n+i+j-2} n \beta_n \theta_i f_j) \\
& = - \frac{4}{\sigma} (1 + \zeta^m \beta_m)^2 (\zeta^n \dot{\theta}_n) \\
& + \frac{(1-4\eta\zeta)}{\sigma} (1 + \zeta^m \beta_m)^2 (\zeta^{n-1} \ddot{\theta}_n) \\
& + \left(\frac{k-1}{4} \right) M_0^2 (1-4\eta\zeta) (\zeta^{m+n-2} \theta_m \ddot{f}_n + \zeta^{i+j-2} \dot{\theta}_i \dot{f}_j)^2 \quad (\text{A-47})
\end{aligned}$$

Again, this equation (A-47) should be valid at any length z or length parameter ζ . Hence, the coefficients of the terms in same powers of the length parameter, after being grouped together on one side of the equation, should be identically equal to zero.

For the terms containing ζ^0 :

$$\frac{1}{\sigma} \ddot{\theta}_1 + f_1 \dot{\theta}_1 + \left(\frac{k-1}{4} \right) M_0^2 (\theta_1 \ddot{f}_1 + \dot{\theta}_1 \dot{f}_1)^2 = 0 \quad (\text{A-48})$$

For the terms containing ζ , after simplification and combination with equation (A-48):

$$\begin{aligned}
& \frac{1}{\sigma} \ddot{\theta}_2 + f_1 \dot{\theta}_2 - \dot{f}_1 \theta_2 + 2 \dot{\theta}_1 \dot{f}_2 \\
& + \left(\frac{k-1}{2} \right) M_0^2 (\theta_1 \ddot{f}_1 + \dot{\theta}_1 \dot{f}_1) (f_1 \dot{\theta}_2 + \dot{f}_1 \theta_2 + \theta_1 \ddot{f}_2 + \dot{\theta}_1 \dot{f}_2) \\
& = K_2(\eta) \quad (\text{A-49})
\end{aligned}$$

where

$$K_2(\eta) \equiv -\frac{2\beta_1}{\sigma} \ddot{\theta}_1 + \frac{4}{\sigma} \dot{\theta}_1 - 2(\beta_1 + 2\eta) f_1 \dot{\theta}_1 - \left(\frac{k-1}{k}\right) \beta_1 f_1 \dot{\theta}_1 \quad (\text{A-50})$$

For the terms containing ξ^2 , after simplification and combination with equation (A-49):

$$\begin{aligned} & \frac{1}{\sigma} \ddot{\theta}_3 + f_1 \dot{\theta}_3 - 2f_1 \dot{\theta}_3 + 3\dot{\theta}_3 f_3 \\ & + \left(\frac{k-1}{2}\right) M_0^2 (\theta_1 \ddot{f}_1 + \dot{\theta}_1 \dot{f}_1) (f_1 \dot{\theta}_3 + f_1 \dot{\theta}_3 + \theta_1 \ddot{f}_3 + \dot{\theta}_1 \dot{f}_3) = K_4(\eta) \quad (\text{A-51}) \end{aligned}$$

where

$$\begin{aligned} K_4(\eta) \equiv & [\theta_2 - \left(\frac{k-1}{k}\right) \beta_1 \theta_1] f_2 \ddot{\theta}_2 - 2[\dot{\theta}_2 + 2(\beta_1 + 2\eta) \dot{\theta}_1] f_2 \dot{\theta}_2 \\ & - \frac{2\beta_1}{\sigma} \ddot{\theta}_2 + \left[\frac{4}{\sigma} - 2(\beta_1 + 2\eta) f_1\right] \dot{\theta}_2 \\ & + \left[\left(\frac{k+1}{k}\right) \beta_1 + 4\eta\right] f_1 \dot{\theta}_2 - \left(\frac{\beta_1^2 + 2\beta_2}{\sigma}\right) \ddot{\theta}_1 \\ & + \frac{8(\beta_1 + 2\eta)}{\sigma} \dot{\theta}_1 - [(\beta_1^2 + 2\beta_2) + 8\eta(\beta_1 + 2\eta)] f_1 \dot{\theta}_1 \\ & - \left(\frac{k-1}{k}\right) [(\beta_1^2 + 2\beta_2) + 4\eta\beta_1] f_1 \dot{\theta}_1 \\ & - \left(\frac{k-1}{4}\right) M_0^2 \left\{ \begin{aligned} & (\theta_1 \ddot{f}_2 + \dot{\theta}_1 \dot{f}_2 + f_1 \ddot{\theta}_2 + \dot{f}_1 \dot{\theta}_2)^2 \\ & + 2(\theta_1 \ddot{f}_1 + \dot{\theta}_1 \dot{f}_1) (\theta_2 \ddot{f}_2 + \dot{\theta}_2 \dot{f}_2) \end{aligned} \right\} \quad (\text{A-52}) \end{aligned}$$

It can be shown that for the terms containing ξ^{n-1} ($n \geq 2$), the equation will be of the form,

$$\begin{aligned} & \frac{1}{\sigma} \ddot{\theta}_n + f_1 \dot{\theta}_n - (n-1) f_1 \theta_n + n \dot{\theta}_1 f_n \\ & + \left(\frac{k-1}{2}\right) M_0^2 (\theta_1 \ddot{f}_1 + \dot{\theta}_1 \dot{f}_1) (f_1 \dot{\theta}_n + f_1 \theta_n + \theta_1 \ddot{f}_n + \dot{\theta}_1 \dot{f}_n) \\ & = K_{2n-2}(\eta) \end{aligned} \quad (\text{A-53})$$

where $K_{2n-2}(\eta)$ will be a function of η , containing f_1, f_2, \dots, f_{n-1} ; $\theta_1, \theta_2, \dots, \theta_{n-1}$; and their derivatives. Note that when the value of n is set to be equal to 1, equation (A-53) is not reducible to equation (A-49).

7. Boundary Conditions

With equations (A-17), (A-19), and (A-22), provided that an isentropic core exists, one obtains,

$$\begin{aligned} w_c &= \frac{w_0}{2} \frac{\rho_0}{\rho_c} \left(\xi^{m-1} f_m \right)_c = \frac{w_0}{2} \frac{(\xi^{m-1} f_m)_c}{(1 + \xi^n \alpha_n)} \\ &= w_0 (1 + \xi^i k_i) \end{aligned}$$

Or,

$$\left(\xi^{m-1} f_m \right)_c = 2(1 + \xi^n \alpha_n)(1 + \xi^i k_i) \quad (\text{A-54})$$

With equation (A-29),

$$\begin{aligned}
 (f_1)_c &= z \\
 (f_2)_c &= z(k_1 + \alpha_1) = z(1 - M_0^2)k_1 \\
 (f_3)_c &= z(k_2 + k_1\alpha_1 + \alpha_2) \\
 &= z k_2(1 - M_0^2) - k_1^2 M_0^2 [3 - (2 - k)M_0^2]
 \end{aligned}
 \quad \left. \vphantom{\begin{aligned} (f_1)_c \\ (f_2)_c \\ (f_3)_c \end{aligned}} \right\} \text{(A-55)}$$

etc.

Or, in general,

$$\begin{aligned}
 (f_{n+1})_c &= z \sum_{i=0}^n k_i \alpha_{n-i} \\
 \text{with} \\
 k_0 = \alpha_0 &= 1, \quad n = 0, 1, 2, \dots
 \end{aligned}
 \quad \left. \vphantom{\begin{aligned} (f_{n+1})_c \\ \text{with} \\ k_0 = \alpha_0 \end{aligned}} \right\} \text{(A-56)}$$

With equations (A-16) and (A-21), provided that an isentropic core exists, one obtains,

$$T_c = T_0 (S^{m-1} \theta_m)_c = T_0 (1 + S^n t_n)$$

Or,

$$(S^{m-1} \theta_m)_c = 1 + S^n t_n \quad \text{(A-57)}$$

With equation (A-28),

$$\left. \begin{aligned} (\theta_1)_c &= 1 \\ (\theta_2)_c &= t_1 = -(k-1)M_0^2 k, \\ (\theta_3)_c &= t_2 = -(k-1)M_0^2 \left(k_2 + \frac{k_2^2}{2}\right) \end{aligned} \right\} \quad (\text{A-58})$$

etc.

Or, in general,

$$\left. \begin{aligned} (\theta_{n+1})_c &= t_n \\ \text{with} \\ t_0 &= 1 \end{aligned} \right\} \quad (\text{A-59})$$

The above boundary conditions are satisfied at the outer edge of the boundary layer, provided that an isentropic core exists. As a limit, they are satisfied as the radius r approaches zero, or as the value of η approaches $\frac{1}{45}$.

At the wall of the circular tube, $r = a$, or $\eta = 0$ for finite length z :

$$u = 0, \text{ or with equation (A-18), } f_n(0) = 0 \quad (\text{A-60})$$

$$w = 0, \text{ or with equation (A-17), } \dot{f}_n(0) = 0 \quad (\text{A-61})$$

For an adiabatic wall,

$$\frac{\partial T}{\partial n} = 0, \text{ or with equation (A-43), } \dot{\theta}_n(0) = 0 \quad (\text{A-62})$$

For a wall maintained at any arbitrary temperature distribution,

$$\frac{T_w}{T_0} = (S^{m-1} \theta_m)_w \equiv \theta_w \quad (\text{A-63})$$

where

$\theta_w \equiv$ the function of the length parameter ξ , representing the given arbitrary temperature distribution at the wall.

Equations (A-56), (A-59), (A-60), (A-61), combined with either (A-62) or (A-63) give the required boundary conditions for solving the differential equations (A-37), (A-42), (A-48), and (A-53).

8. Evaluation of Constants k_m

$$\begin{aligned} \text{Mass Rate of Flow} &= 2\pi \int_0^a \rho w r dr = 2\pi \int_0^a \frac{\partial \Psi}{\partial r} dr \\ \text{at Any Length } z &= 2\pi (\Psi_{r=a} - \Psi_{r=0}) \\ &= \rho_0 w_0 \pi a^2 = \text{constant} \end{aligned} \quad (\text{A-64})$$

where $\Psi_{r=a}$ and $\Psi_{r=0}$ are evaluated at their respective radii at a certain length z or length parameter ξ .

From equations (A-15) and (A-60),

$$\Psi_{r=a} = 0 \quad (\text{A-65})$$

Also, from equation (A-15),

$$\Psi_{r=0} = -a^2 \rho_0 w_0 (S^m f_m)_{r=0} \quad (\text{A-66})$$

Substitution into equation (A-64) gives

$$(S^m f_m)_{r=0} = \frac{1}{2} \quad (\text{A-67})$$

Integration of equations (A-55) and (A-56) gives

$$\left. \begin{aligned} (f_1)_c &= z\eta + C_1 \\ (f_2)_c &= z(k_1 + \alpha_1)\eta + C_2 \\ (f_3)_c &= z(k_2 + k_1\alpha_1 + \alpha_2)\eta + C_3 \end{aligned} \right\} \quad (\text{A-68})$$

etc.

Or, in general,

$$(f_m)_c = z \left(\sum_{i=0}^{m-1} k_i \alpha_{m-1-i} \right) \eta + C_m \quad (\text{A-69})$$

where C_1, C_2, \dots are the respective integration constants.

At $r = 0$, or $\eta = \frac{1}{4g}$, one obtains,

$$(f_m)_{r=0} = \frac{1}{2r} \left(\sum_{i=0}^{m-1} k_i \alpha_{m-1-i} \right) + C_m \quad (\text{A-70})$$

Substituting equation (A-70) into equation (A-67) and equating the coefficients of the terms in same powers of the length parameter, one obtains,

$$\left. \begin{aligned} \sum_{i=0}^m k_i \alpha_{m-i} + z C_m &= 0 \\ \text{with} \end{aligned} \right\} \quad (\text{A-71})$$

$$k_0 = \alpha_0 = 1, \quad m = 1, 2, \dots$$

In particular,

$$\left. \begin{aligned} C_1 &= -\frac{1}{2}(k_1 + \alpha_1) = \frac{k_1}{2}(M_0^2 - 1) \\ C_2 &= -\frac{1}{2}(k_2 + k_1\alpha_1 + \alpha_2) \\ &= \frac{k_2}{2}(M_0^2 - 1) + \frac{k_1^2 M_0^2}{4} [3 - (2 - k_1)M_0^2] \end{aligned} \right\} \text{(A-72)}$$

etc.

Or,

$$\left. \begin{aligned} k_1 &= \frac{2C_1}{M_0^2 - 1} \\ k_2 &= \frac{2C_2}{M_0^2 - 1} - \frac{2M_0^2 [3 - (2 - k_1)M_0^2]}{(M_0^2 - 1)^3} C_1^2 \end{aligned} \right\} \text{(A-73)}$$

etc.

9. Summary of Important Relationships

Combining equations (A-17), (A-4), (A-16), (A-21), (A-22), and (A-19), one obtains,

$$\frac{w}{w_c} = \frac{s^{m+n-2} \theta_m f_n}{2(1 + s^k \alpha_k)(1 + s^i t_i)(1 + s^j k_j)} \quad \text{(A-74)}$$

Combining equations (A-16) and (21), one obtains,

$$\frac{T}{T_c} = \frac{s^{m-1} \theta_m}{1 + s^n t_n} \quad \text{(A-75)}$$

The shearing stress at the tube wall is found as

$$\tau_w = -\mu \left(\frac{\partial w}{\partial r} \right)_{r=a} \quad \text{(A-76)}$$

With equation (A-31) and defining the local true friction coefficient f_z as

$$f_z \equiv \frac{\tau_w}{\frac{1}{2} \rho_c w_c^2} \quad (\text{A-77})$$

one obtains,

$$f_z = \frac{1}{2} \left(\frac{p_0}{p} \right) \left(\frac{\rho_0}{\rho_c} \right) \left(\frac{w_0}{w_c} \right)^2 \left(\frac{y_0}{w_{0j}} \right)^{1/2} \left(\int_0^{\eta} e^{m+n-2} \theta_m f_n'' + \int_0^{i+j-2} \theta_i f_j' \right)_{\eta=0} \quad (\text{A-78})$$

Or,

$$f_z \left(\frac{w_{0j}}{y_0} \right)^{1/2} = \frac{1}{2} \left(\frac{p_0}{p} \right) \left(\frac{\rho_0}{\rho_c} \right) \left(\frac{w_0}{w_c} \right)^2 \left(\int_0^{\eta} e^{m+n-2} \theta_m f_n'' + \int_0^{i+j-2} \theta_i f_j' \right)_{\eta=0} \quad (\text{A-79})$$

A mean apparent friction coefficient \bar{f}_a convenient for design purposes may be defined as

$$4 \bar{f}_a \left(\frac{z}{D} \right) \equiv \frac{\Delta p}{\frac{1}{2} \rho_0 w_0^2} \quad (\text{A-80})$$

where

$$\Delta p \equiv p_0 - p, \text{ for incompressible and subsonic flows,}$$

and

$$\Delta p \equiv p - p_0, \text{ for supersonic flows.}$$

For incompressible flow, using equation (25) of Atkinson and Goldstein (10) and Bernoulli's relationship,

$$4 \bar{f}_a \left(\frac{z}{D} \right) = (1 + \int_0^z k_n)^2 - 1 \quad (\text{A-81})$$

For compressible flow, with equations (A-20), (A-4), and (A-27),

$$4\bar{f}_a\left(\frac{\dot{f}}{D}\right) = \frac{2}{kM_0^2} (\delta^n \beta_n) \quad (\text{A-82})$$

Assuming a constant value of the absolute viscosity and using the respective definitions of the two length Reynolds numbers,

$$\left. \begin{aligned} \text{and} \\ Re_{j_0} &\equiv \frac{w_0 \dot{f}}{\nu_0} \\ Re_{j_c} &\equiv \frac{w_c \dot{f}}{\nu_c} \end{aligned} \right\} \quad (\text{A-83})$$

one obtains,

$$\frac{Re_{j_0}}{Re_{j_c}} = \left(\frac{\rho_0}{\rho_c}\right) \left(\frac{w_0}{w_c}\right) \quad (\text{A-84})$$

The local recovery factor \bar{r} is defined through the following equation:

$$\bar{r} \equiv \frac{T_{aw} - T_c}{T_s - T_c} = \left(\frac{T_{aw}}{T_0} - \frac{T_c}{T_0}\right) / \left(\frac{T_s}{T_0} - \frac{T_c}{T_0}\right) \quad (\text{A-85})$$

With equations (A-16), (A-21), and the well-known adiabatic relationship

$$\frac{T_s}{T_0} = 1 + \left(\frac{k-1}{2}\right) M_0^2 \quad (\text{A-86})$$

one obtains,

$$\bar{r} \equiv \frac{\delta^{m-1} \theta_m(0) - (1 + \delta^n t_n)}{\left(1 + \frac{k-1}{2} M_0^2\right) - (1 + \delta^n t_n)} \quad (\text{A-87})$$

The local heat-transfer coefficient h_z based on the difference of actual wall temperature and the adiabatic-wall temperature is obtained through the thermal boundary condition at the tube wall,

$$q = \lambda \left(\frac{\partial T}{\partial r} \right)_{r=a} = h_z (T_w - T_{aw}) \quad (\text{A-88})$$

The adiabatic-wall temperature is obtained as the function of the length parameter for the adiabatic case of identical entrance Mach number.

With equations (A-43), (A-16), and defining

$$\left. \begin{aligned} G_o &\equiv \rho_o w_o \\ G_c &\equiv \rho_c w_c \end{aligned} \right\} \quad (\text{A-89})$$

one obtains,

$$\frac{h_z}{c_p G_o} = - \frac{1}{2\sigma} \left(\frac{\gamma_o'}{w_o z} \right)^{1/2} \frac{(S^{m-1} \dot{\theta}_m)_w}{(S^{n-1} \theta_n)_w - (S^{i-1} \theta_i)_{aw}} \quad (\text{A-90})$$

or,

$$\frac{h_z}{c_p G_c} = - \frac{1}{2\sigma} \left(\frac{G_o}{G_c} \right)^{1/2} \left(\frac{\gamma_c}{w_c z} \right)^{1/2} \frac{(S^{m-1} \dot{\theta}_m)_w}{(S^{n-1} \theta_n)_w - (S^{i-1} \theta_i)_{aw}} \quad (\text{A-91})$$

Since

$$\frac{h_z D}{\lambda} = \left(\frac{h_z}{c_p G_o} \right) \left(\frac{G_o D}{\mu} \right) \left(\frac{c_p \mu}{\lambda} \right) \quad (\text{A-92})$$

one obtains,

$$\frac{h_z D}{\lambda} = - \frac{(S^{m-2} \dot{\theta}_m)_w}{(S^{n-1} \theta_n)_w - (S^{i-1} \theta_i)_{aw}} \quad (\text{A-93})$$

With equations (A-43) and (A-88), one obtains,

$$q a / \lambda T_o = - \frac{1}{2} (S^{m-2} \dot{\theta}_m)_w \quad (\text{A-94})$$

APPENDIX B

METHOD OF SOLVING THE DIFFERENTIAL EQUATIONS
WITH THE AID OF THE M.I.T. DIFFERENTIAL ANALYZER

The transformed boundary-layer equations derived in Appendix A (A-37, A-42, A-48, and A-53) were solved with the aid of the M.I.T. Differential Analyzer. Since there are available only eighteen integrators in this differential analyzer, the following transformations were made, so that the machine may be used to solve these simultaneous differential equations:

$$F_1 \equiv \theta_1 \dot{f}_1 \quad (B-1)$$

and

$$F_n \equiv \theta_1 \dot{f}_n + \dot{f}_1 \theta_n, \text{ with } n \geq 2 \quad (B-2)$$

Equations (A-37) and (A-48) are thus transformed into

$$\ddot{F}_1 + \dot{f}_1 F_1 = 0 \quad (B-3)$$

and

$$\frac{1}{\sigma} \ddot{\theta}_1 + \dot{f}_1 \dot{\theta}_1 + \frac{k-1}{4} M_0^2 \dot{F}_1^2 = 0 \quad (B-4)$$

Equations (A-42) and (A-53) are transformed into, with $n \geq 2$,

$$\ddot{F}_n + \dot{f}_1 \dot{F}_n - (n-1) \dot{f}_1 F_n + n \dot{f}_n F_1 = K_{2n-3}(\eta) \quad (B-5)$$

and

$$\begin{aligned} \frac{1}{\sigma} \ddot{\theta}_n + \dot{f}_1 \dot{\theta}_n - (n-1) \dot{f}_1 \theta_n + n \dot{f}_n \dot{\theta}_1 \\ + \frac{k-1}{2} M_0^2 \dot{F}_1 \dot{F}_n = K_{2n-2}(\eta) \end{aligned} \quad (B-6)$$

It is observed that the first set of the differential equations (B-3 and B-4) are non-linear, while the general differential equations with $n \geq 2$ (B-5 and B-6) are linear.

It is also observed from equations (A-56), (A-59), (A-60), (A-61), (A-62), and (A-63) that the boundary conditions of the differential equations are known at two boundaries; viz., at the tube wall and at the outer edge of the boundary layer.

Since the equations (B-3) and (B-4) are non-linear, it was necessary to guess $\dot{F}_1(0)$ and $\theta_1(0)$ or $\dot{\theta}_1(0)$, and to run the differential analyzer to some large value of η . If the final values of F_1 and θ_1 approach asymptotically 2 and 1 respectively, the original choices of $\dot{F}_1(0)$ and $\theta_1(0)$ or $\dot{\theta}_1(0)$ were satisfactory.

Since the equations (B-5) and (B-6) are linear, it is not necessary to use this trial-and-error method. Linear combinations of the solutions to the general differential equations and the corresponding homogeneous differential equations may be adjusted to satisfy all the boundary conditions. For example, for case A ($M_0 = 2.8$, adiabatic wall) and $n = 2$, the required boundary conditions are:

$$\text{At } \eta = 0, \quad f_2 = \dot{f}_2 = \dot{\theta}_2 = 0 \quad (\text{B-7})$$

$$\left. \begin{aligned} \text{As } \eta \rightarrow \text{large,} \quad \dot{f}_2 &\rightarrow 2(1-M_0^2)k_1 \\ \theta_2 &\rightarrow -(k-1)M_0^2 k_1 \end{aligned} \right\} \quad (\text{B-8})$$

With the transformation equation (B-2), the required boundary

conditions become,

$$\text{At } \eta = 0, \quad f_2 = F_2 = \dot{\theta}_2 = 0 \quad (\text{B-9})$$

$$\text{As } \eta \rightarrow \text{large}, \quad \left. \begin{aligned} F_2 &\rightarrow 2(1-kM_0^2)k_1 \\ \theta_2 &\rightarrow -(k-1)M_0^2 k_1 \end{aligned} \right\} (\text{B-10})$$

Let the general differential equations be denoted by

$$L_1(\eta) = K_1(\eta)$$

$$L_2(\eta) = K_2(\eta)$$

and the corresponding homogeneous differential equations be denoted by

$$L_1(\eta) = 0$$

$$L_2(\eta) = 0.$$

The required solutions F_2 and θ_2 may be represented by the following linear combinations:

$$\left. \begin{aligned} F_2 &= F_{2a} + bF_{2b} + cF_{2c} \\ \theta_2 &= \theta_{2a} + b\theta_{2b} + c\theta_{2c} \end{aligned} \right\} (\text{B-11})$$

where F_{2a} , θ_{2a} ; F_{2b} , θ_{2b} ; and F_{2c} , θ_{2c} are respectively the solutions to the differential equations, which are listed in Table B-1 in the columns headed by the same letters as those of the subscripts. The corresponding initial conditions are also shown.

TABLE B-1

Differential Equations	(2a) $L_1(\gamma) = K_1$ $L_2(\gamma) = K_2$	(2b) $L_1(\gamma) = 0$ $L_2(\gamma) = 0$	(2c) $L_1(\gamma) = 0$ $L_2(\gamma) = 0$
$f_2(0)$	0	0	0
$F_2(0)$	0	0	0
$\dot{F}_2(0)$	0	1	$\ddot{f}_1(0)$
$\theta_2(0)$	0	0	1
$\dot{\theta}_2(0)$	0	0	0

According to equation (B-10), the constant coefficients b and c in equation (B-11) are obtained by solving the following simultaneous algebraic expressions:

As $\gamma \rightarrow$ large,

$$\left. \begin{aligned} F_{2a} + bF_{2b} + cF_{2c} &\longrightarrow 2(1-kM_0^2)k_1 \\ \theta_{2a} + b\theta_{2b} + c\theta_{2c} &\longrightarrow -(k-1)M_0^2 k_1 \end{aligned} \right\} \quad (B-12)$$

With b and c thus determined, the required solutions in terms of F_2 and θ_2 are obtained through equation (B-11). In particular, the required initial conditions are

$$\left. \begin{aligned}
 f_2(0) &= F_2(0) = \dot{\theta}_2(0) = 0 \\
 \dot{F}_2(0) &= b + cf_1''(0) \\
 \theta_2(0) &= c
 \end{aligned} \right\} \quad (B-13)$$

With either heating or cooling at the tube wall, $\theta_2(0)$ is given according to equation (A-63), but $\dot{\theta}_2(0)$ needs to be determined. A similar method may be followed to find the required solution, by using the linear combinations

$$\left. \begin{aligned}
 F_2 &= F_{2a} + bF_{2b} + cF_{2c} + dF_{2d} \\
 \theta_2 &= \theta_{2a} + b\theta_{2b} + c\theta_{2c} + d\theta_{2d}
 \end{aligned} \right\} \quad (B-14)$$

where F_{2a} , θ_{2a} ; F_{2b} , θ_{2b} ; F_{2c} , θ_{2c} ; and F_{2d} , θ_{2d} are respectively the solutions to the differential equations, which are listed in Table B-2 in the columns headed by the same letters as those of the subscripts. The corresponding initial conditions are also shown.

TABLE B-2

	(2a)	(2b)	(2c)	(2d)
Differential Equations	$L_1(\eta) = K_1$ $L_2(\eta) = K_2$	$L_1(\eta) = 0$ $L_2(\eta) = 0$	$L_1(\eta) = 0$ $L_2(\eta) = 0$	$L_1(\eta) = 0$ $L_2(\eta) = 0$
$f_2(0)$	0	0	0	0
$F_2(0)$	0	0	0	0
$\dot{F}_2(0)$	0	1	$f_1''(0)$	0
$\theta_2(0)$	0	0	1	0
$\dot{\theta}_2(0)$	0	0	0	1

The constant coefficient c is determined from the given value of $\theta_2(0)$, while b and d are determined by solving the following simultaneous algebraic expressions:

As $\gamma \rightarrow$ large,

$$\left. \begin{aligned} F_{2a} + bF_{2b} + cF_{2c} + dF_{2d} &\rightarrow 2(1-kM_0^2)k_1 \\ \theta_{2a} + b\theta_{2b} + c\theta_{2c} + d\theta_{2d} &\rightarrow -(k-1)M_0^2 k_1 \end{aligned} \right\} \quad (B-15)$$

With b , c , and d thus determined, the required solution is obtained through equation (B-14). In particular, the required initial conditions are

$$\left. \begin{aligned} f_2(0) = F_2(0) &= 0 \\ \theta_2(0) &= c \\ \dot{F}_2(0) &= b + c\ddot{f}_1(0) \\ \dot{\theta}_2(0) &= d \end{aligned} \right\} \quad (B-16)$$

APPENDIX C

TABULATION OF RESULTS

TABLE C-1

Limiting Values of η for Calculation
of Boundary Layer Thicknesses

<u>Case</u>	<u>Entrance Mach Number</u>	<u>Thermal Condition at Wall</u>	<u>η_x</u>	<u>η_r</u>
A	2.8	Adiabatic	3.9	4.4
B	2.8	Cooling, $\theta_w = 2$	3.7	4.2
C	2.8	Heating, $\theta_w = 3$	4.3	4.7
D	2	Adiabatic	3.7	4.1
E	2	Cooling, $\theta_w = 1.445$	3.5	4.0
F	2	Heating, $\theta_w = 2.167$	3.9	4.2
G	Incompressible	Adiabatic	3.3	

TABLE 0-2

Values of F_n and θ_n

(1) Case A, $M_0 = 2.8$, Adiabatic

<u>η</u>	<u>F_1</u>	<u>θ_1</u>	<u>F_2</u>	<u>θ_2</u>	<u>F_3</u>	<u>θ_3</u>
0	0	2.330	0	0.85	0	1.8
0.5	0.484	2.262	4.99	0.97	5.8	4.7
1.0	0.953	2.065	11.31	0.52	40.3	7.6
1.5	1.371	1.775	17.64	-1.03	96.1	4.5
2.0	1.691	1.465	21.75	-2.50	144.3	6.8
2.5	1.886	1.220	22.82	-2.18	130.2	28.1
3.0	1.971	1.079	21.99	-0.23	67.8	46.3
3.5	1.996	1.022	21.20	1.72	37.0	39.5
4.0	2.001	1.005	21.01	2.77	30.8	20.2
4.5	2.001	1.002	20.95	3.09	29.6	7.4
5.0	2.001	1.002	20.95	3.17	29.7	3.1

TABLE C-2, Continued

Values of F_n and θ_n (ii) Case C, $M_0 = 2.8$, Heating, $\theta_w = 3$

η	F_1	θ_1	F_2	θ_2	F_3	θ_3
0	0	3	0	0	0	0
0.5	0.451	2.803	4.84	0.01	-2.3	7.1
1.0	0.891	2.495	11.35	-0.60	36.4	14.0
1.5	1.293	2.107	18.16	-2.44	109.1	12.1
2.0	1.620	1.703	23.42	-4.47	190.7	11.2
2.5	1.840	1.364	25.61	-4.67	214.5	33.5
3.0	1.953	1.147	25.15	-2.37	134.7	67.9
3.5	1.992	1.046	24.02	0.65	52.9	70.2
4.0	2.002	1.011	23.42	2.63	30.6	40.7
4.5	2.003	1.003	23.27	3.42	29.1	14.5
5.0	2.003	1.002	23.28	3.61	30.4	2.6

TABLE C-3

Values of β_n , t_n , α_n , and k_n

<u>Case</u>	<u>β_1</u>	<u>β_2</u>	<u>β_3</u>	<u>t_1</u>	<u>t_2</u>	<u>t_3</u>
A	11.29	50.1	248	3.225	1.33	39.2
B*	10.53			3.008		
C	12.78	60.2	330	3.650	0.559	58.8
D	10.27	57.9		2.934	5.77	
E*	9.434			2.696		
F*	11.70			3.344		
<u>Case</u>	<u>α_1</u>	<u>α_2</u>	<u>α_3</u>	<u>k_1</u>	<u>k_2</u>	<u>k_3</u>
A	8.063	22.8	125	-1.028	-0.951	-13.5
B*	7.519			-0.9591		
C	9.126	26.4	170	-1.164	-0.855	-19.7
D	7.335	30.6		-1.834	-5.29	
E*	6.739			-1.685		
F*	8.360			-2.090		
G				3.434	-9.16	

* Computations for $n = 2$ are still in progress.

TABLE C-4

Values of $\dot{F}_n(0)$, $\ddot{f}_n(0)$, $\theta_n(0)$, and $\dot{\theta}_n(0)$

<u>Case</u>	<u>$\dot{F}_1(0)$</u>	<u>$\dot{F}_2(0)$</u>	<u>$\dot{F}_3(0)$</u>	<u>$\ddot{f}_1(0)$</u>	<u>$\ddot{f}_2(0)$</u>	<u>$\ddot{f}_3(0)$</u>
A	0.971	7.7	-17	0.417	3.1	-7.5
B*	1.013			0.507		
C	0.903	7.6	-35	0.301	2.5	-12
D	1.099	4.1		0.653	2.2	
E*	1.147			0.794		
F*	1.024			0.473		
G	1.328			1.328		

<u>Case</u>	<u>$\theta_1(0)$</u>	<u>$\theta_2(0)$</u>	<u>$\theta_3(0)$</u>	<u>$\dot{\theta}_1(0)$</u>	<u>$\dot{\theta}_2(0)$</u>	<u>$\dot{\theta}_3(0)$</u>
A	2.330	0.85	1.8	0	0	0
B*	2			0.154		
C	3	0	0	-0.277	-0.059	6.3
D	1.683	0.66		0	0	
E*	1.445			0.124		
F*	2.167			-0.227		

* Computations for $n = 2$ are still in progress.

APPENDIX D

RECOMMENDATIONS FOR FUTURE WORK

Along with the "exact" analysis presented in this thesis, some preliminary work was done, based on the Karman-Pohlhausen integral method, in which a linear velocity distribution was assumed to exist inside the laminar boundary layer of a steady, compressible flow in the entrance region of a tube. The predicted distribution of the static pressure along the length of the tube obtained with this approximate method was found to agree fairly well with that obtained in the more exact analysis presented here. It appears very encouraging to extend this approximate method by employing a parabolic velocity distribution inside the laminar boundary layer.

The present analysis should be extended to cover the region where the laminar boundary layer already fills the entire cross-section of the tube. The transitional and turbulent regimes of the tube flow should also deserve thorough investigations.

Using the theoretical results obtained in this thesis, the problem of stability of the laminar boundary layer of a steady, compressible flow in the entrance region of a tube may be analyzed in detail.

With the present analysis, the effect of variable surface temperature may be investigated. It has been shown in Appendix B that the value of the constant coefficient c in equation (B-14) may be

assigned arbitrarily according to a given distribution of the surface temperature at the tube wall, the values of the constant coefficients b and d may be calculated through the algebraic expression (B-15), and a new set of values may then be obtained for the functions $F_n(\eta)$ and $\theta_n(\eta)$.

One of the assumptions made in the present analysis is that the value of the absolute viscosity of the compressible fluid is taken as a constant. However, the effect of the change in absolute viscosity with temperature should be carefully studied. The method presented here may easily be extended to cover the case where the absolute viscosity is represented by a power series of the absolute temperature with integral exponents.

In order to obtain a better understanding of the tube problem presented here, it is worthwhile to measure experimentally with a tiny probe the velocity and temperature profiles inside the boundary layer, the radial distribution of static pressure across any section of the tube, the effects of the interactions between shock and transition on the radial distribution of the static pressure, etc., etc.

APPENDIX E

BIBLIOGRAPHY

1. "Report of Progress on Measurements of Friction Coefficients, Recovery Factors, and Heat Transfer Coefficients for Supersonic Flow of Air in a Pipe," by J. Kaye, J. H. Keenan, and W. H. McAdams, Heat Transfer and Fluid Mechanics Institute, June, 1949, pp. 147-164.
 2. "Measurement of Recovery Factors and Friction Coefficients for Supersonic Flow of Air in a Tube," by J. Kaye, J. H. Keenan, and R. H. Shoulberg, presented in the General Discussion on Heat Transmission, London, England, September, 1951.
 3. "Measurement of Recovery Factors and Friction Coefficients for Supersonic Flow of Air in a Tube," by J. Kaye, J. H. Keenan, K. K. Klingensmith, G. M. Ketchum, and T. Y. Toong, presented at the Annual Meeting of the ASME, Atlantic City, N. J., November 25-30, 1951.
 4. "Measurement of Recovery Factors and Friction Coefficients for Supersonic Flow of Air in a Tube," by J. Kaye, T. Y. Toong and R. H. Shoulberg, presented at the Annual Meeting of the ASME, Atlantic City, N. J., November 25-30, 1951.
 5. "Über die Bestimmung der Zähigkeit einer Flüssigkeit durch den Ausfluß aus Röhren," by E. Hagenbach, Poggendorff's Annalen der Physik und Chemie (4), vol. 109, 1860, pp. 385-426.
 6. "Einleitung in die theoretische Physik," by F. E. Neumann, Leipzig, 1883, p. 262.
 7. "Études sur le frottement des liquides," by M. Couette, Annales de Chimie et de Physique (6), vol. 21, 1890, pp. 494-510.
 8. "Sur la manière dont les vitesses, dans un tube cylindrique de section circulaire, évasé à son entrée, se distribuent depuis cette entrée jusqu'aux endroits où se trouve établi un régime uniforme," by J. Boussinesq, Comptes Rendus, vol. 113, 1891, pp. 9-15.
- "Calcul de la moindre longueur que doit avoir un tube circulaire, évasé à son entrée, pour qu'un régime sensiblement uniforme s'y établisse, et de la dépense de charge qu'y entraîne l'établissement de ce régime," by J. Boussinesq, Comptes Rendus, vol. 113, 1891, pp. 49-51.

9. "Untersuchungen über laminare und turbulente Strömung," by L. Schiller, Forschungsarbeiten, V. D. I., vol. 248, 1922, pp. 17-36.

"Die Entwicklung der laminaren Geschwindigkeitsverteilung und ihre Bedeutung für Zähigkeitsmessungen," by L. Schiller, Zeitschrift für angewandte Mathematik und Mechanik, vol. 2, 1922, pp. 96-106.
10. "Modern Developments in Fluid Dynamics," edited by S. Goldstein, Oxford University Press, London, England, 1938, vol. 1, Atkinson-Goldstein, pp. 304-306.
11. "Steady Flow in the Transition Length of a Straight Tube," by H. L. Langhaar, Journal of Applied Mechanics, Trans. ASME, vol. 64, 1942, pp. A-55 - A-58.
12. "Concerning the Effect of Compressibility on Laminar Boundary Layers and Their Separation," by L. Howarth, Proceedings of the Royal Society of London, series A, vol. 194, 1948, p. 25.
13. "Experimental Investigation of Heat Transfer Coefficients for Air Flowing in a Tube at Supersonic Velocities," by R. H. Shoulberg, W. J. Larkin, and W. L. England, S.M. Thesis, Mechanical Engineering Department, Massachusetts Institute of Technology, 1949.
14. "Temperature Effects in a Laminar Compressible-Fluid Boundary Layer Along a Flat Plate," by H. W. Emmons and J. G. Brainerd, Journal of Applied Mechanics, Trans. ASME, vol. 63, 1941, pp. A-105 - A-110.
15. "Grenzschichten in Flüssigkeiten mit kleiner Reibung," by H. Blasius, Zeitschrift für Mathematik und Physik, vol. 56, 1908, pp. 1-37.
16. "Der Wärmeaustausch zwischen festen Körpern und Flüssigkeiten mit kleiner Reibung und kleiner Wärmeleitung," by E. Pohlhausen, Zeitschrift für angewandte Mathematik und Mechanik, vol. 1, 1921, pp. 115-121.
17. "Temperature and Velocity Profiles in the Compressible Laminar Boundary Layer with Arbitrary Distribution of Surface Temperature," by D. R. Chapman and M. W. Rubesin, Journal of the Aeronautical Sciences, vol. 16, 1949, pp. 547-565.
18. "Gas Tables," by J. H. Keenan and J. Kaye, John Wiley & Sons, New York, N. Y., 1948.

APPENDIX F

BIOGRAPHICAL NOTE

The author, Tau-Yi Toong, was born in Shanghai, China on August 15, 1918.

He attended the Chinese Primary School in Kobe, Japan, and the Nanyang Model Middle School in Shanghai, China. From 1936 to 1940, he studied in the National Chiao-Tung University in China. He received the degree of Bachelor of Science in Mechanical Engineering in June 1940 with great distinction, and was elected the honorary membership of Phi Tau Phi Society for Higher Learning.

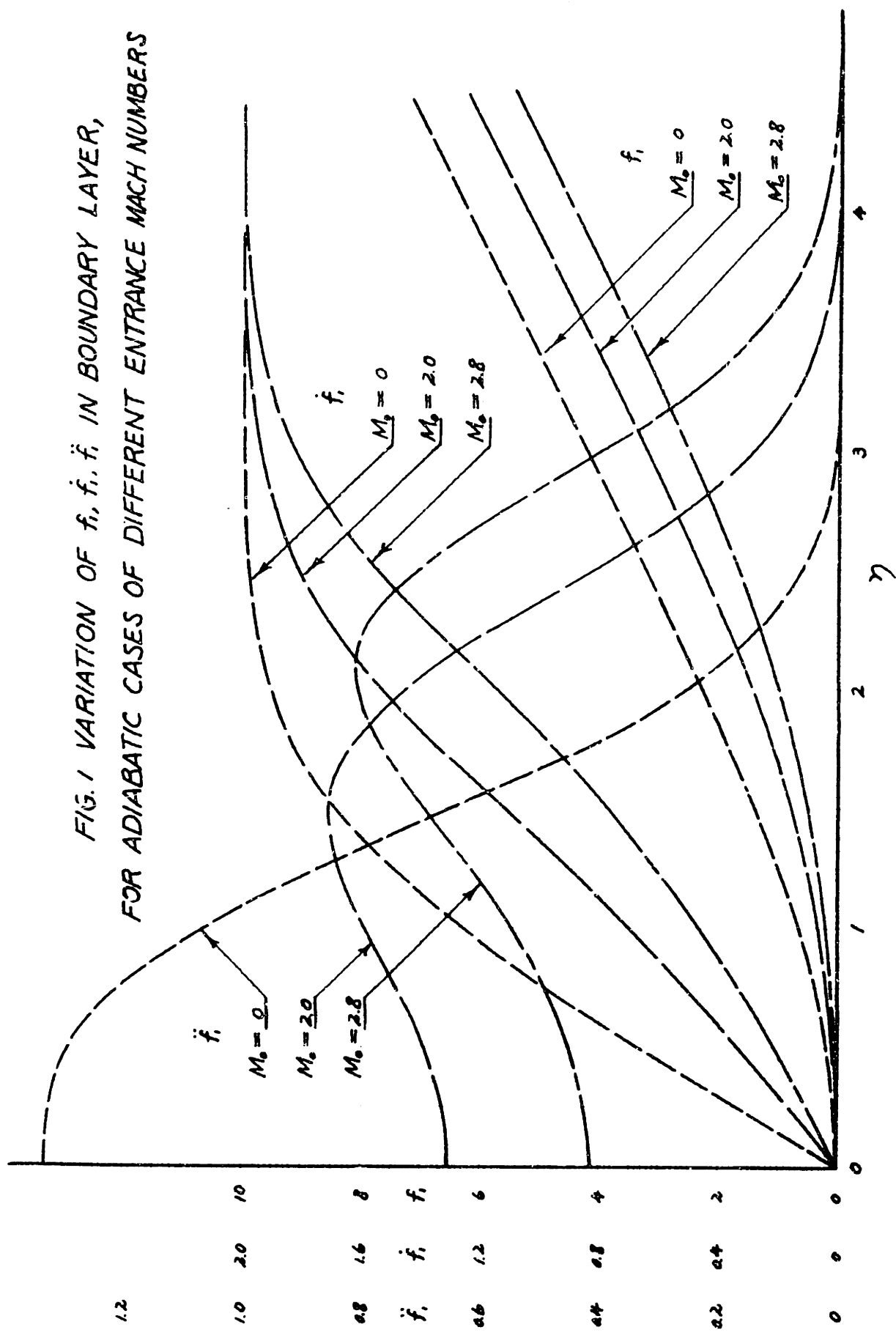
After graduation till 1947, he worked as testing engineer in the China General Omnibus Company, manager of the Nanyang Engineering Corporation, and plant superintendent of the Shanghai Transit Company.

In 1947, after a series of competitive examinations, he was granted a governmental scholarship and came to the Massachusetts Institute of Technology for advanced study. In June 1948, he obtained the degree of Master of Science in the Department of Mechanical Engineering. He was elected an Associate Member of the Sigma Xi Society.

He joined the staff of the Massachusetts Institute of Technology as Assistant from 1948 to 1949, as Research Assistant from 1949 to 1951, and is now an Instructor in the Department of Mechanical Engineering.

He has written three papers and three theses. The first paper appeared in series in the Far Eastern Engineer in China, and the other two, of which he is one of the authors, will be published in the Journal of Applied Mechanics.

FIG. 1 VARIATION OF f_i , f_i , f_i IN BOUNDARY LAYER,
FOR ADIABATIC CASES OF DIFFERENT ENTRANCE MACH NUMBERS



1.2

1.0 2.0 10

0.8 1.6 8

f_i 1.2 6

0.6 0.8 4

0.2 0.4 2

0 0 0

0

1

2

3

4

f_i

$M_0 = 0$

$M_0 = 2.0$

$M_0 = 2.8$

f_i

$M_0 = 0$

$M_0 = 2.0$

$M_0 = 2.8$

f_i

$M_0 = 0$

$M_0 = 2.0$

$M_0 = 2.8$

f_i

$M_0 = 0$

$M_0 = 2.0$

$M_0 = 2.8$

f_i

$M_0 = 0$

$M_0 = 2.0$

$M_0 = 2.8$

f_i

0

FIG. 2 VARIATION OF f IN BOUNDARY LAYER,
 FOR DIFFERENT ENTRANCE MACH NUMBERS
 AND THERMAL CONDITIONS AT TUBE WALL

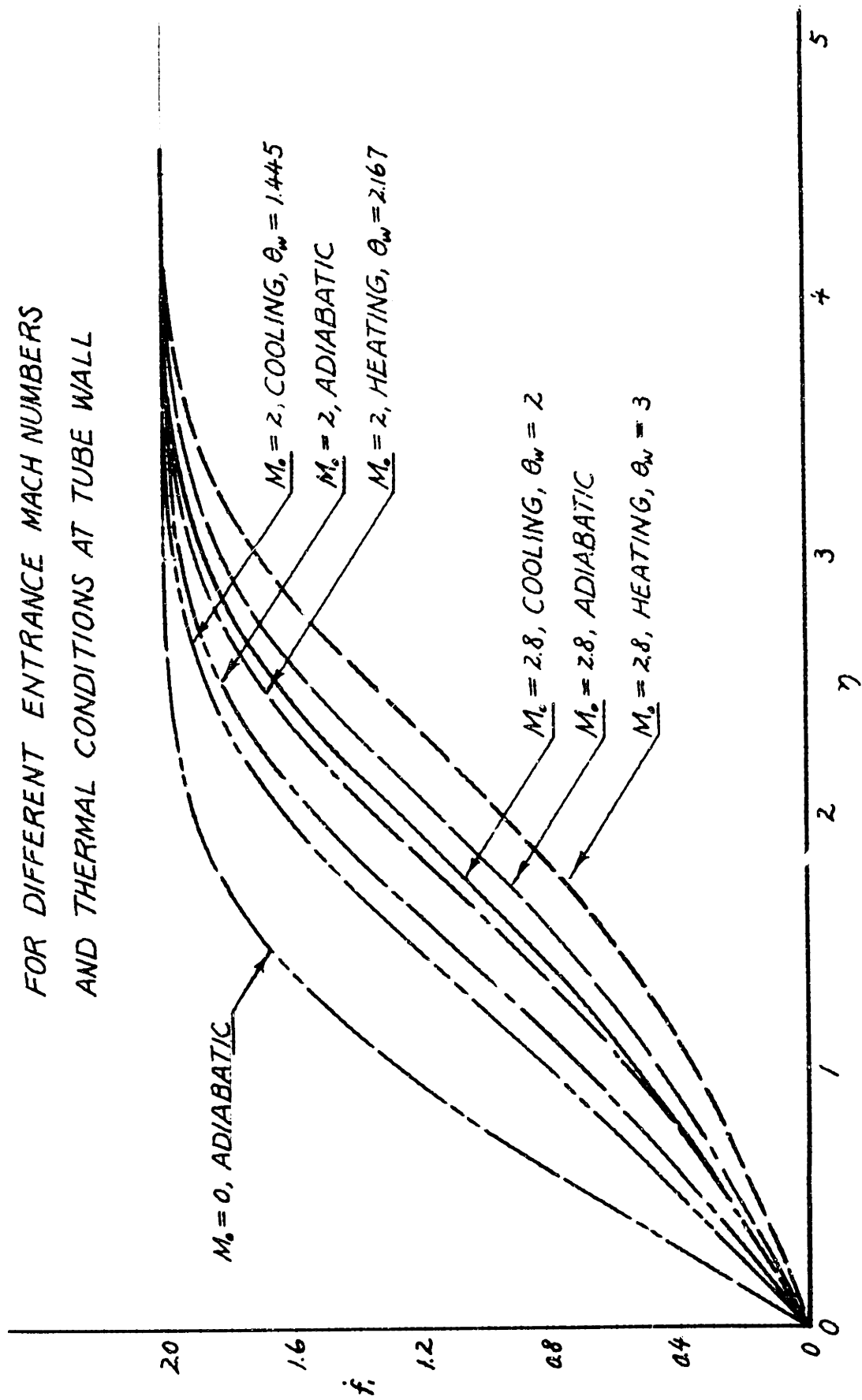


FIG. 3 VARIATION OF θ , IN BOUNDARY LAYER,
FOR DIFFERENT ENTRANCE MACH NUMBERS
AND THERMAL CONDITIONS AT TUBE WALL

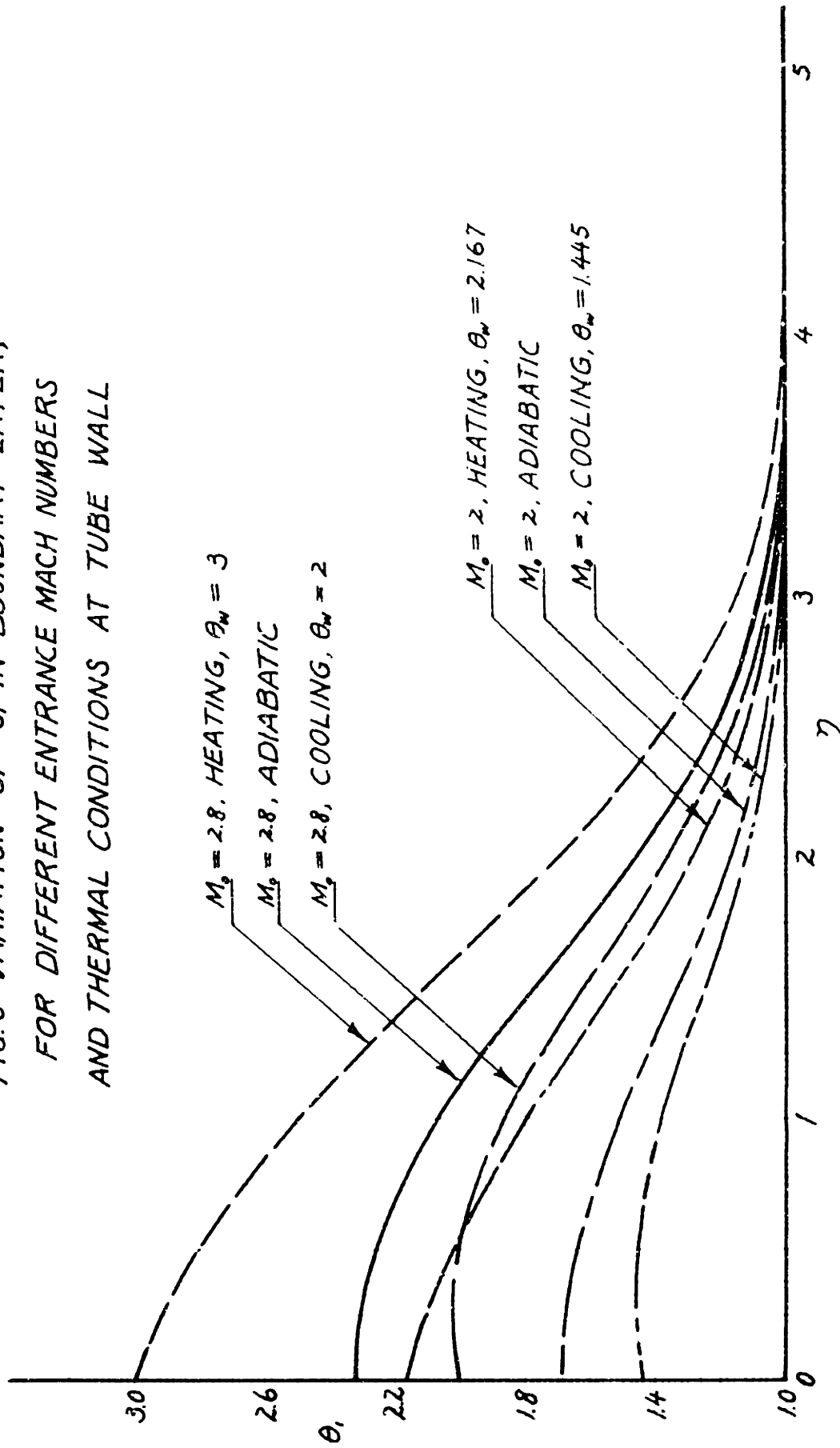


FIG. 4 VARIATION OF θ , IN BOUNDARY LAYER,
FOR DIFFERENT ENTRANCE MACH NUMBERS
AND THERMAL CONDITIONS AT TUBE WALL

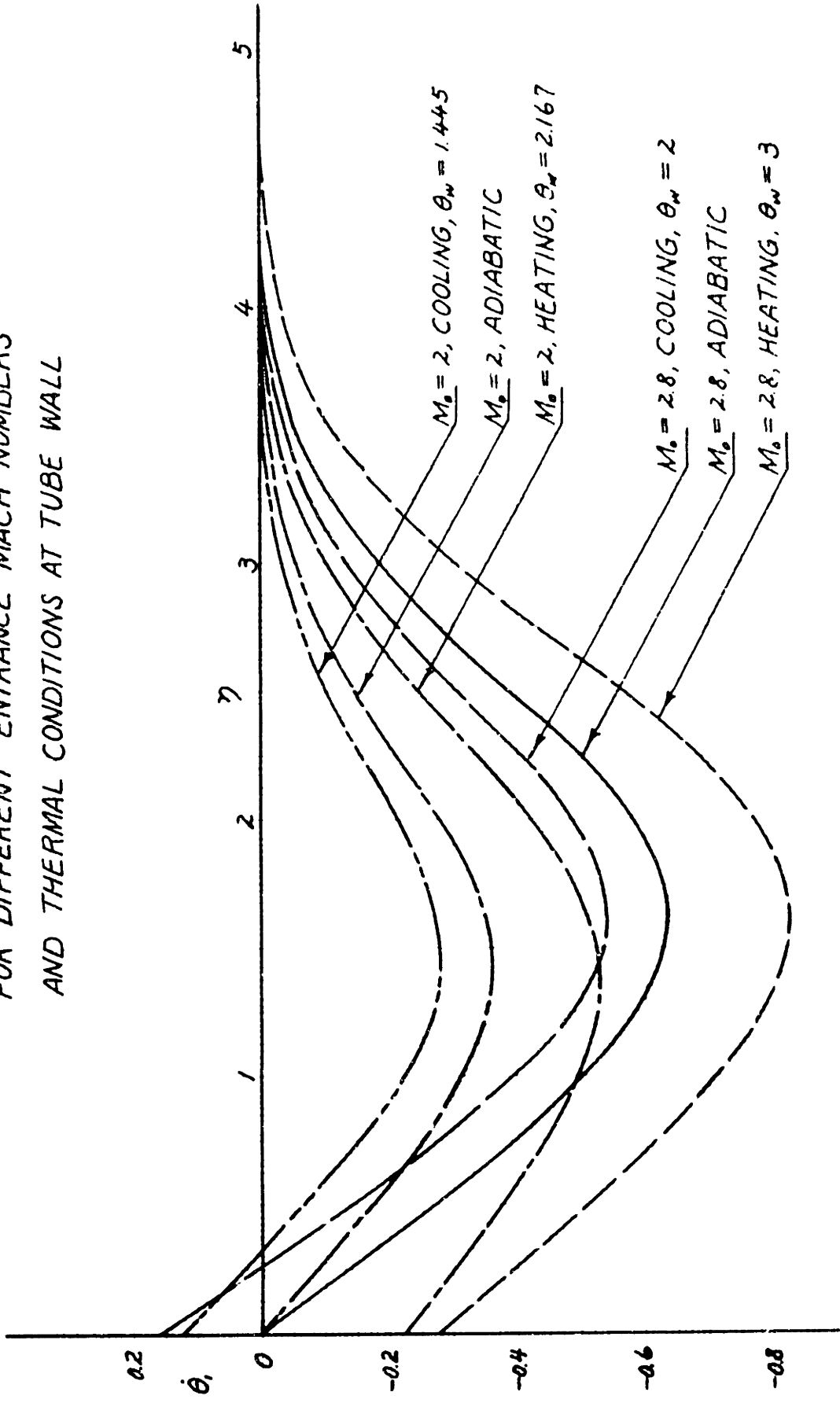


FIG. 5 FIRST APPROXIMATION TO VELOCITY PROFILE
 IN BOUNDARY LAYER, FOR DIFFERENT ENTRANCE MACH NUMBERS
 AND THERMAL CONDITIONS AT TUBE WALL

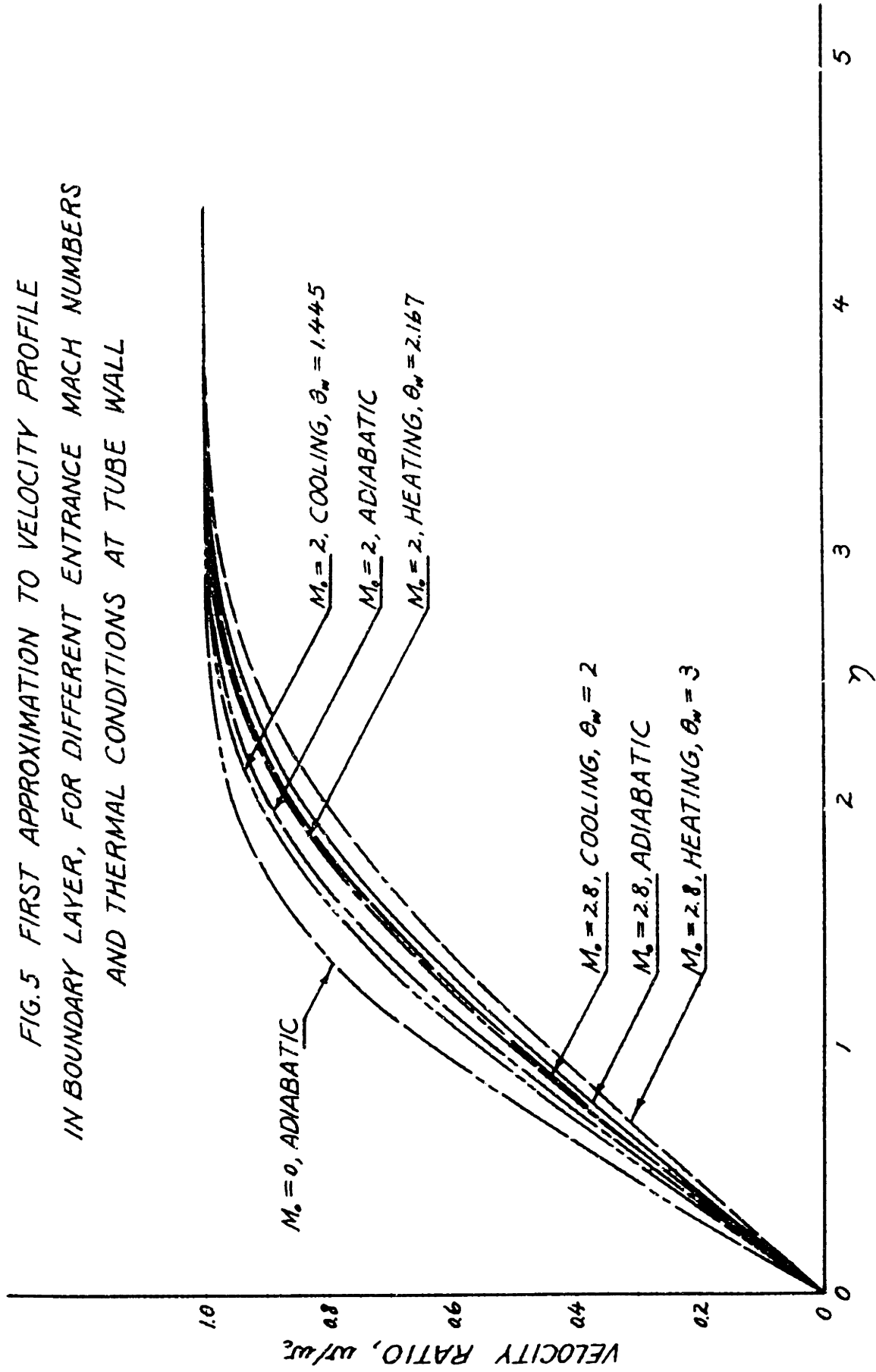


FIG. 6 BOUNDARY-LAYER THICKNESS-RATIO
 VERSUS LENGTH PARAMETER,
 FOR ENTRANCE MACH NUMBER OF 2.8 AND
 DIFFERENT THERMAL CONDITIONS AT TUBE WALL

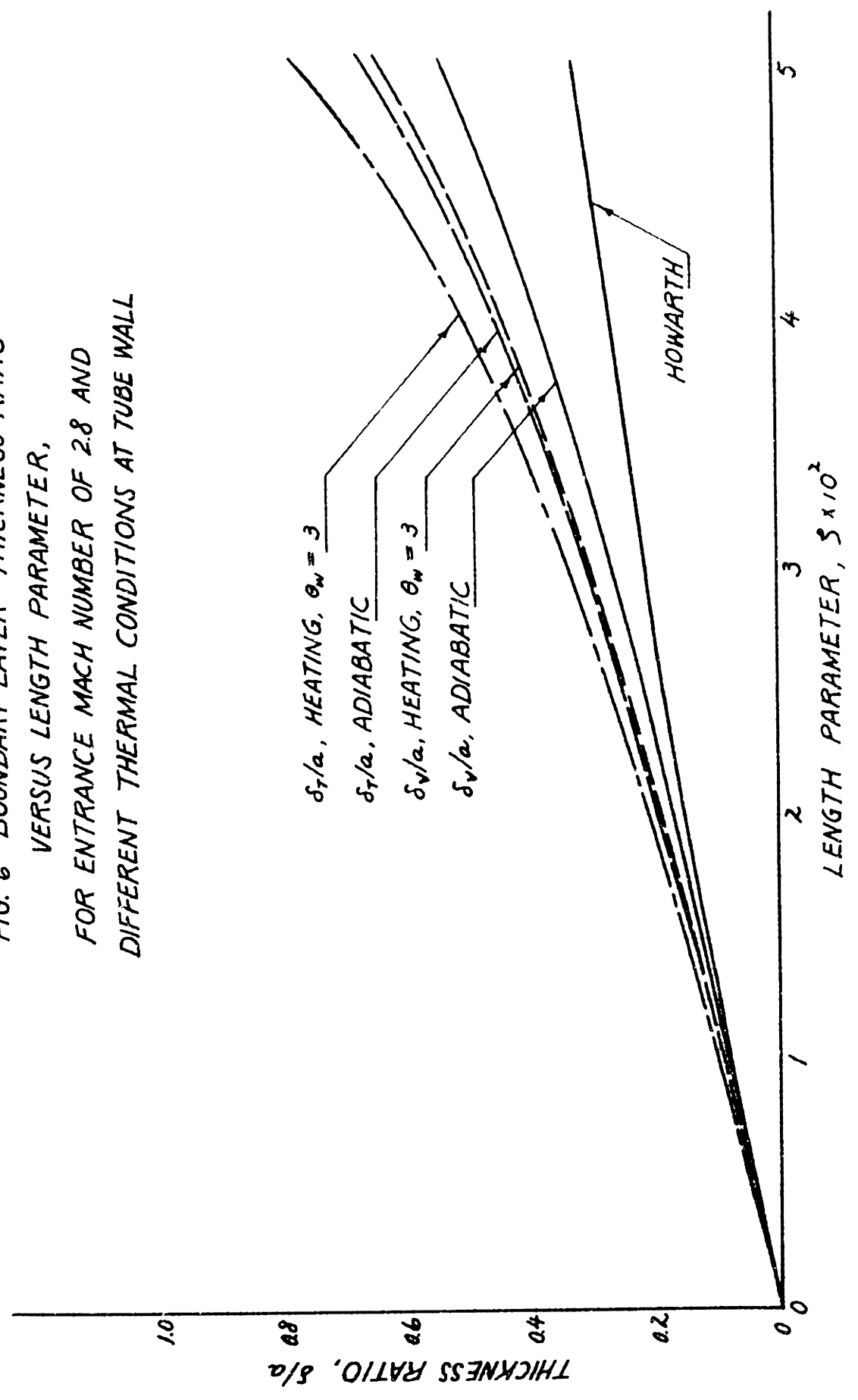


FIG. 7 BOUNDARY-LAYER THICKNESS-RATIO
 VERSUS LENGTH REYNOLDS NUMBER,
 FOR ENTRANCE MACH NUMBERS OF 2.8 AND
 DIFFERENT THERMAL CONDITIONS AT TUBE WALL

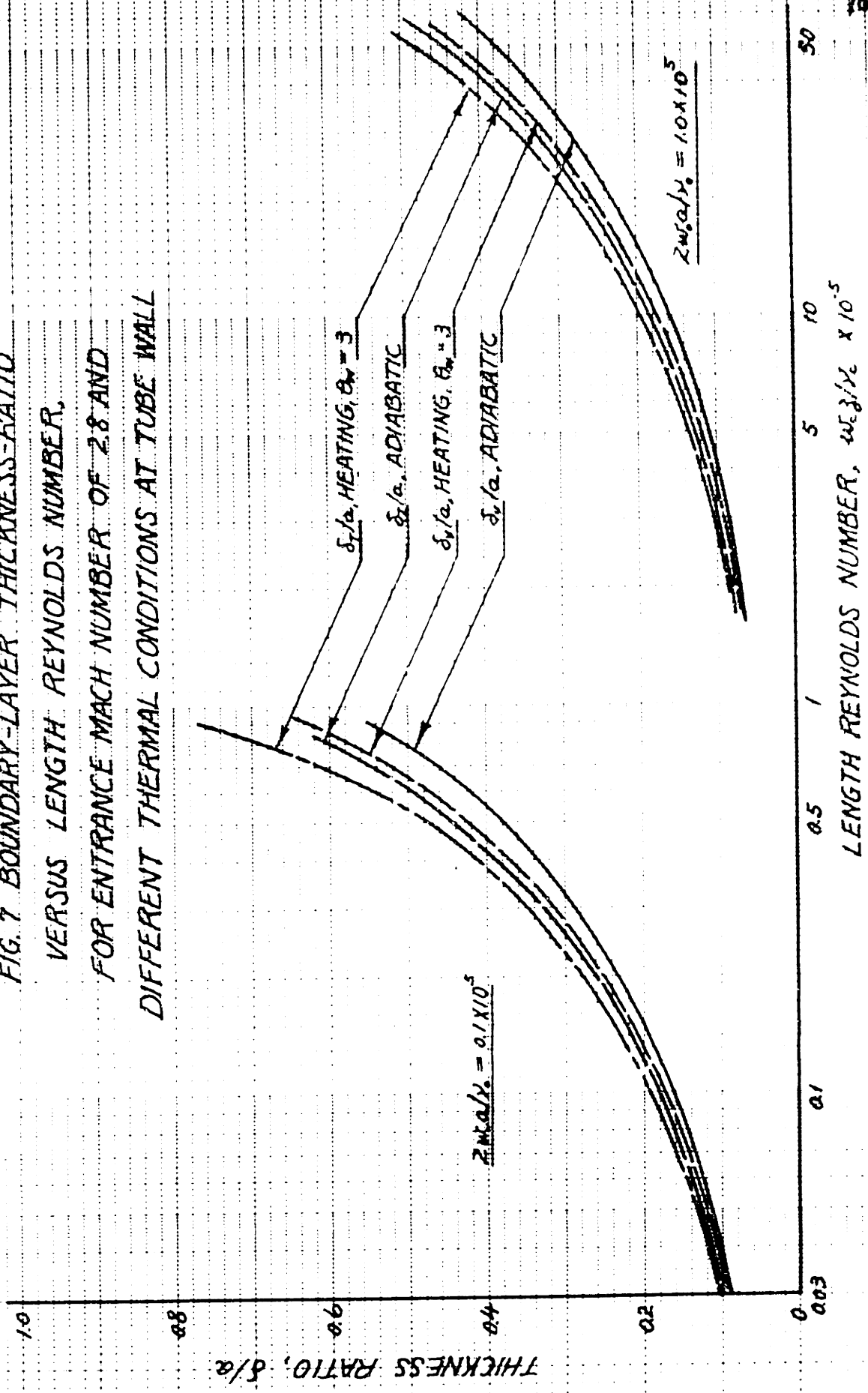
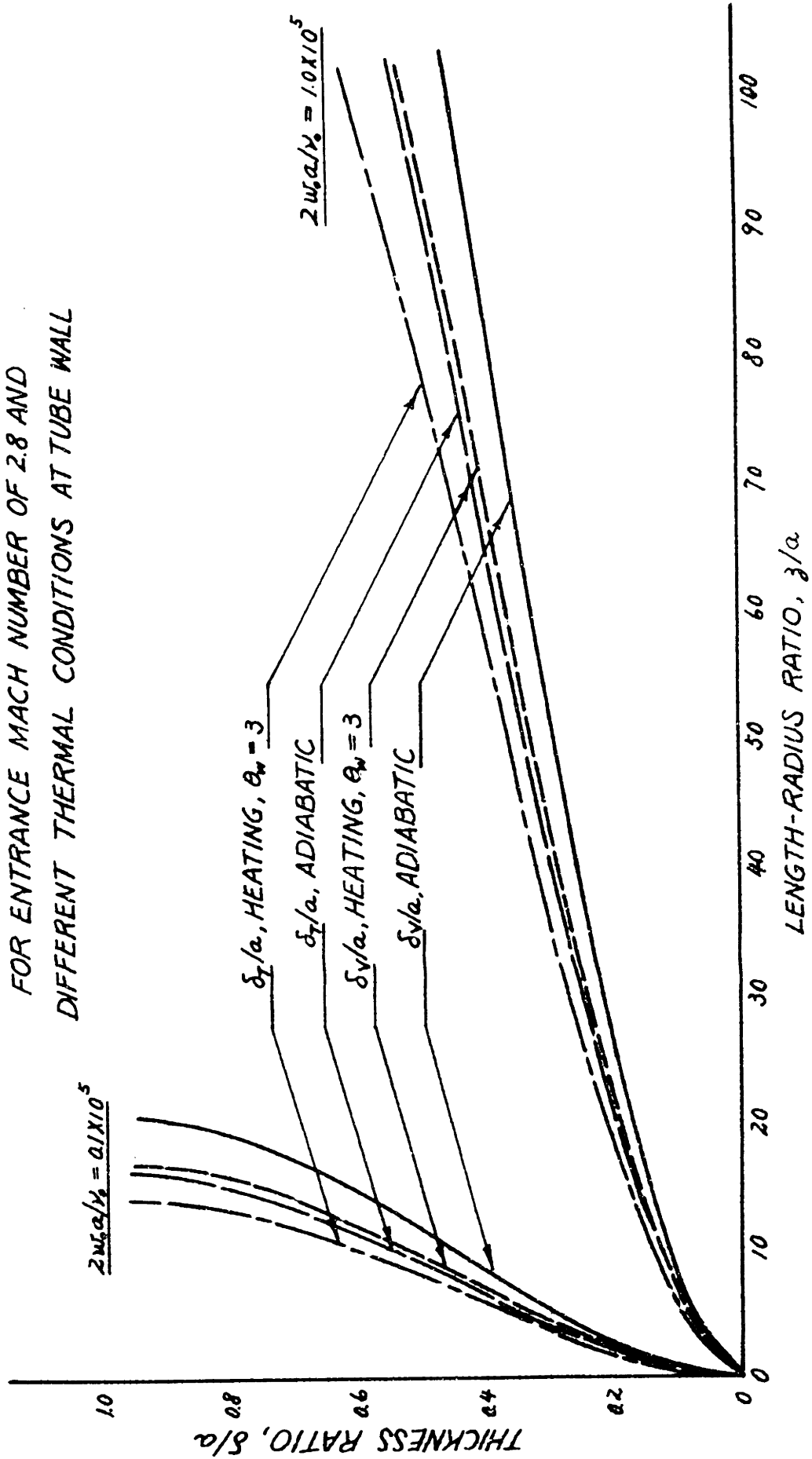


FIG. 8 BOUNDARY-LAYER THICKNESS-RATIO
 VERSUS LENGTH-RADIUS RATIO,
 FOR ENTRANCE MACH NUMBER OF 2.8 AND
 DIFFERENT THERMAL CONDITIONS AT TUBE WALL



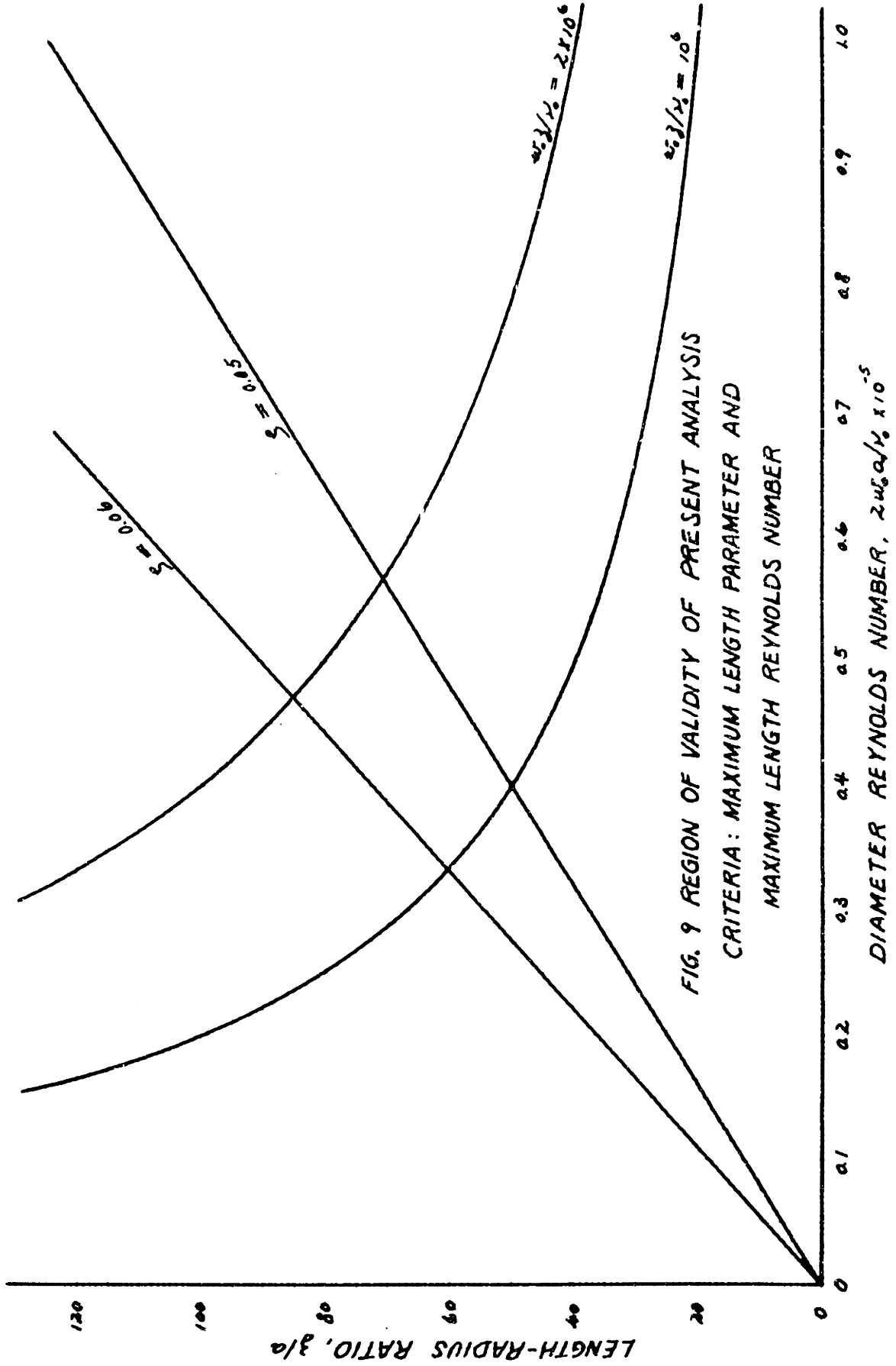
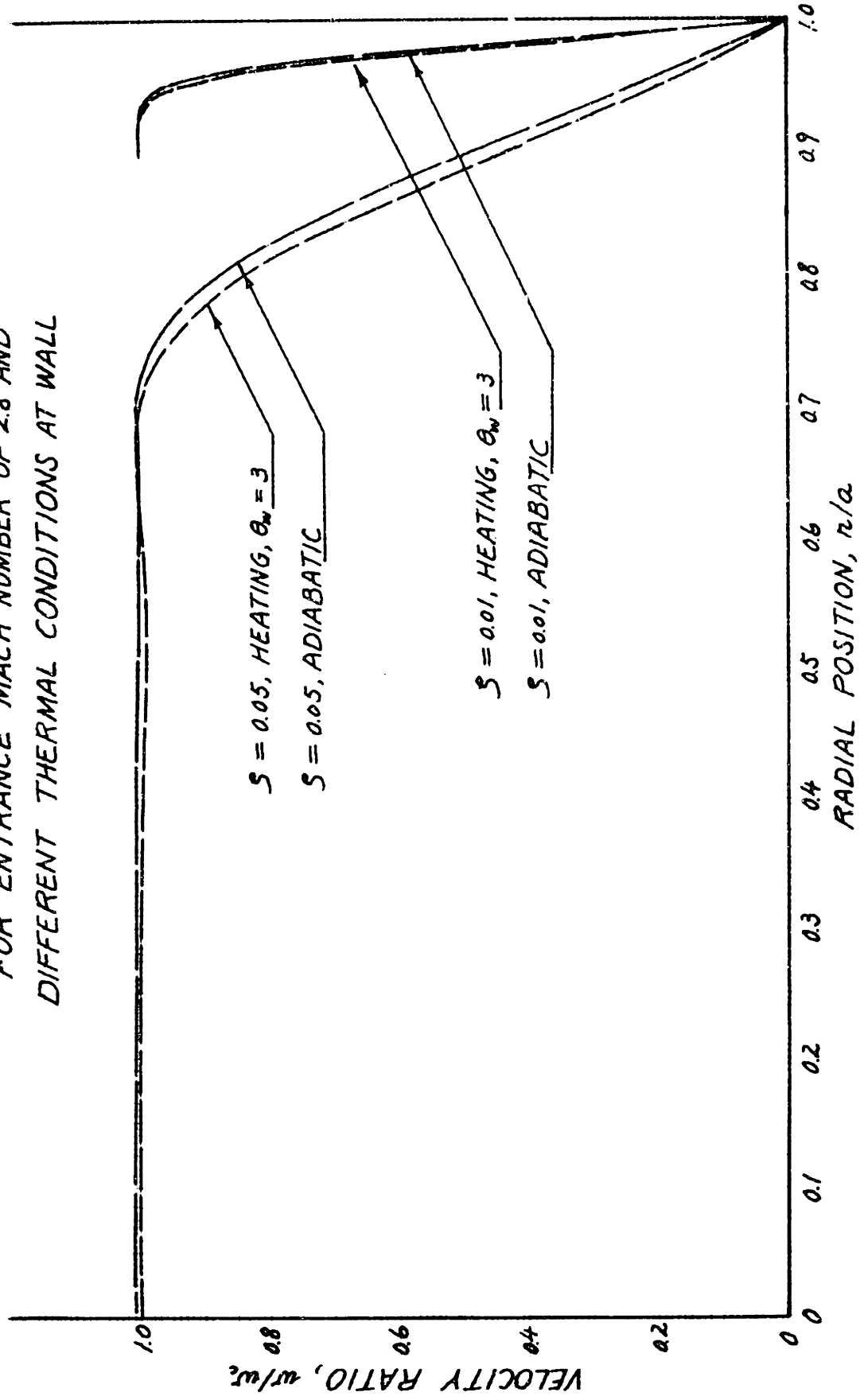


FIG. 9 REGION OF VALIDITY OF PRESENT ANALYSIS
 CRITERIA: MAXIMUM LENGTH PARAMETER AND
 MAXIMUM LENGTH REYNOLDS NUMBER

FIG.10 VELOCITY PROFILE IN BOUNDARY LAYER,
FOR ENTRANCE MACH NUMBER OF 2.8 AND
DIFFERENT THERMAL CONDITIONS AT WALL



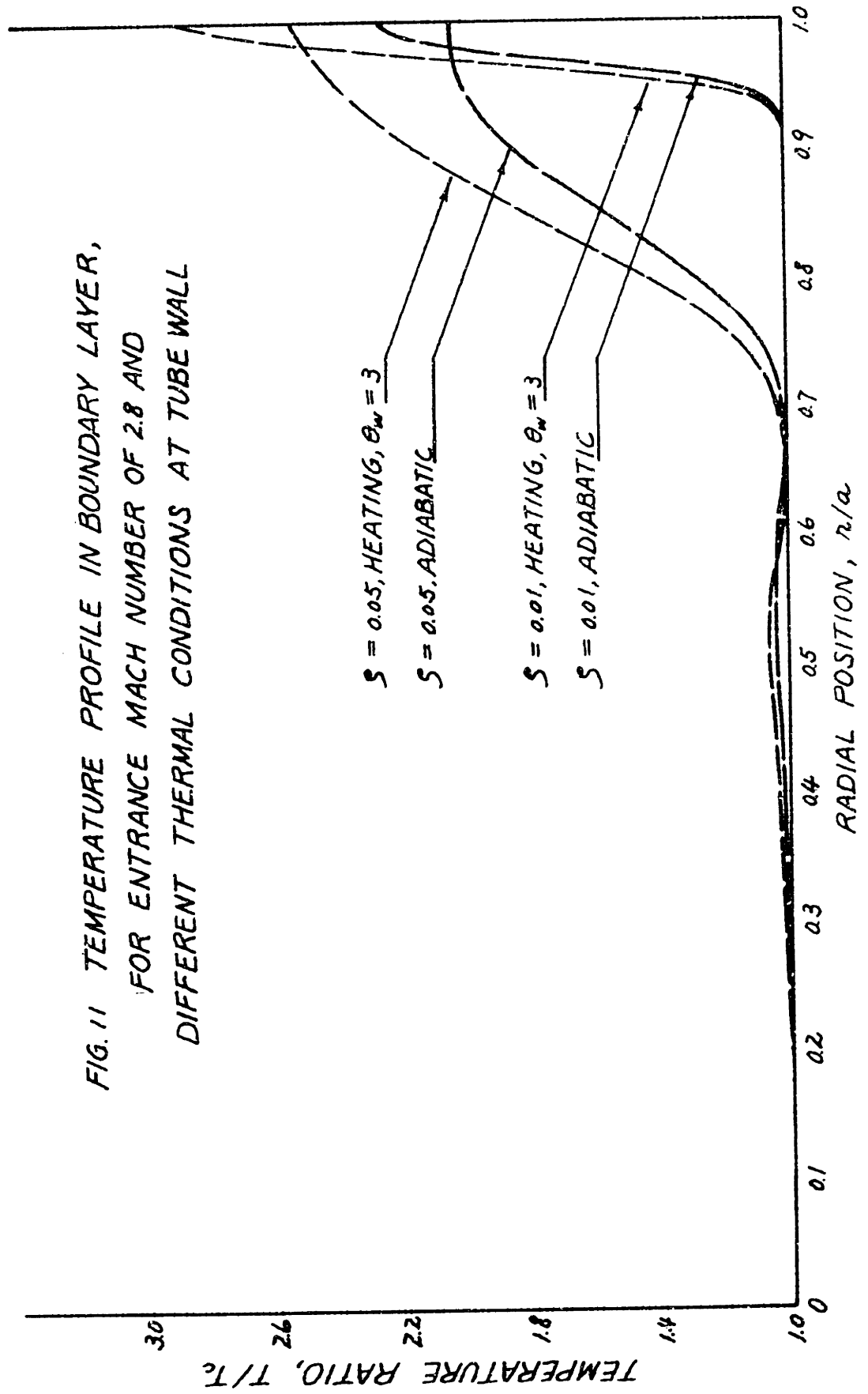


FIG. 12 PRESSURE RATIO VERSUS LENGTH PARAMETER,
 FOR ADIABATIC CASE OF ENTRANCE MACH NUMBER OF 2.8

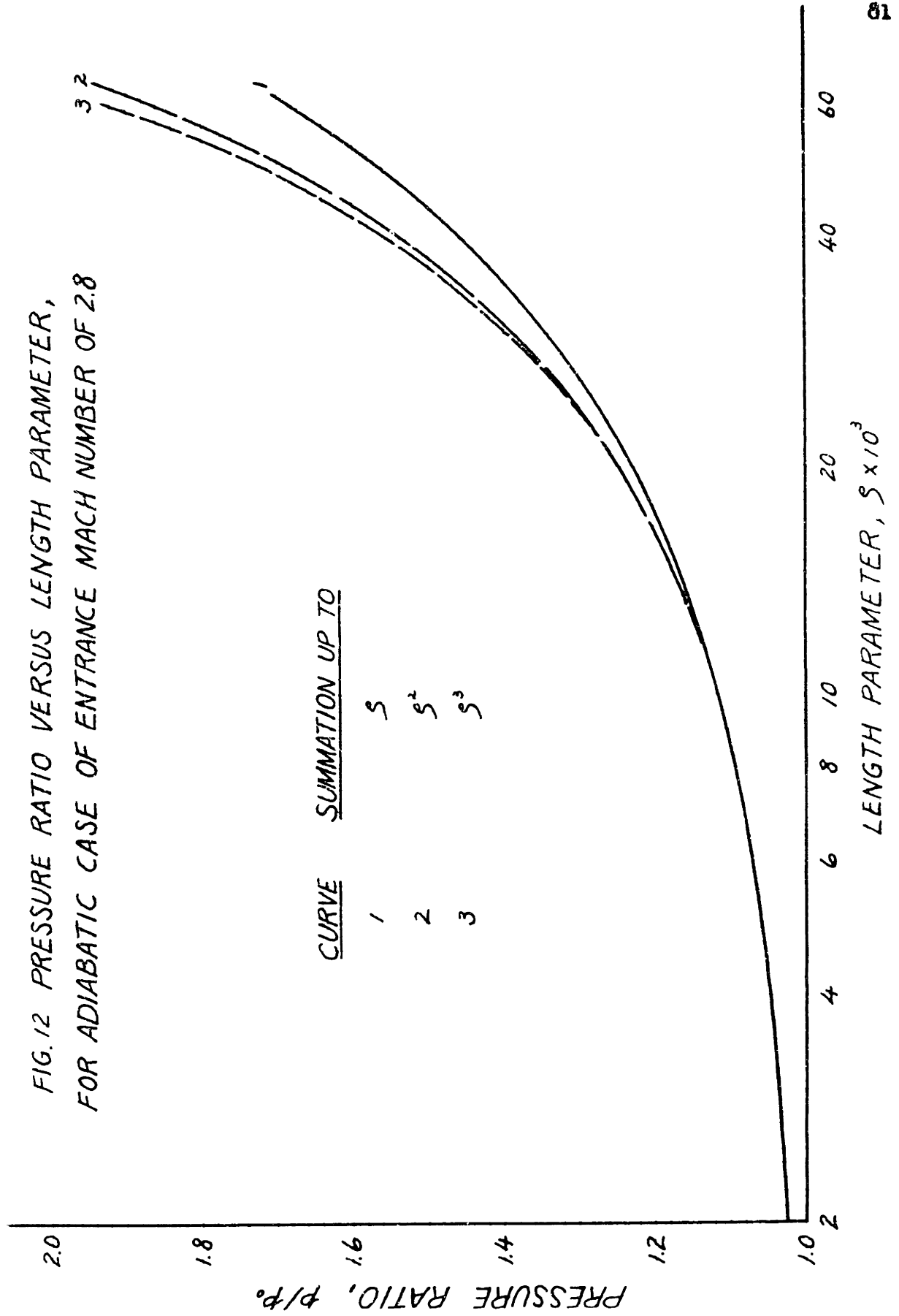


FIG. 13 MEASURED VALUE OF PRESSURE RATIO
 VERSUS MODIFIED LENGTH PARAMETER,
 TEST COMBINATION B, ADIABATIC APPARATUS (3, 4)

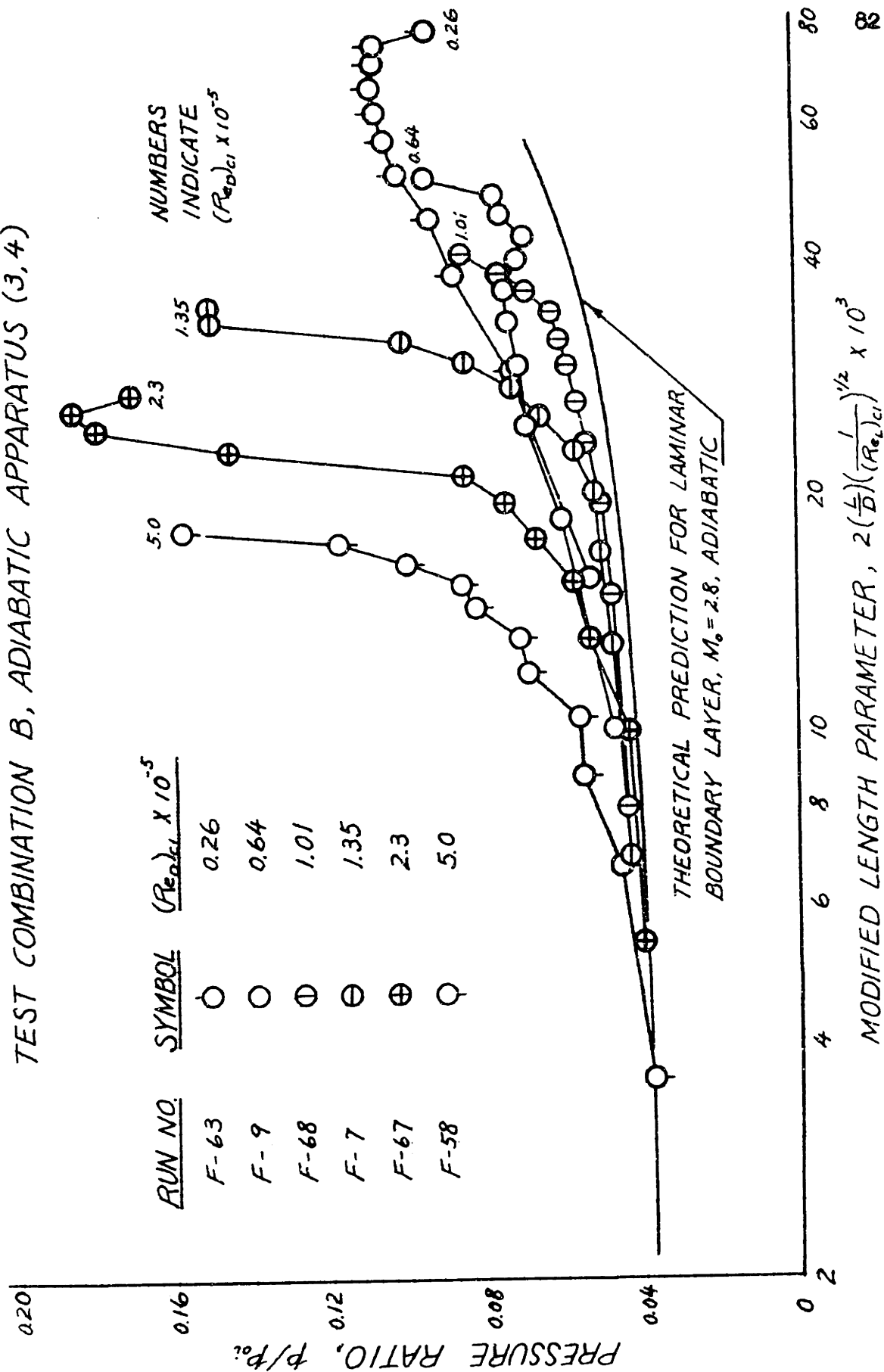


FIG.14 MEASURED VALUE OF PRESSURE RATIO
 VERSUS LENGTH REYNOLDS NUMBER,
 TEST COMBINATION B, ADIABATIC APPARATUS (3,4)

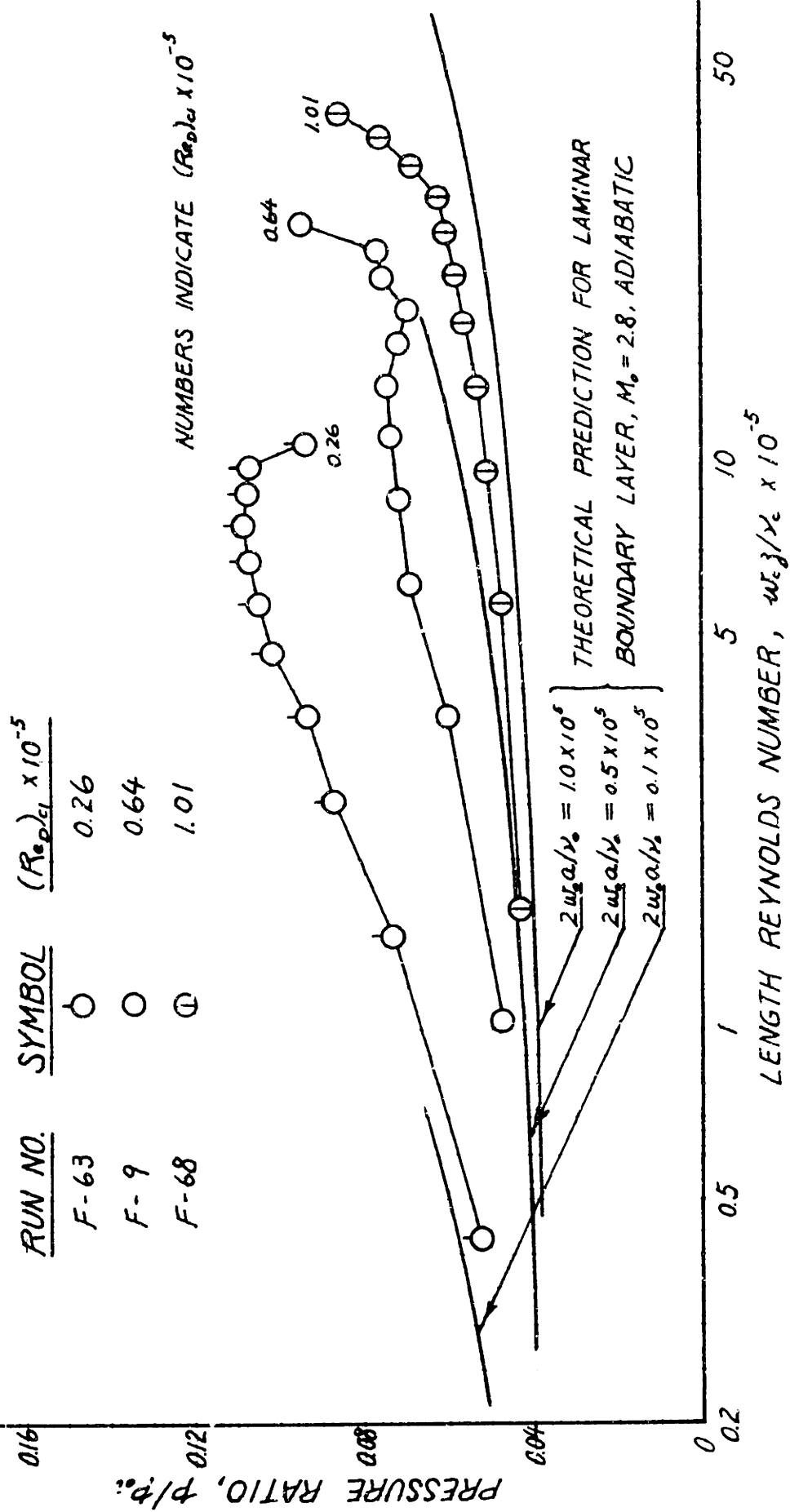


FIG.15 PRESSURE RATIO VERSUS LENGTH PARAMETER,
 FOR ENTRANCE MACH NUMBER OF 2.8
 WITH HEATING AT TUBE WALL ($\theta_w = 3$)

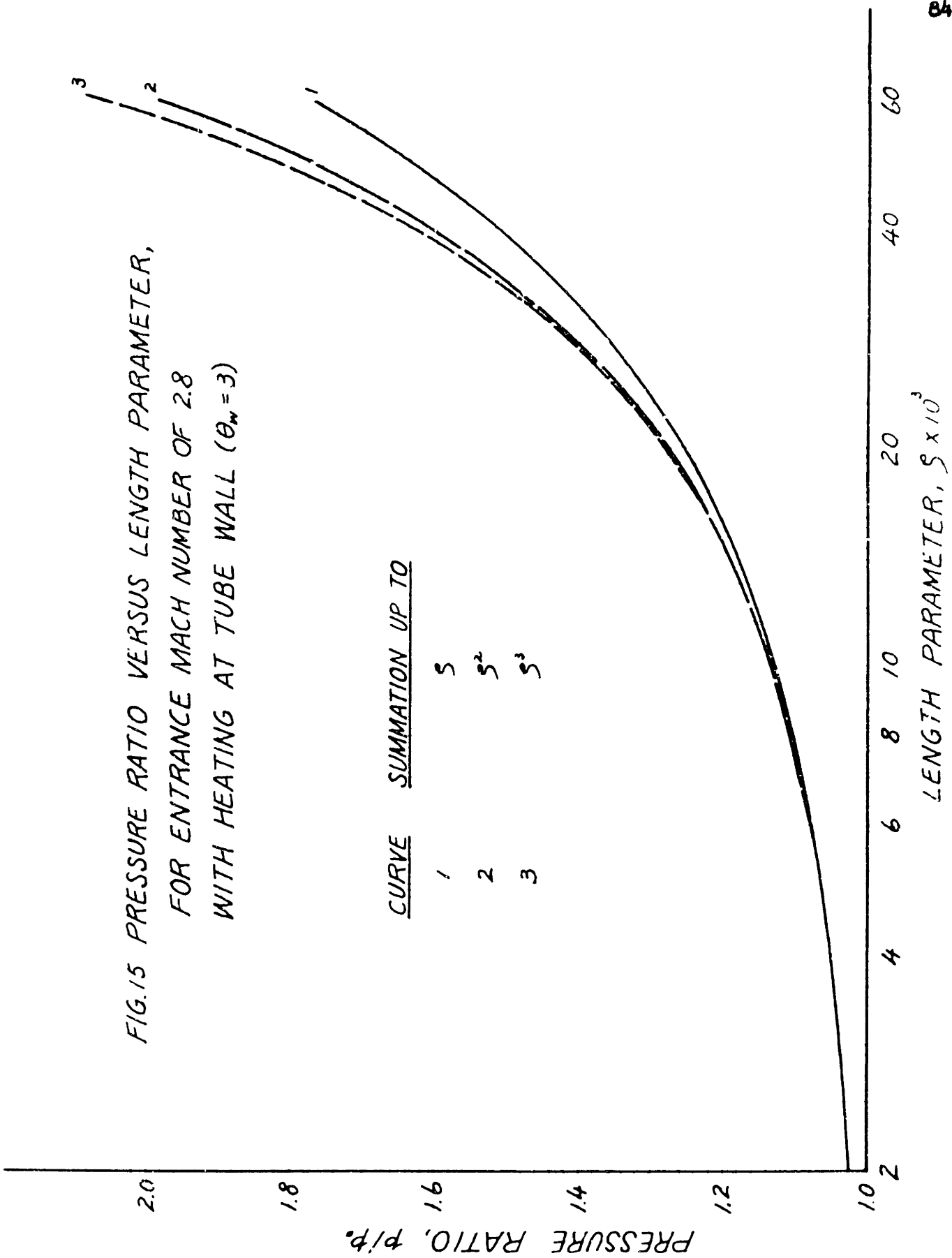
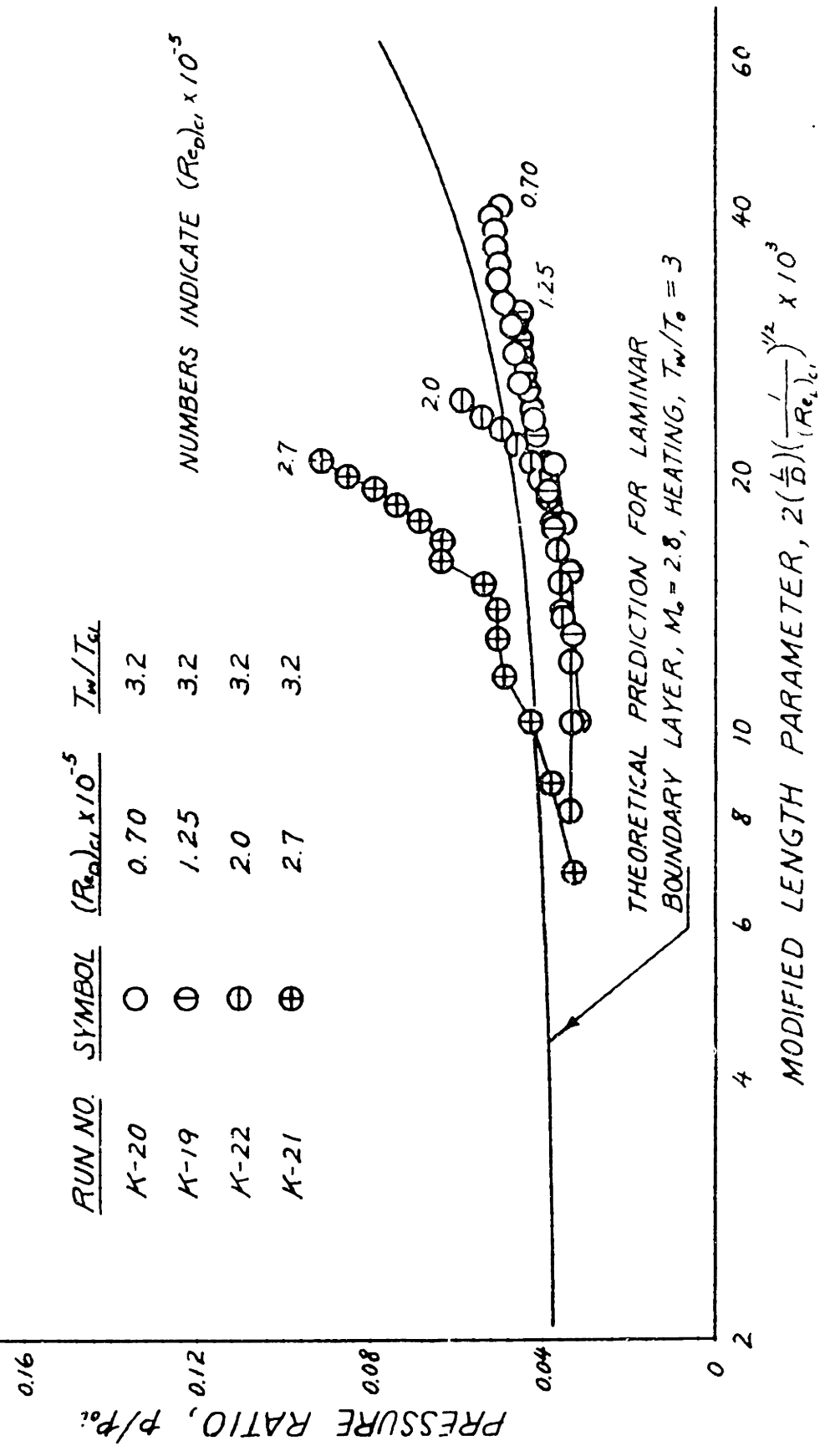


FIG. 16 MEASURED VALUE OF PRESSURE RATIO
 VERSUS MODIFIED LENGTH PARAMETER,
 HEAT-TRANSFER APPARATUS (13)



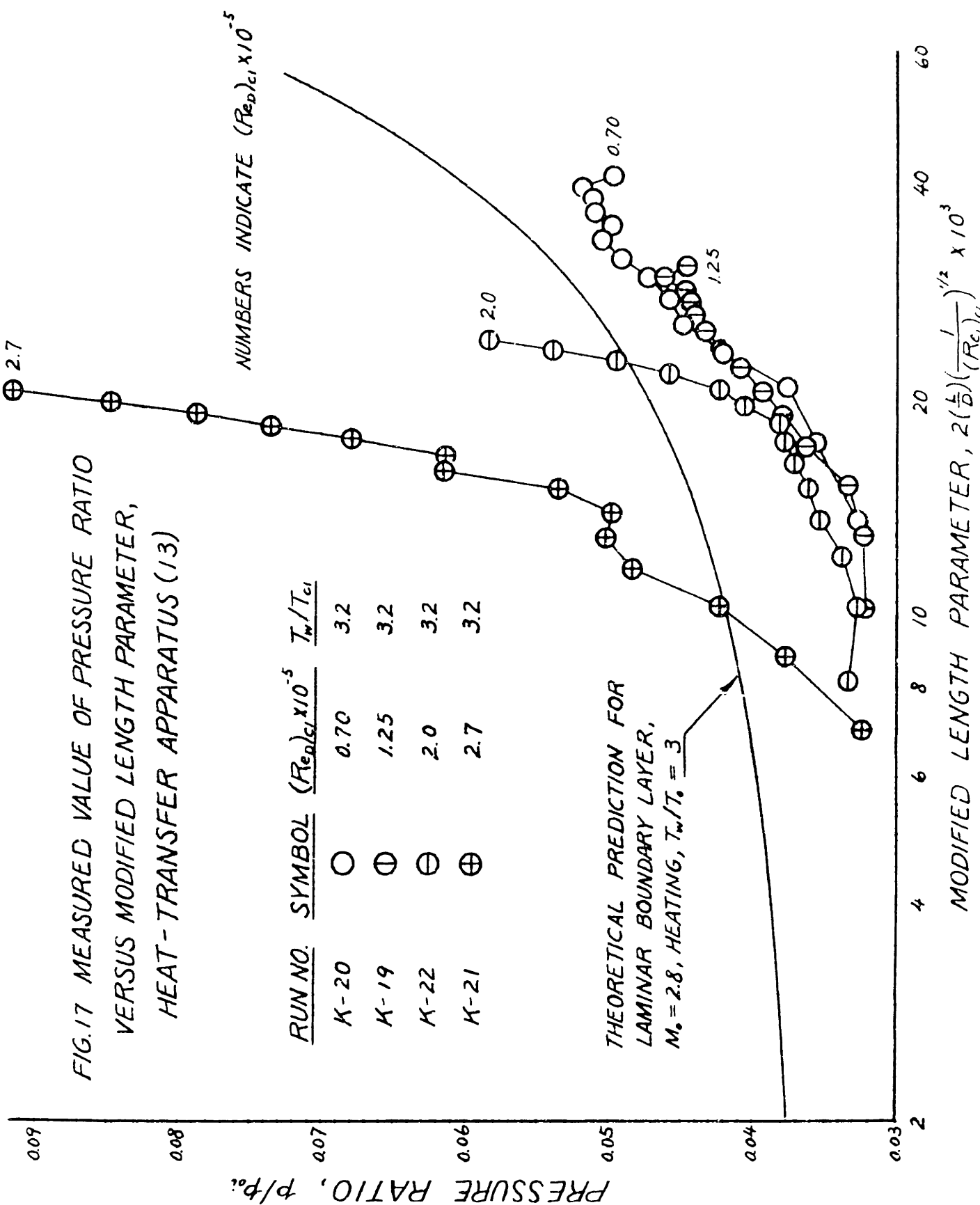


FIG.18 FIRST APPROXIMATION TO PRESSURE RATIO
 VERSUS LENGTH PARAMETER, FOR DIFFERENT ENTRANCE MACH NUMBERS
 AND THERMAL CONDITIONS AT TUBE WALL

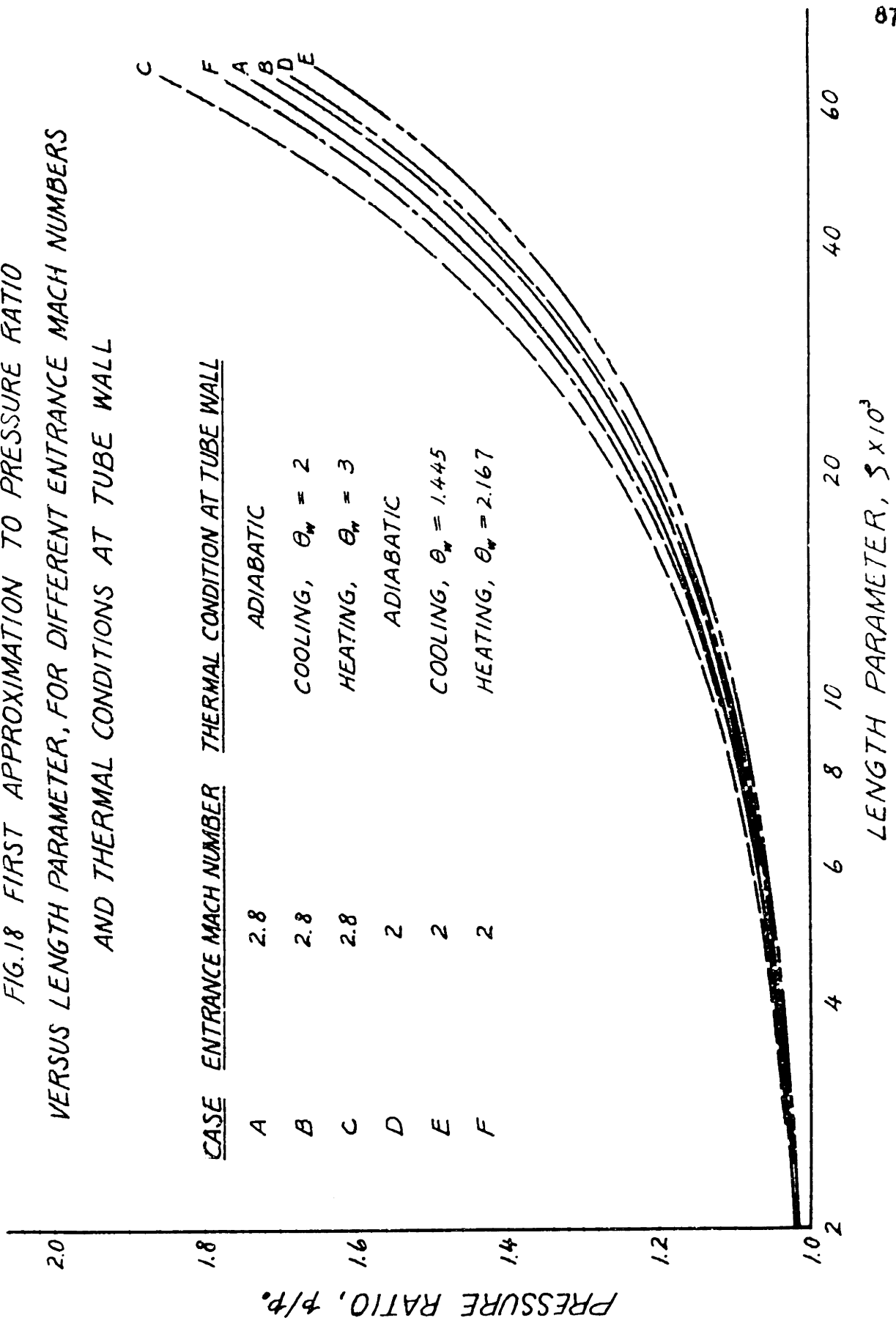


FIG. 19 ADIABATIC - WALL TEMPERATURE - RATIO
 VERSUS LENGTH PARAMETER,
 FOR ENTRANCE MACH NUMBER OF 2.8

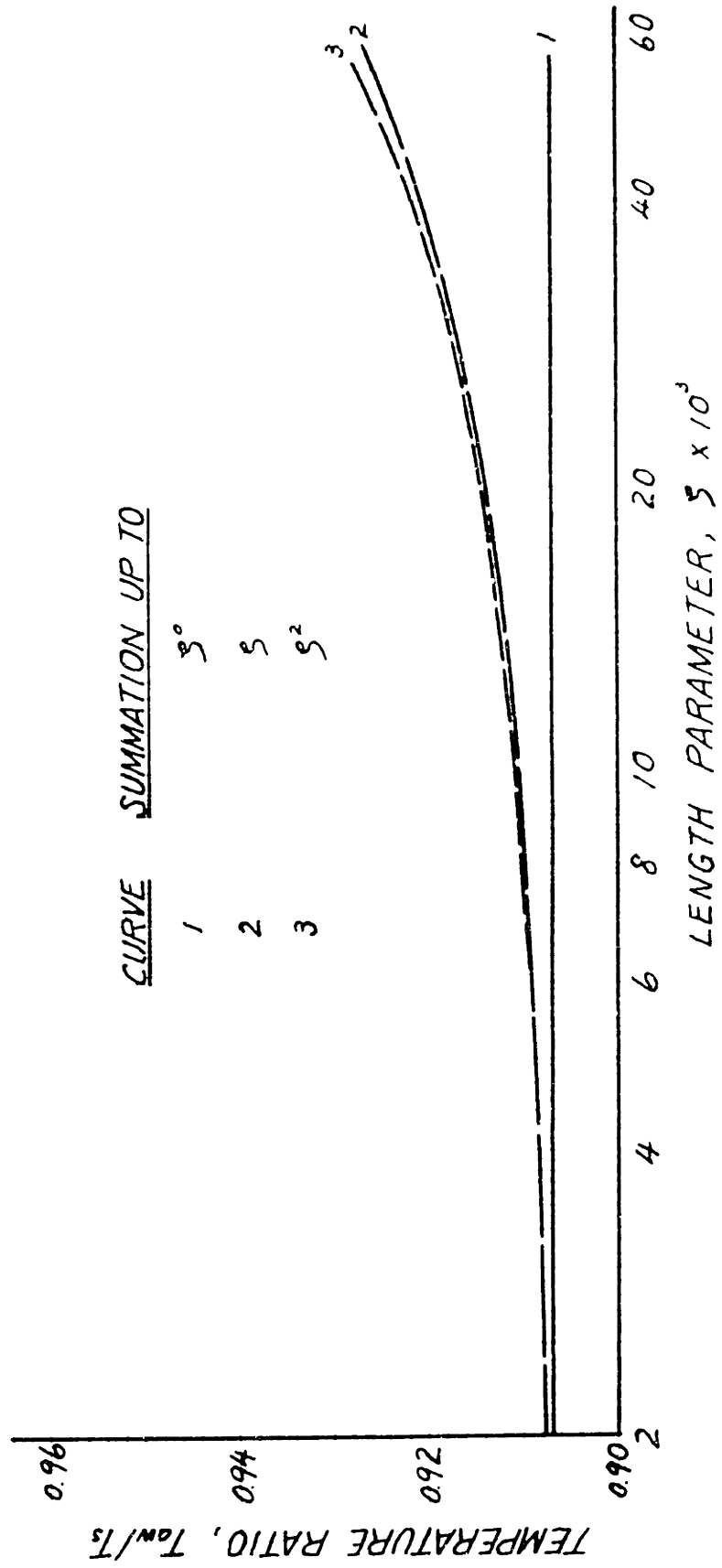


FIG. 20 MEASURED VALUE OF ADIABATIC-WALL TEMPERATURE-RATIO
 VERSUS MODIFIED LENGTH PARAMETER,
 TEST COMBINATION B, ADIABATIC APPARATUS (3, 4)

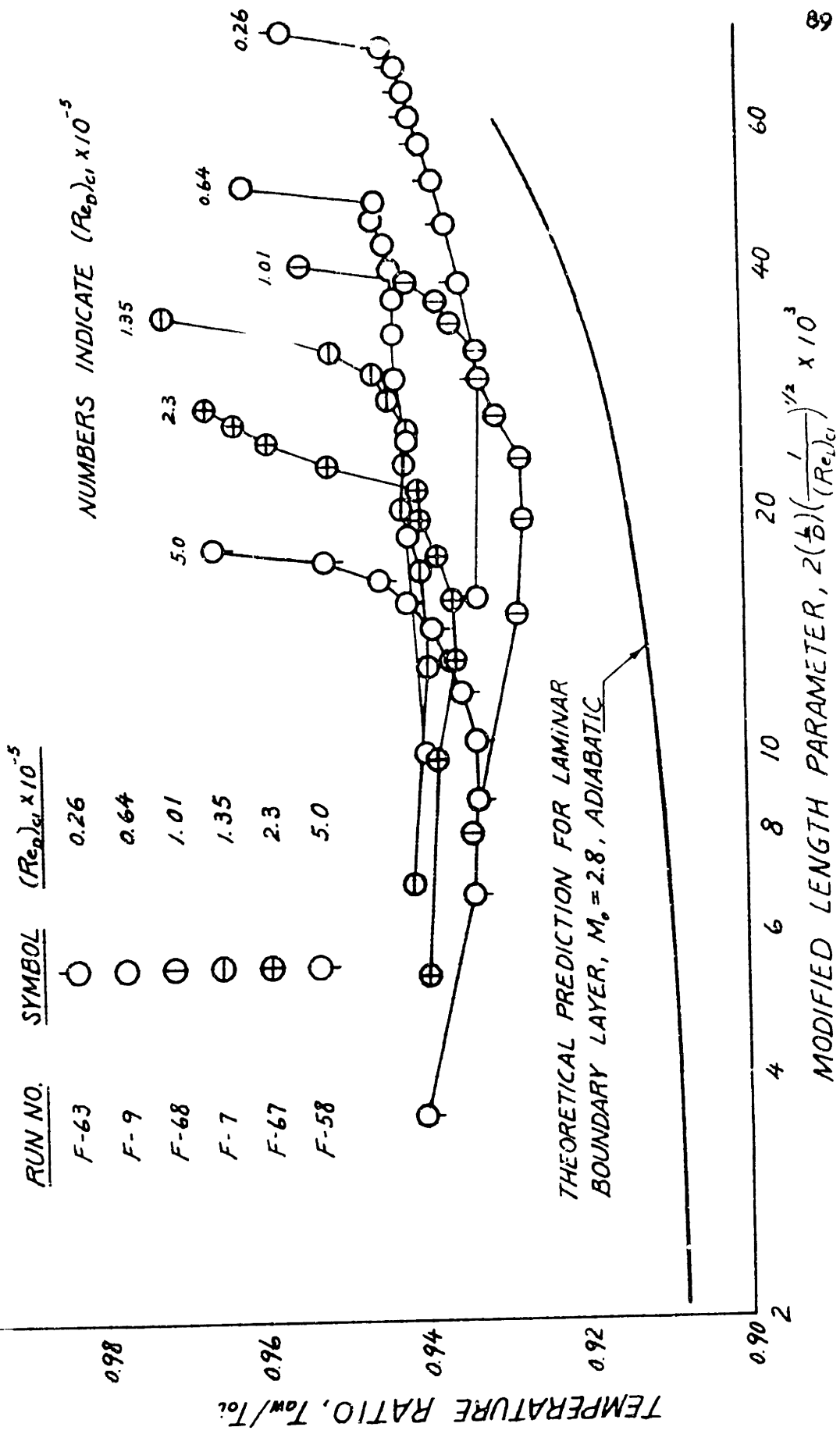


FIG. 21 ADIABATIC-WALL TEMPERATURE-RATIO
 VERSUS LENGTH PARAMETER,
 FOR ENTRANCE MACH NUMBERS OF 2 AND 2.8

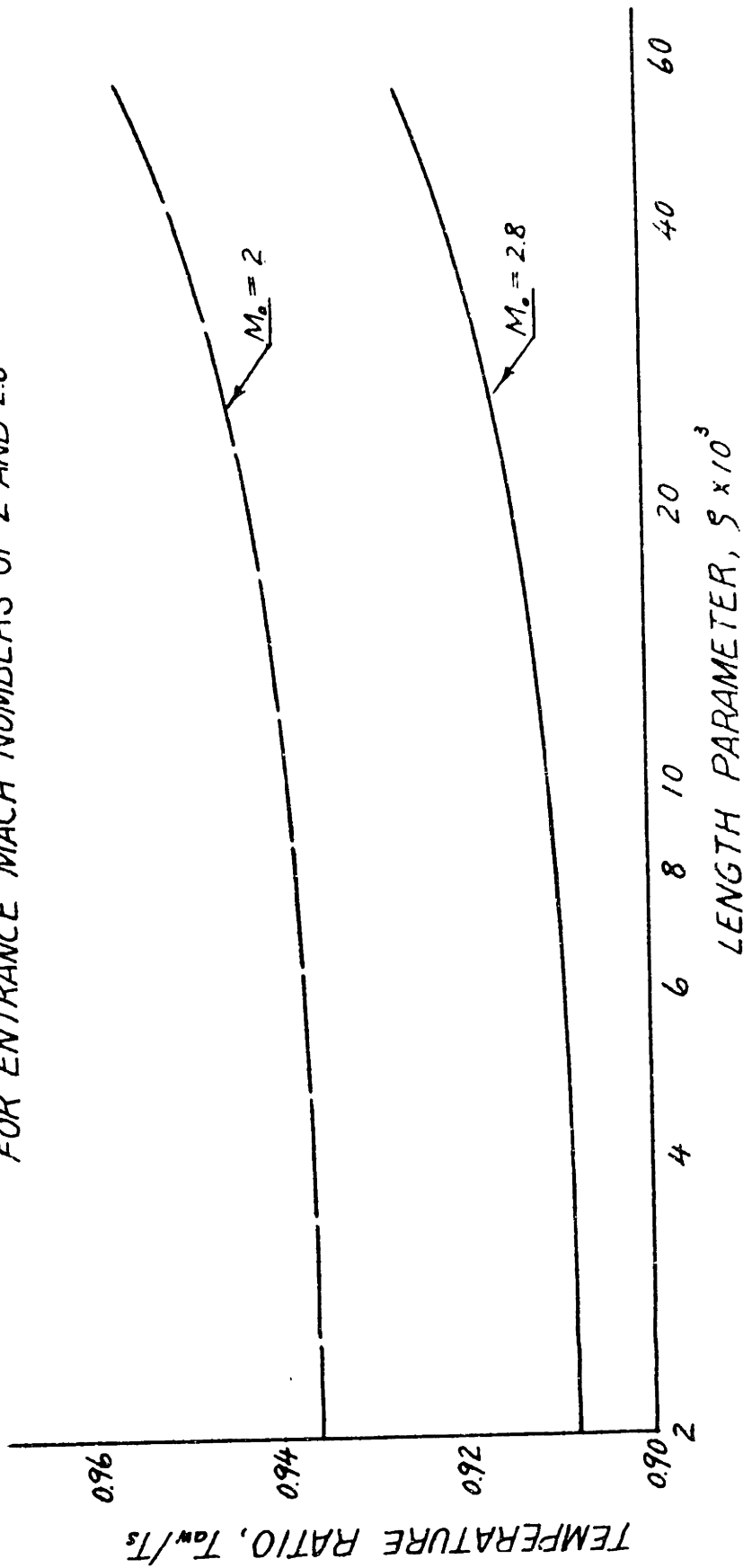


FIG. 22 LOCAL RECOVERY FACTOR VERSUS LENGTH PARAMETER,
FOR ENTRANCE MACH NUMBERS OF 2 AND 2.8

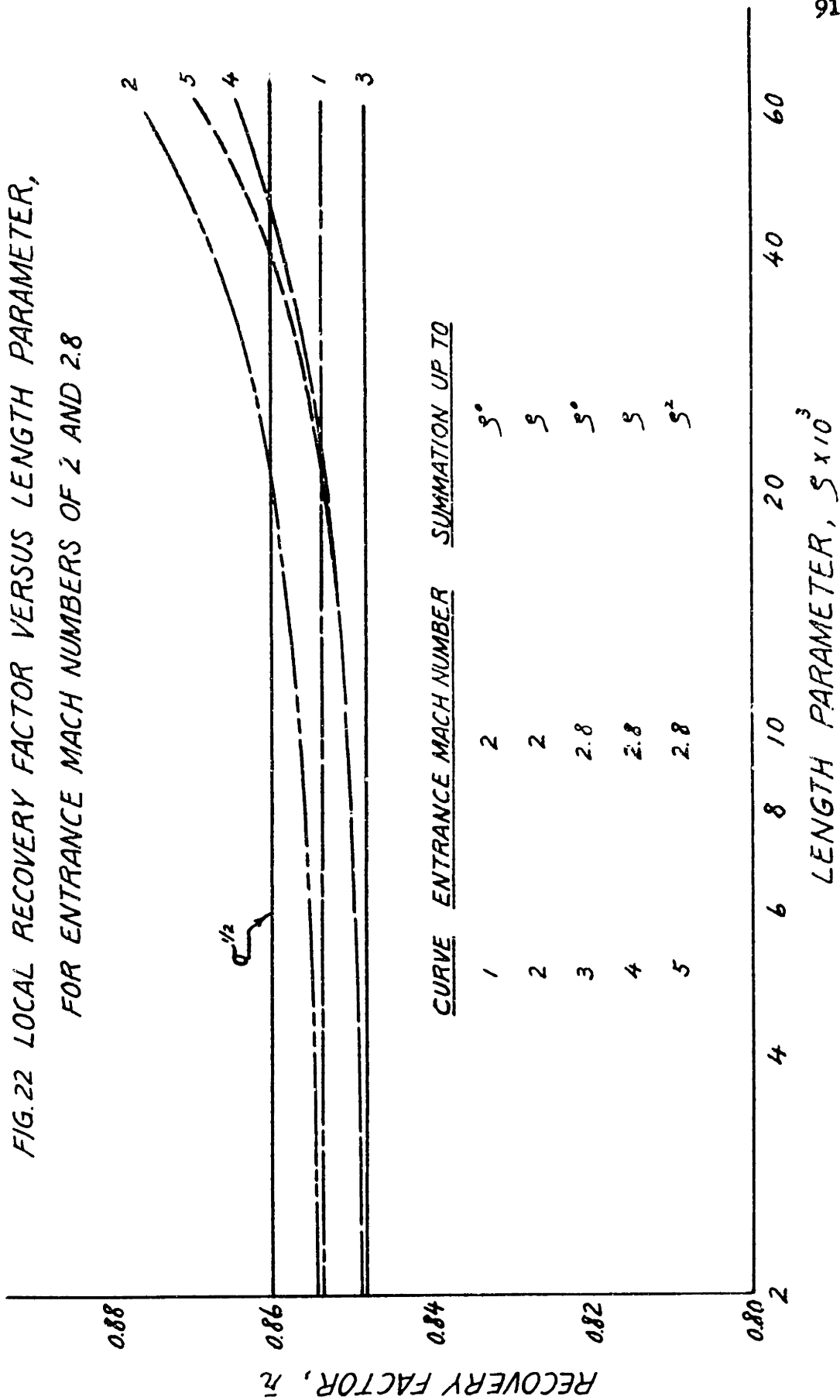


FIG. 23 LOCAL TRUE FRICTION COEFFICIENT
 VERSUS LENGTH REYNOLDS NUMBER,
 FOR ADIABATIC CASE OF ENTRANCE MACH NUMBER OF 2.8

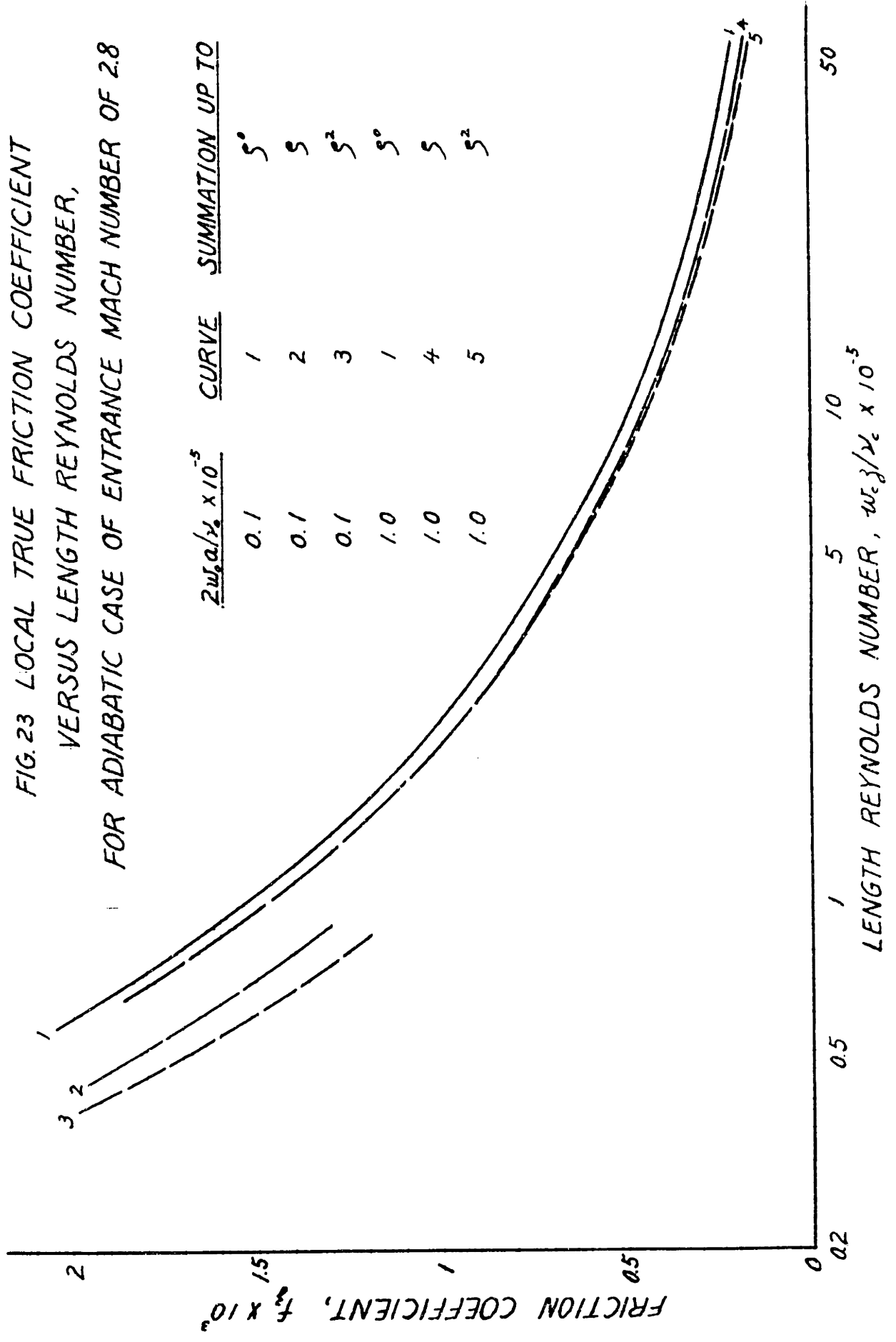


FIG. 24 LOCAL TRUE FRICTION COEFFICIENT
 VERSUS LENGTH REYNOLDS NUMBER,
 FOR ADIABATIC CASES OF DIFFERENT ENTRANCE MACH NUMBERS

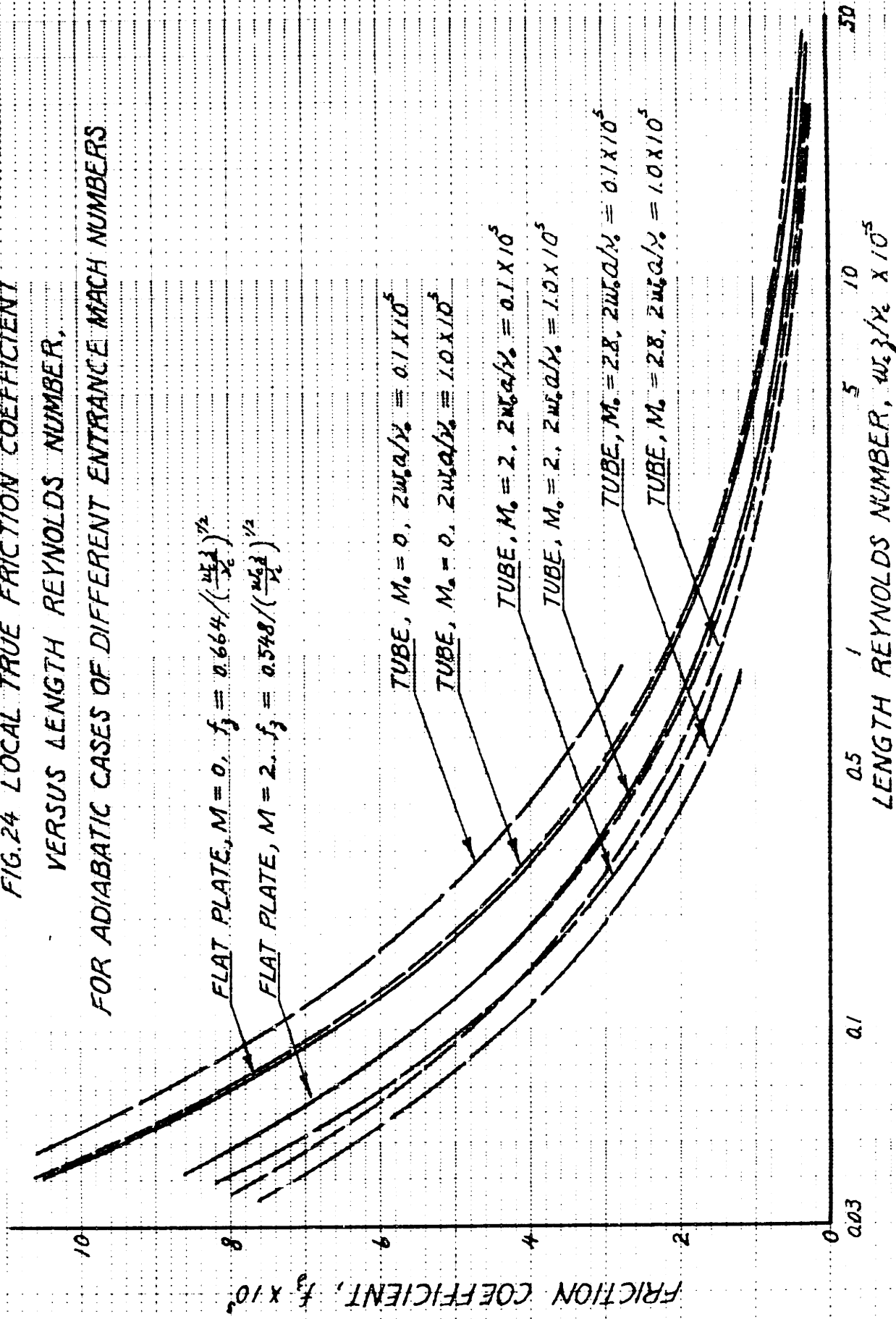


FIG.25 LOCAL TRUE FRICTION COEFFICIENT
 VERSUS LENGTH REYNOLDS NUMBER,
 FOR ADIABATIC CASES OF
 DIFFERENT ENTRANCE MACH NUMBERS

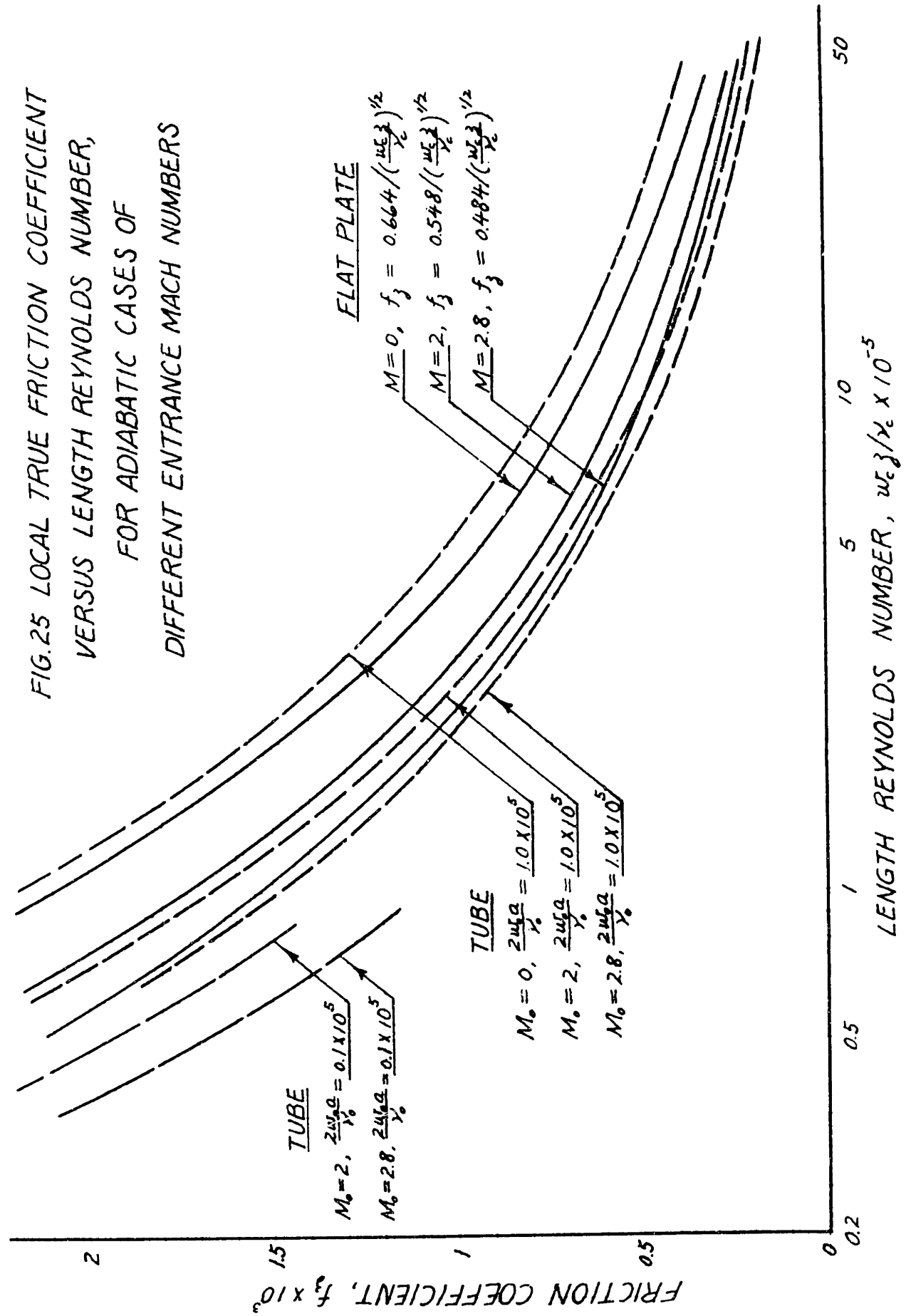


FIG. 26 LOCAL TRUE FRICTION COEFFICIENT
 VERSUS LENGTH REYNOLDS NUMBER,
 FOR ENTRANCE MACH NUMBERS OF 2.8 AND
 DIFFERENT THERMAL CONDITIONS AT TUBE WALL

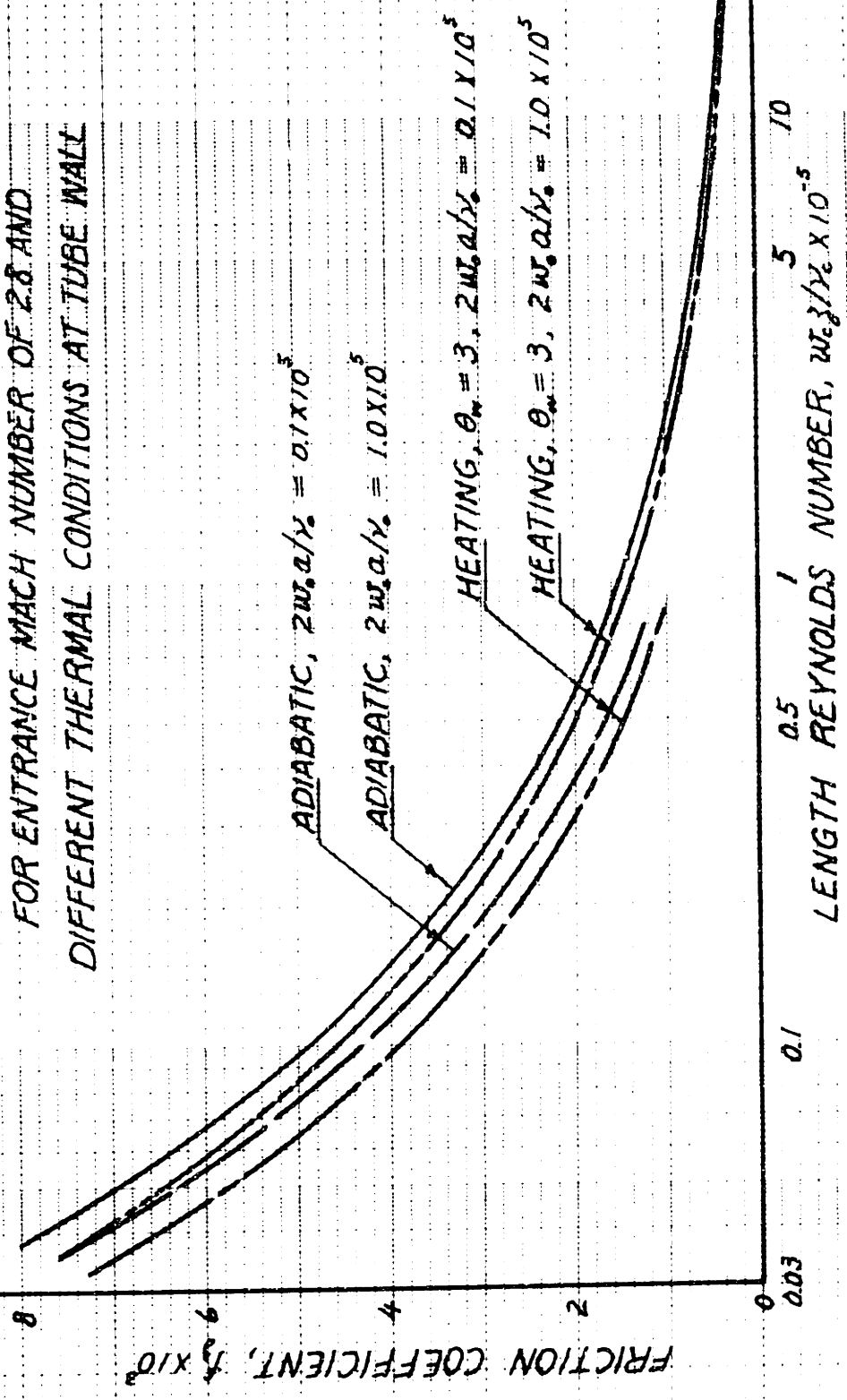


FIG. 27 $f_3 \left(\frac{M_0^2}{\gamma} \right)^{1/2}$ VERSUS LENGTH PARAMETER,
 FOR DIFFERENT ENTRANCE MACH NUMBERS
 AND THERMAL CONDITIONS AT TUBE WALL

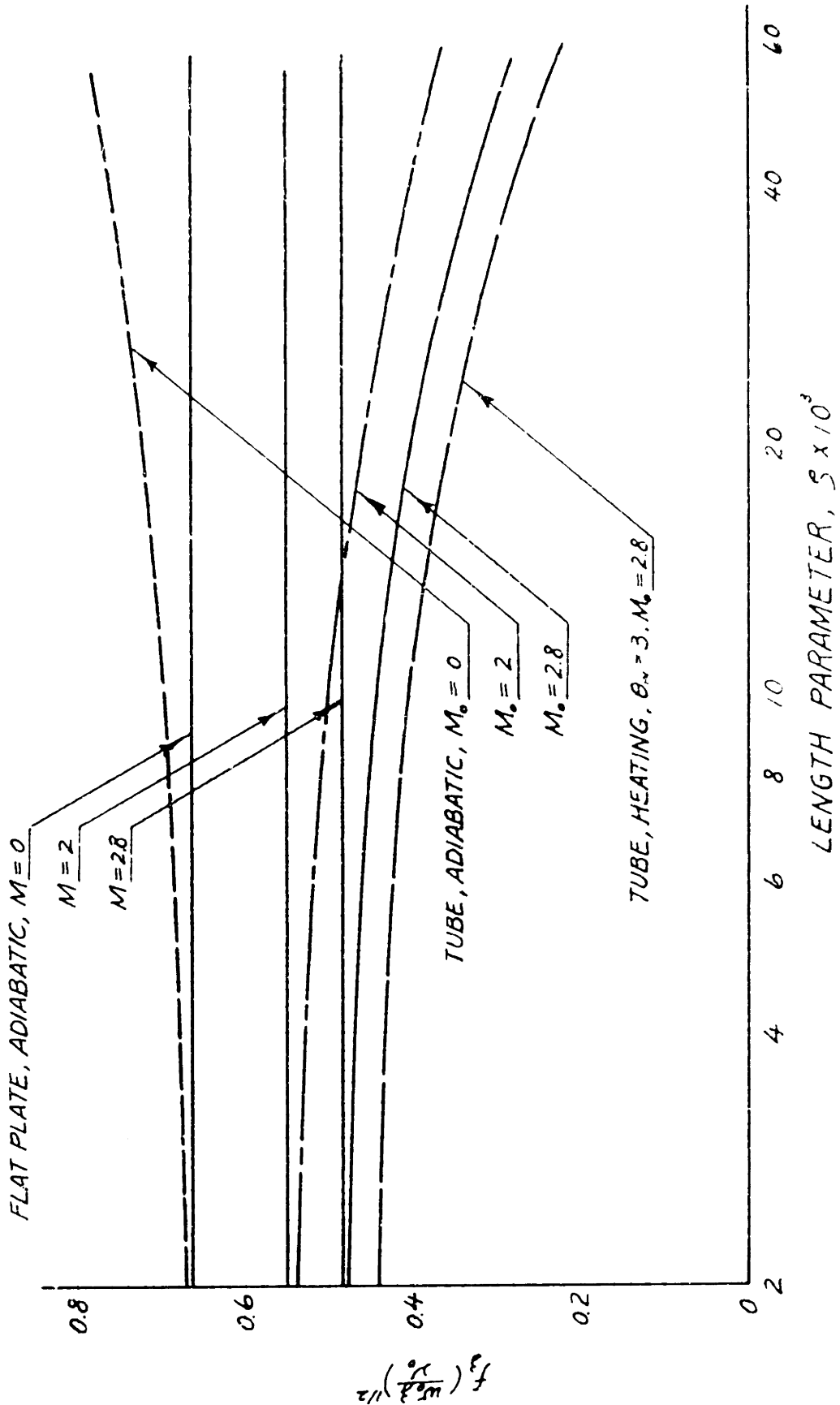


FIG. 28 FIRST APPROXIMATION TO $f_3 \left(\frac{4.5z}{x_0} \right)^{1/2}$
 VERSUS LENGTH PARAMETER, 5×10^3
 FOR DIFFERENT ENTRANCE MACH NUMBERS
 AND THERMAL CONDITIONS AT TUBE WALL

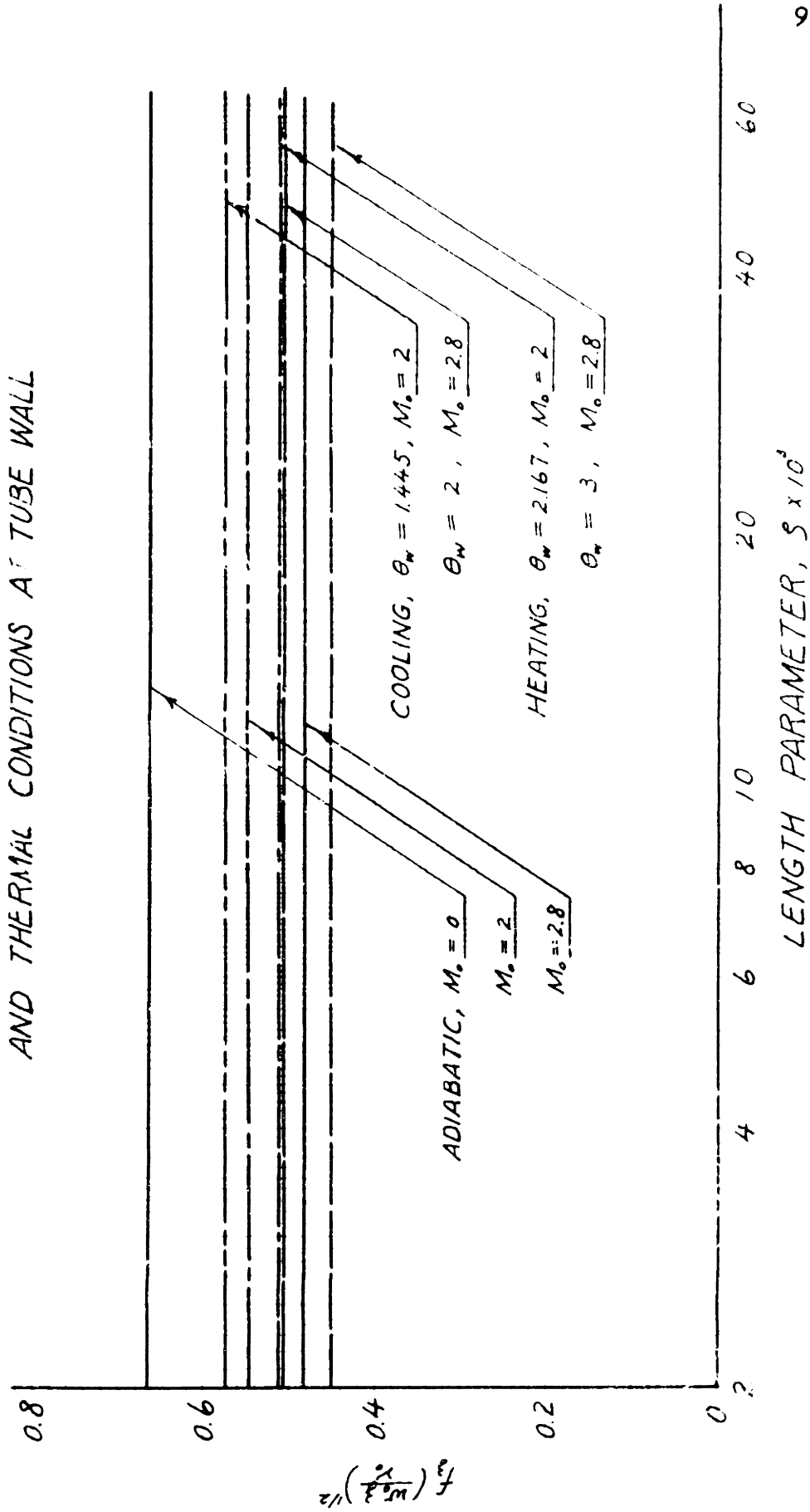
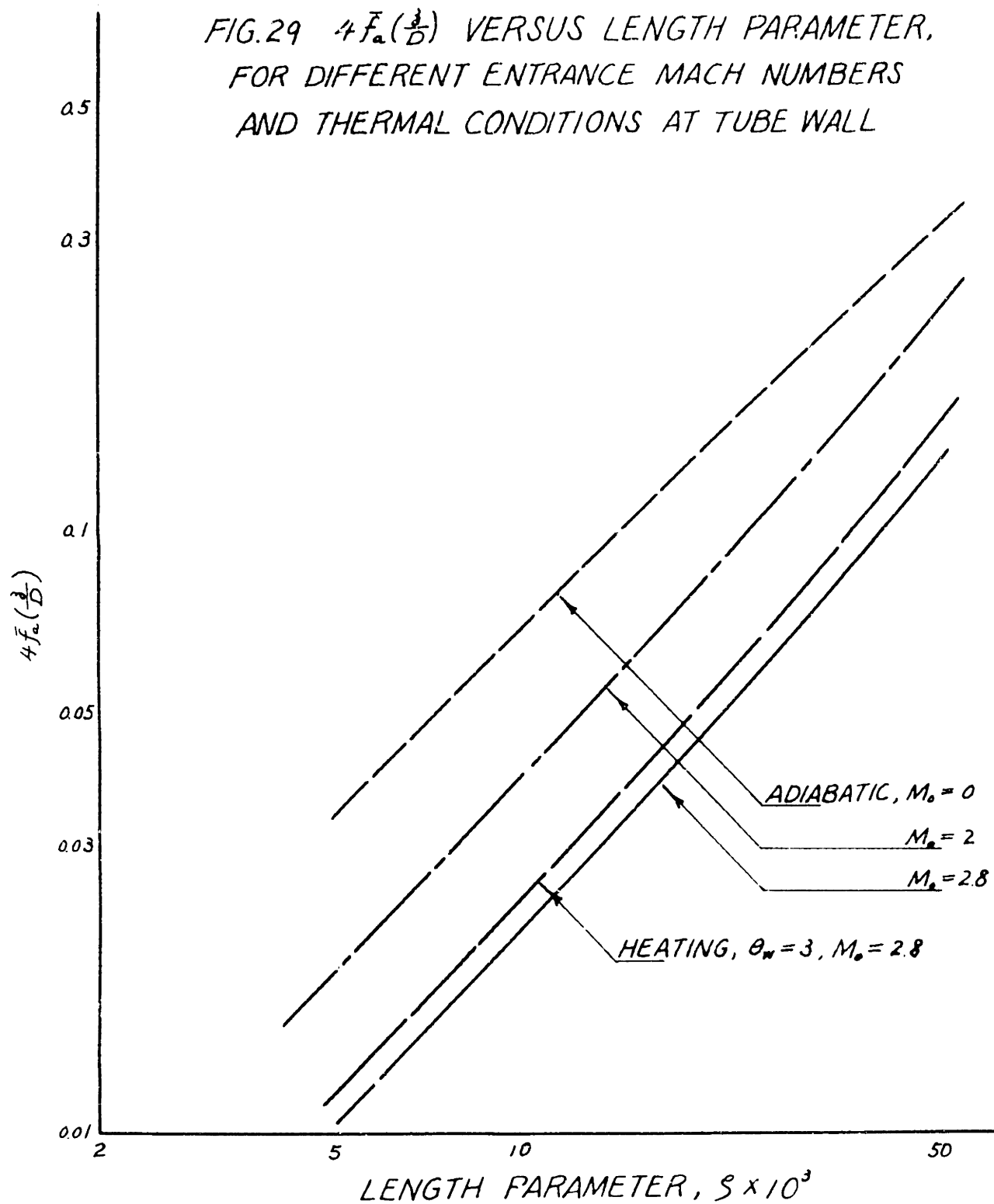


FIG.29 $4\bar{f}_a(\frac{z}{D})$ VERSUS LENGTH PARAMETER,
FOR DIFFERENT ENTRANCE MACH NUMBERS
AND THERMAL CONDITIONS AT TUBE WALL



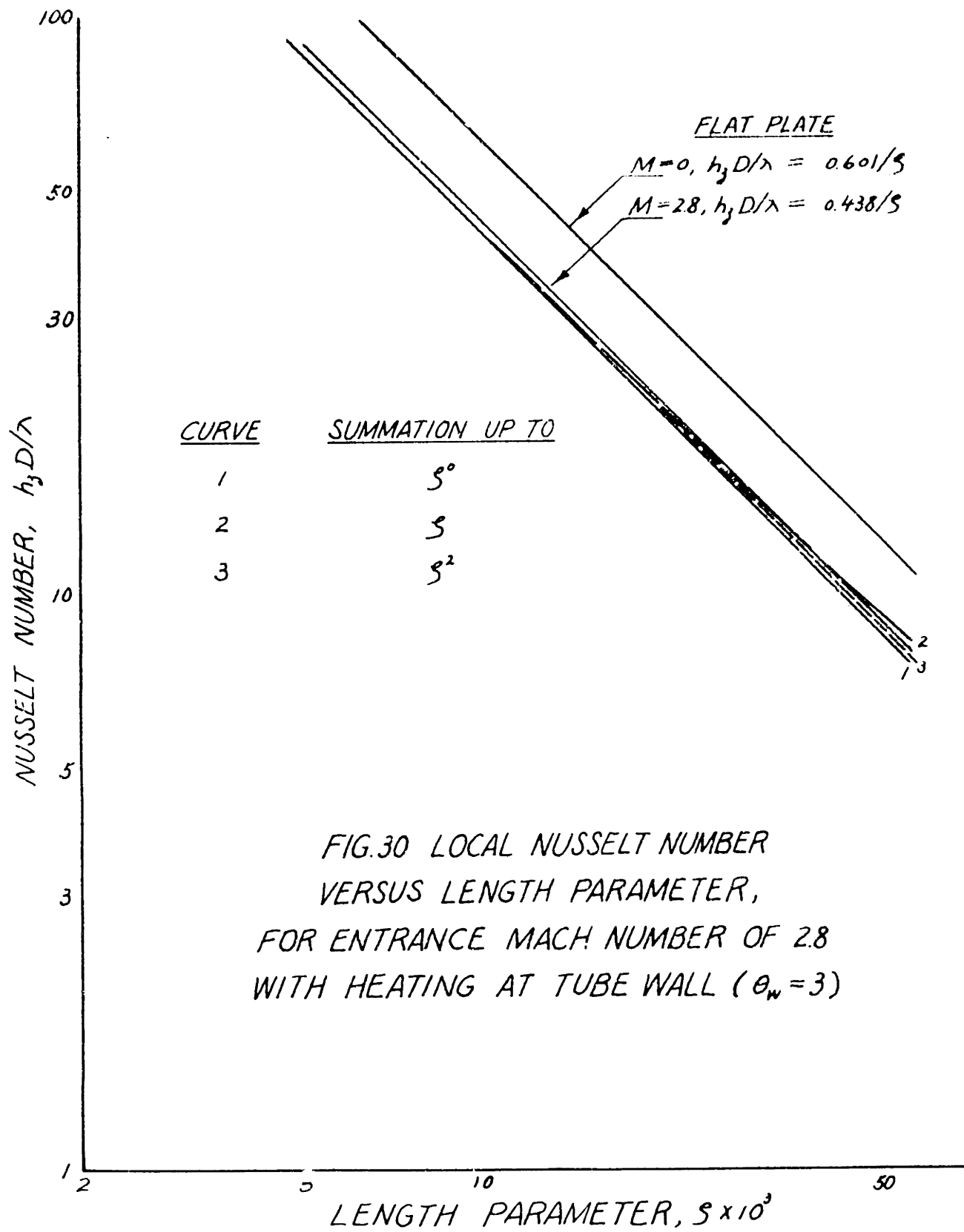


FIG. 31 LOCAL STANTON NUMBER VERSUS
 LENGTH REYNOLDS NUMBER,
 FOR ENTRANCE MACH NUMBER OF 2.8
 WITH HEATING AT TUBE WALL ($\theta_w = 3$)

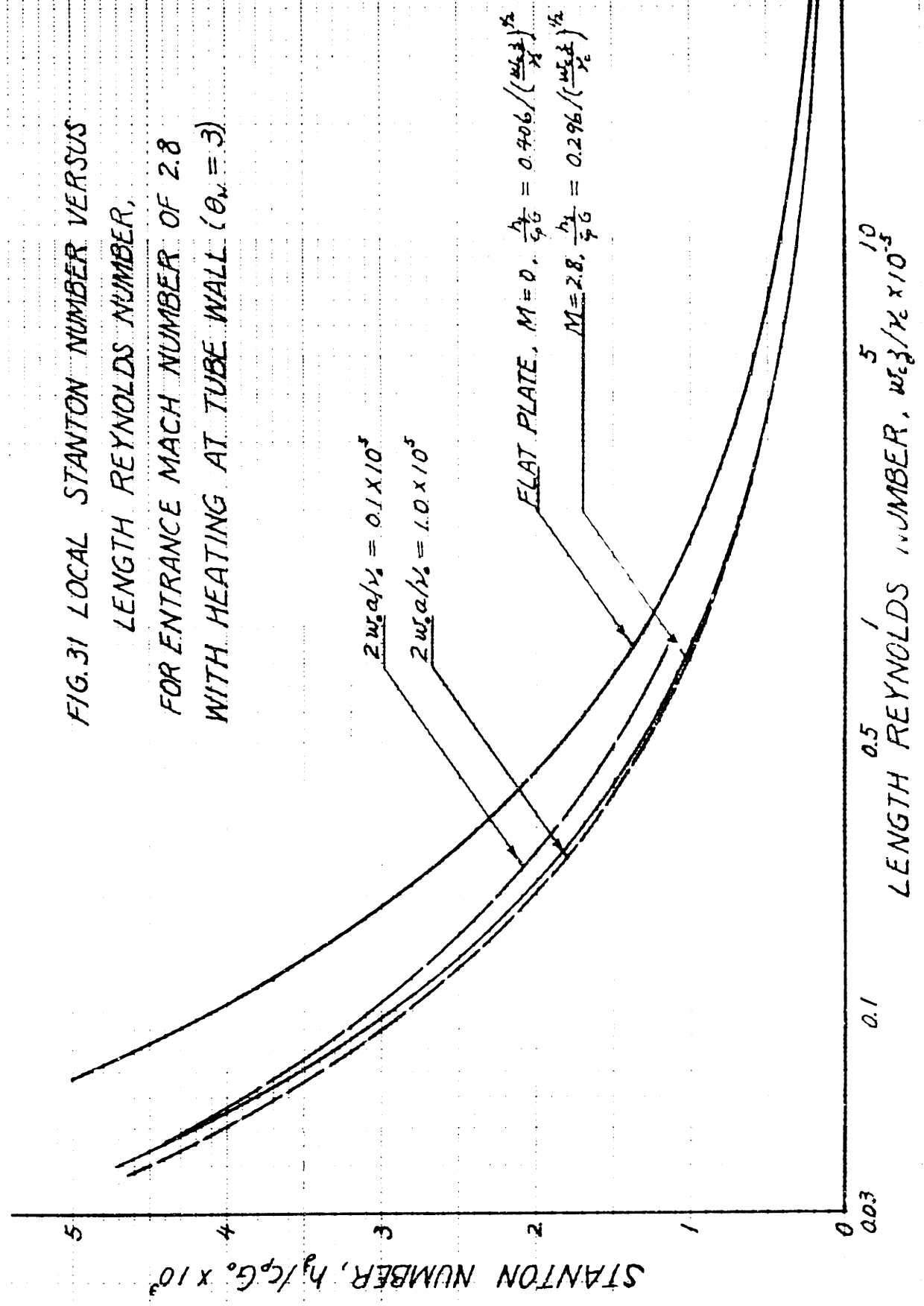


FIG. 32 LOCAL STANTON NUMBER VERSUS
 LENGTH REYNOLDS NUMBER,
 FOR ENTRANCE MACH NUMBER OF 2.8
 WITH HEATING AT TUBE WALL ($\theta_w = 3$)

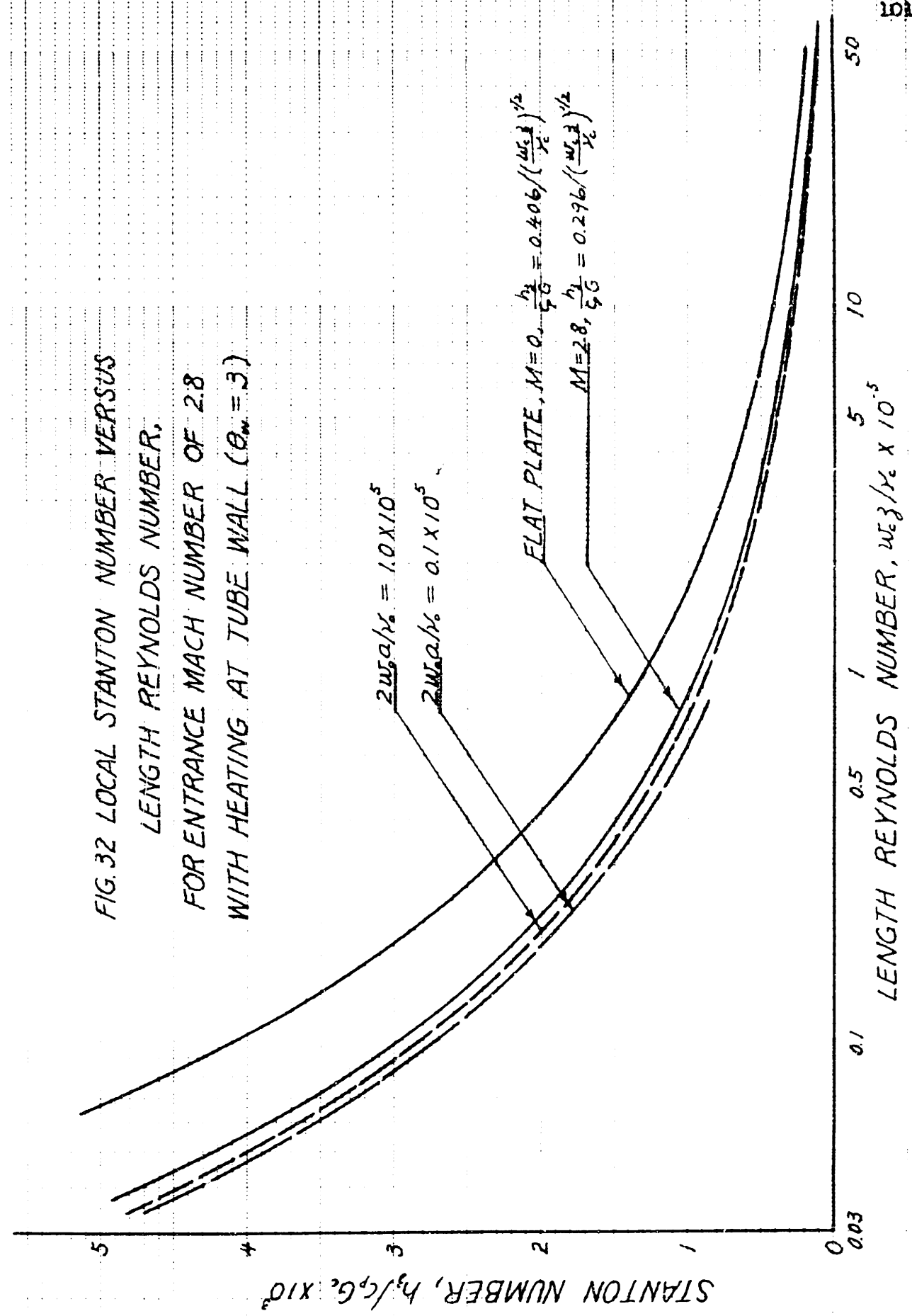
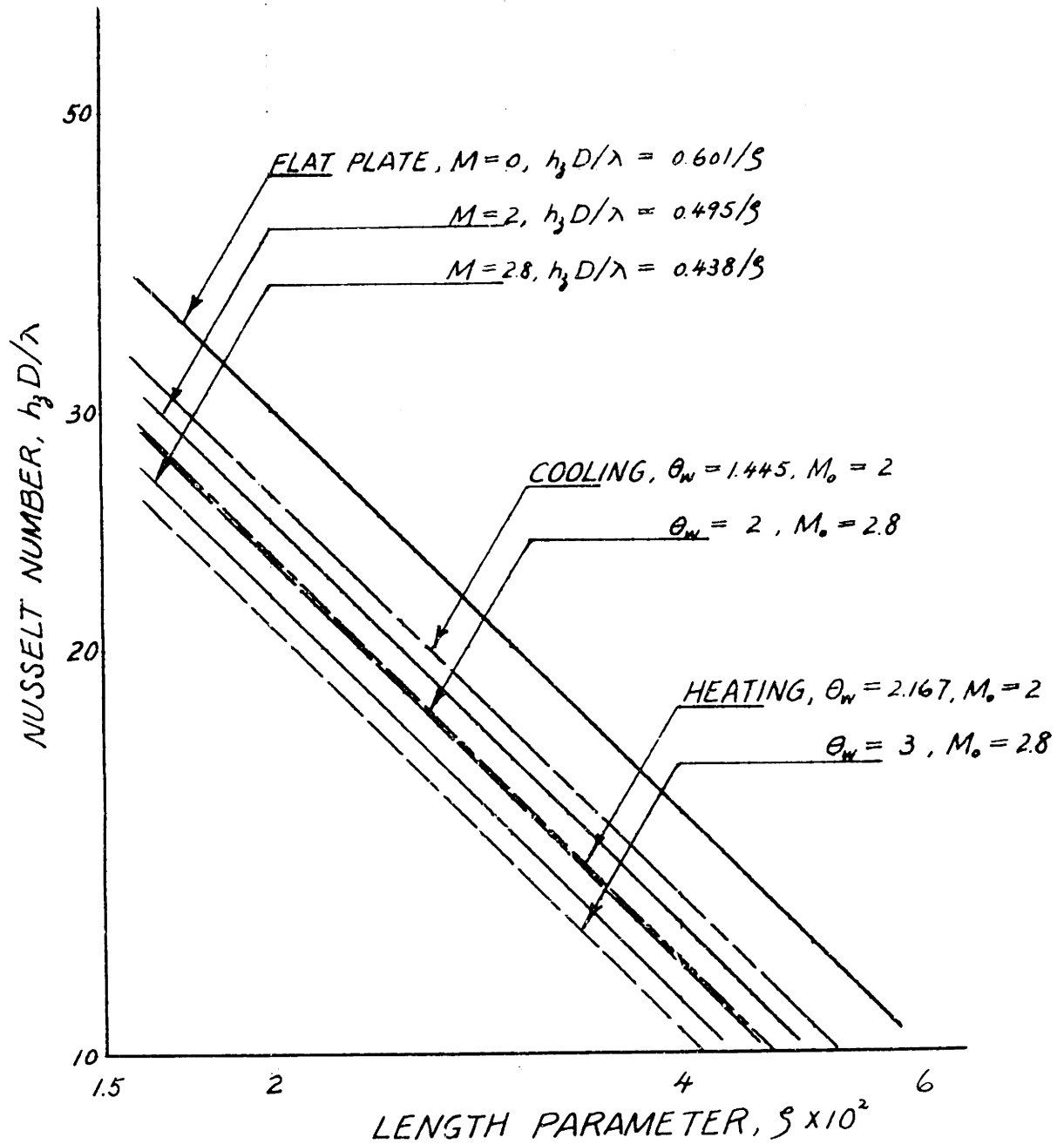
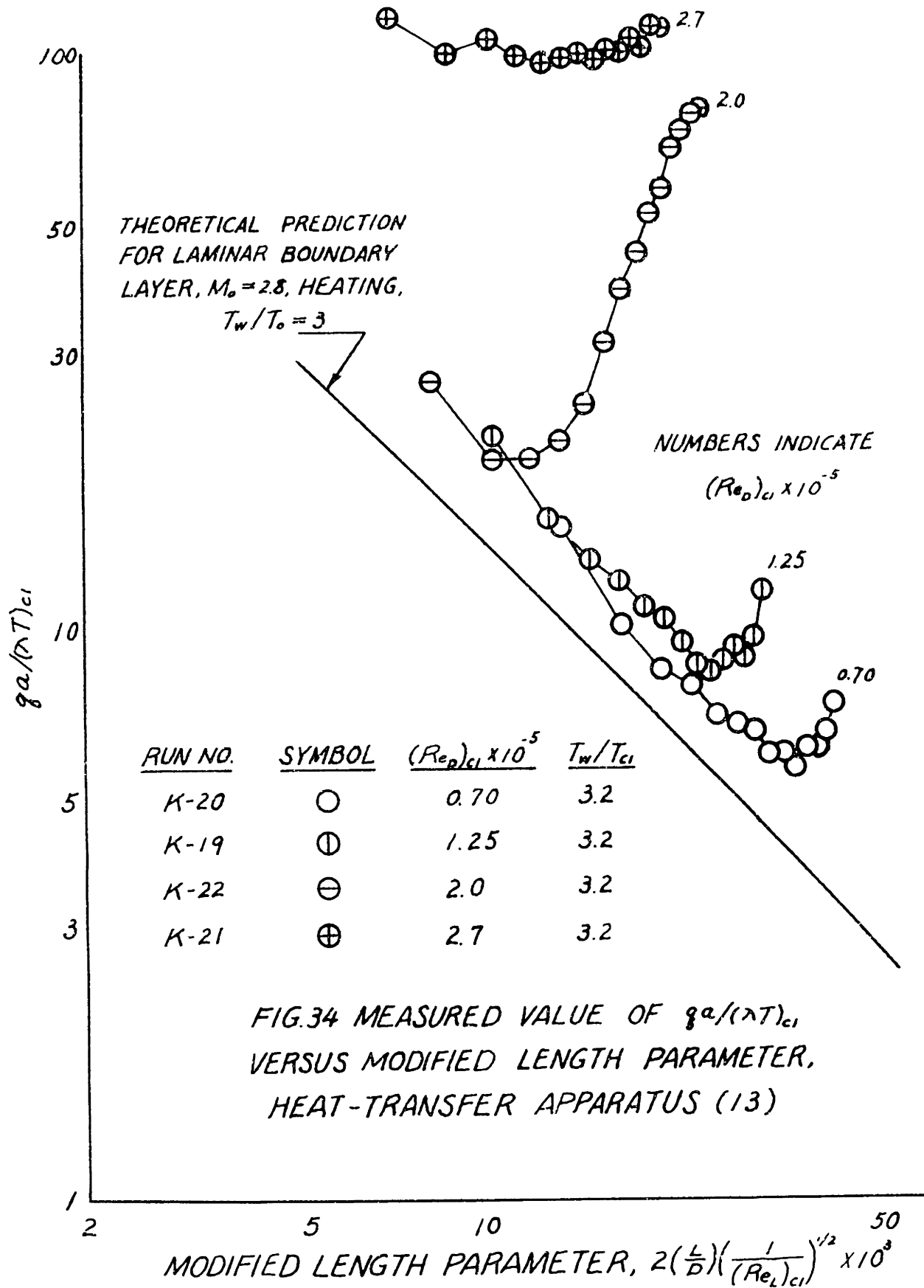


FIG.33 FIRST APPROXIMATION TO
 LOCAL NUSSELT NUMBER
 VERSUS LENGTH PARAMETER,
 FOR DIFFERENT ENTRANCE MACH NUMBERS
 AND THERMAL CONDITIONS AT TUBE WALL





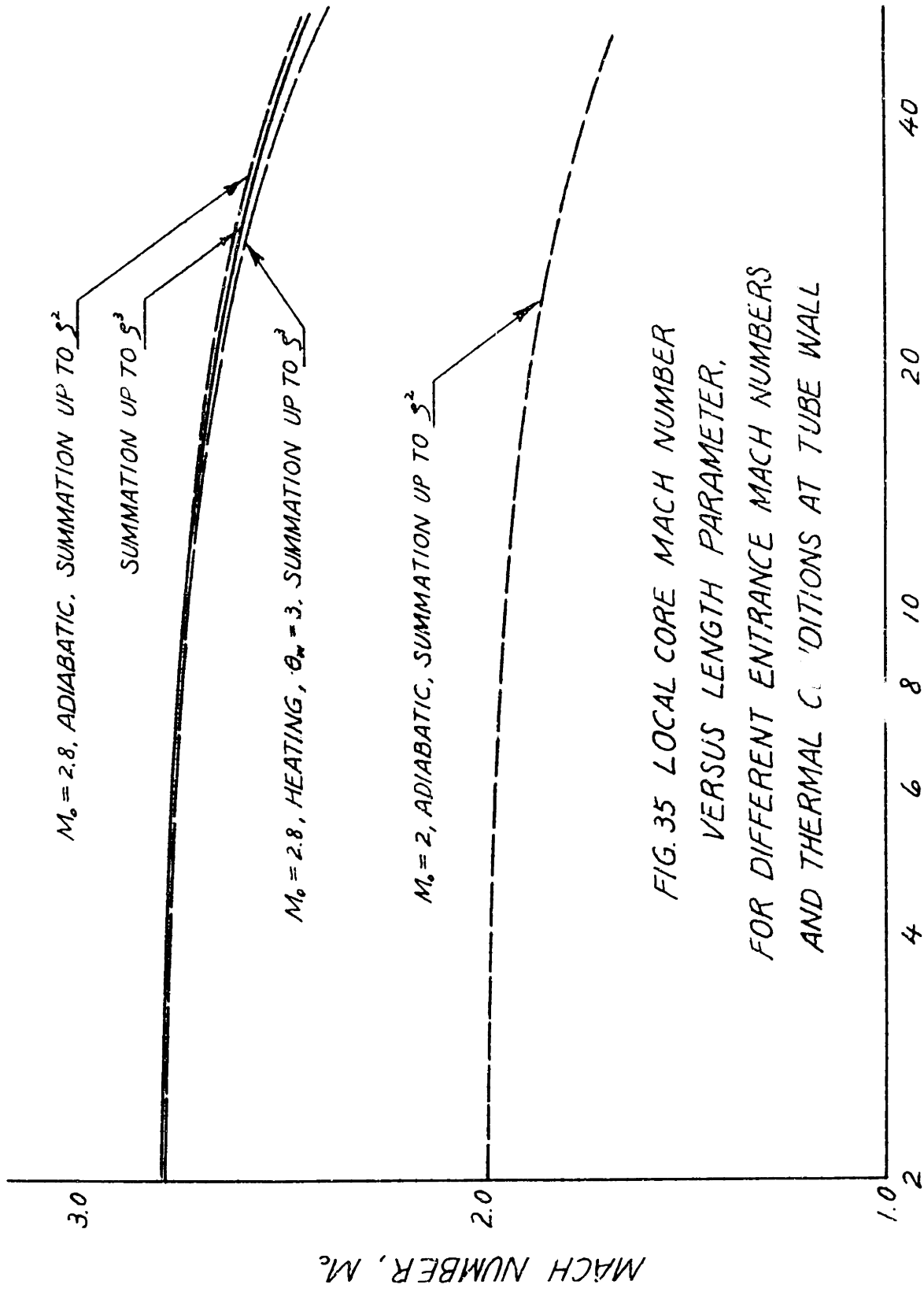


FIG. 35 LOCAL CORE MACH NUMBER
 VERSUS LENGTH PARAMETER,
 FOR DIFFERENT ENTRANCE MACH NUMBERS
 AND THERMAL CONDITIONS AT TUBE WALL

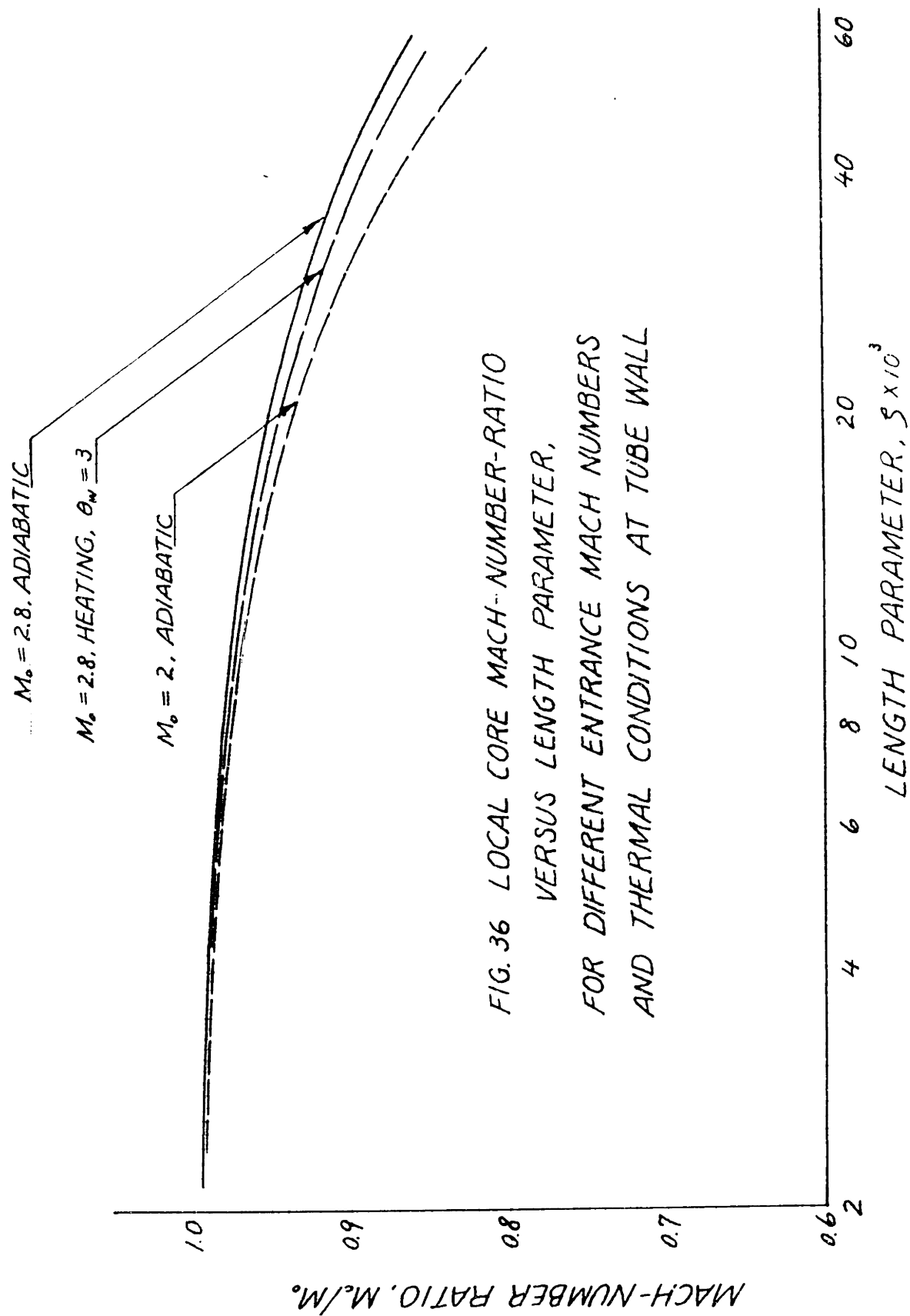


FIG. 36 LOCAL CORE MACH-NUMBER-RATIO
 VERSUS LENGTH PARAMETER,
 FOR DIFFERENT ENTRANCE MACH NUMBERS
 AND THERMAL CONDITIONS AT TUBE WALL

FIG.37 LOCAL CORE DENSITY-RATIO
VERSUS LENGTH PARAMETER,
FOR DIFFERENT ENTRANCE MACH NUMBERS
AND THERMAL CONDITIONS AT TUBE WALL

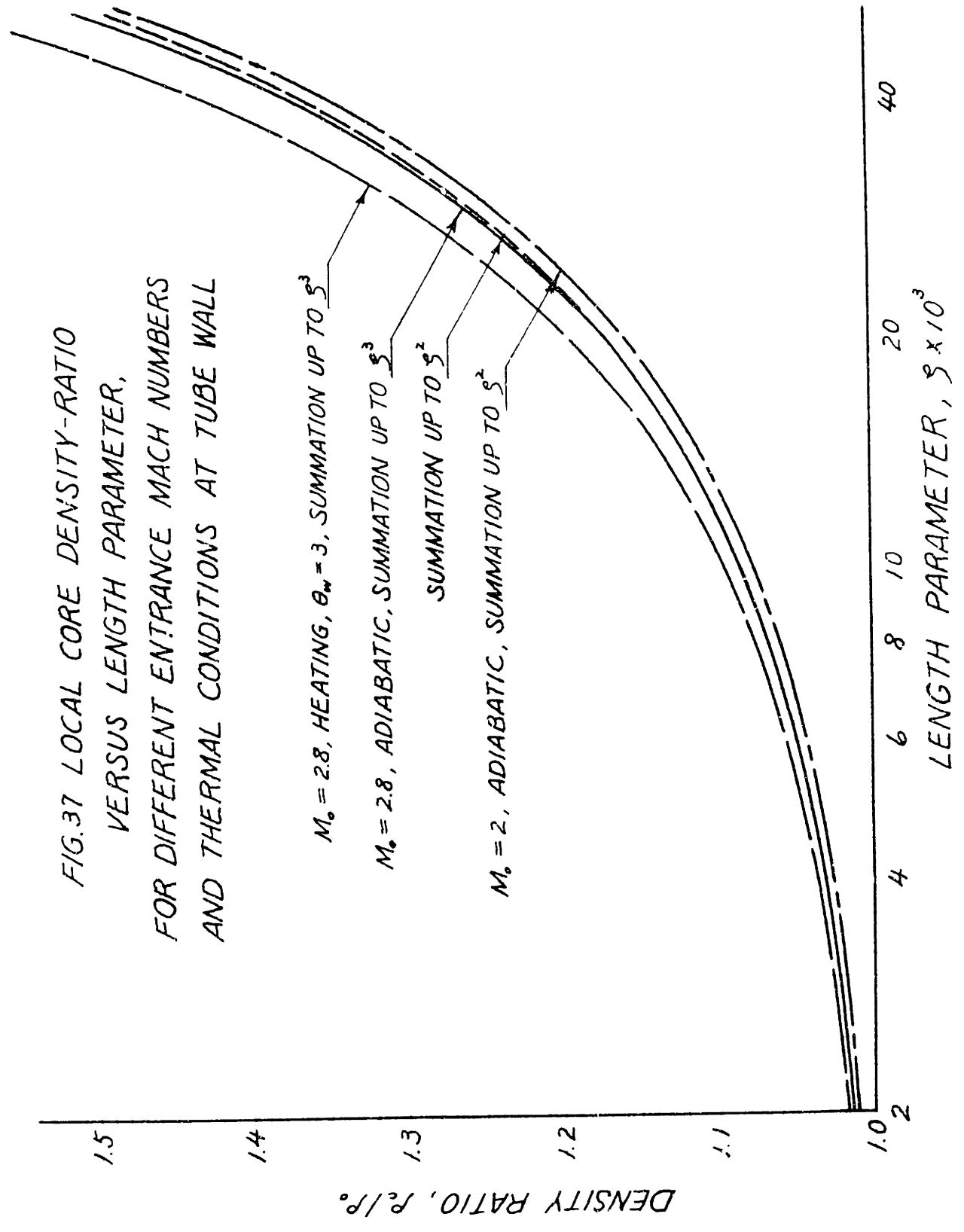


FIG. 38 LOCAL CORE TEMPERATURE-RATIO
 VERSUS LENGTH PARAMETER,
 FOR DIFFERENT ENTRANCE MACH NUMBERS
 AND THERMAL CONDITIONS AT TUBE WALL

